Development and Performance Assessment of Gaseous fuel based Porous Radiant Burners

A thesis submitted in partial fulfillment of the requirements for the degree of

Doctor of Philosophy

by

M. Arun Kumar

(Roll No: 186151001)

School of Energy Science and Engineering

Indian Institute of Technology Guwahati

Guwahati-781039, India

August-2023

School of Energy Science and Engineering,
Indian Institute of Technology Guwahati,
Guwahati – 781039, India

THESIS CERTIFICATE

It is certified that the work contained in the thesis entitled **Development and Performance Assessment of Gaseous fuel based Porous Radiant Burners** by M. Arun Kumar, a student in the School of Energy Science and Engineering, Indian Institute of Technology Guwahati, India, for the award of the degree of the **Doctor of Philosophy** has been carried out under my supervision and that this work has not been submitted elsewhere for the degree.

Dr. P. Muthukumar
Professor
Department of Mechanical Engineering
Indian Institute of Technology Guwahati
Guwahati – 781039, Assam, India.

Dedicated to

My Family, Friends and Supervisor

Acknowledgement

I thank my thesis supervisor, Prof. P. Muthukumar, for his invaluable guidance throughout my Ph.D. program. The attention given by him during my difficult times will never be forgotten. He stayed actively involved in the work I did for my thesis, from framing the research topic to the final experimental results and their physical interpretations. He gave me a lot of creative ideas, which were very useful for completing the present thesis. I am immensely grateful for every moment of my association with him. His superior intellect and outstanding professionalism motivated me a lot. I enjoyed every moment of working under his supervision and learned a lot of things from him, which will be an asset for my future research.

I am thankful to my Doctoral Committee members, Prof. S. Senthilmurugan, Dr. R. Anandalakshmi and Dr. Pankaj Kalita for their valuable suggestions and encouragement during the period of my research work. I would like to express my sincere thanks to Dr. Archana M Nair, Dr. Sharmistha Banerjee, Dr. Pratul Chandra Kalita and Dr. Ranjith Thangavel for their support and guidance. I especially thank Mr. Dilip Chetry and Mr. Gakul Das for their help during the fabrication of the setup and also for their assistance when needed during my experimental studies. I am grateful to Mr. Pratap Chandra Das, Mr. Parvej Ahmed and Mr. Gabindo Boro for their assistance and support in performing the experiments.

I wish to express my deep gratitude to all those who have helped me in various ways during the tenure of my Ph.D. program at IIT Guwahati. I have been supported and accompanied by many people, and each one has played an indispensable role during my work. I am grateful to all of them. I am extremely thankful to my seniors Dr. Lav Kumar Kaushik and Dr. Sunita deb for guiding and helping me with research work, and also for the moral support given by them during my Ph.D. program. I express my sincere gratitude to my seniors and labmates, Mr. G. Surreandhar, Dr. Sangjukta Devi, Dr. Jenne Sunku Prasad, Dr. Alok Kumar, Dr. Vigneshwaran, Dr. Pratibha Maurya, Dr. Mrinal Bhowmik, Dr. Nithin Narmada Raju, Dr. Gurpreet Singh Sodhi, Mr. Sayantan Jana, Mr. Aswin Karthick, Mr. Abhishek Parida, Mr. Shubham Parashar, Mr. Hemanth Krishna Kommu, Mr. N. Umapathi, Mr. Mukesh Gupta, Dr. Viswanth Ramba, Dr. B. Kiran Naik, Dr. Chilaka Ravichandra Rao, Mr. Puneet Kumar Nema, Ms. Juri Sonowal, Dr. Sofia Rani Shaik, Ms. Akshini More, Ms. Nayanita Kalita, Mr. Tat Suraj Arun, Mr. Masresha Adasho Achomo and Dr. Najrul Haque for their unwavering support and

encouragement throughout my Ph.D. program at IIT Guwahati. Their support has been invaluable, and I could not have accomplished this without them. I also extend my gratitude to Dr. Muniraja Tippa, Mr. Arnab Kumar Pal, Mr. Arup Dutta, Mr. Samar Das, Mr. Amit Jain, Mr. Chandan Kakati, Mr. Rabindra Kangsha Banik, Mr. Arun Sathiyan, Mr. Shayaram Basumatary, Mr. Biswajyoti Kakoti and Mr. Barenya Deka for their help and support at different segments of my life in IIT Guwahati.

A special mention to my closest friends Ms. Rashmi Ananda Selvam, Ms. Rismita Khaund, Dr. A. Rahul Narasimhan, Dr. Robin Marlar Rajendran, Dr. Vijay Velu, Dr. K. S. Pragadeesh, Mr. Harish Nanda, Mr. M. Manoj Kumar, Ms. Padma Sheeba, Mr. S. Arunsaikiran and Mr. Janarthanan Mani for enriching my life with the bond of friendship and for supporting me during all the difficult times and being available at any hour of need.

I owe my profound gratitude to my family for their patience and enormous trust in me. My deepest thanks to them for supporting me and being a pillar of my steadfastness during difficult times.

In conclusion, I would like to express my sincere gratitude to my family, faculties and friends who have supported me. Your unwavering support, encouragement, and friendship mean the world to me. Thank you.

M. Arun Kumar

Abstract

In contemporary times, the issue of energy has gained tremendous significance in all conversations and gatherings worldwide. The survival and advancement of humanity depend heavily on it. There are two categories of energy sources - renewable and non-renewable. Fossil fuels, nuclear power, natural gas, etc., belong to the non-renewable category, while solar, geothermal, biomass, wind, and other forms of energy belong to the renewable category. Non-renewable energy sources, primarily fossil fuels, meet the primary energy demand on the planet. Fossil fuels are currently under enormous pressure to meet global primary energy demand and are being consumed at a faster rate than they are generated. This trend, if it continues, could lead to a significant energy crisis in the near future. Additionally, global warming is a severe issue that is expected to cause significant climate changes in the years ahead. To address these challenges, sustainable development is required in all sectors, and there is a growing focus on maximizing energy efficiency and effectiveness. To address this, the United Nations (UN) unveiled 17 Sustainable Development Goals (SDGs) at the UN Sustainable Development Summit in 2015, which are intended to be achieved by 2030.

In India, around 57.4% of the primary energy demand is met by non-renewable sources such as coal, oil, and natural gas, indicating the country's reliance on these sources for survival and growth. As of 2021, India was the world's third-largest consumer of energy. The Indian government has established many initiatives and programs in an effort to move towards renewable sources and locally accessible fuels. However, the nation still lacks efficient technology and machinery for renewables and locally available fuels, which means that the country continues to depend on fossil fuels, oil, and natural gas to meet its energy needs. The government has taken several steps towards sustainable development across all sectors and invested in the development of energy-efficient machinery and modifications to existing machinery to improve performance. The majority of energy is consumed by heating applications, mostly through the use of combustion devices that rely on non-renewable sources. Combustion devices are widely used in many industrial sectors, such as power plants, metal industries, mining industries, food industries, etc., and account for the largest portion of energy consumption. A combustion device converts the chemical energy of fuels (solid, liquid and gases) into heat energy. This process occurs within the combustion device and is exothermic, as heat energy is released in the combustion process. Combustion devices play a vital role in

almost all thermal-oriented industries and cooking applications. Combustion devices contribute to a large amount of energy consumption in domestic and industrial applications. Combustion devices generally work on the following two principles (i) Free Flame Combustion (FFC) and (ii) Porous Medium Combustion (PMC). Conventional burners used for heating purposes in both domestic and industrial applications operate based on the FFC principle. In FFC based combustion devices, the fuel-air mixture combusts above the device head in an open environment, with heat transfer primarily occurring through convection. Due to the low thermal conductivity and emissivity of burnt flue gases, conduction and radiation have insignificant contributions to heat transfer. Although preheating the fuel-air mixture can enhance combustion efficiency, FFC based combustion devices lack heat energy recirculation, resulting in incomplete combustion and emission of pollutants. Researchers worldwide have conducted numerous studies to overcome the limitations of FFC combustion devices and improve combustion efficiency by developing new technologies. PMC based combustion devices have recently attracted attention as an alternative to FFC based combustion devices because of their performance, feasibility, and effectiveness.

PMC based combustion devices use a Porous Medium (PM) which acts as a flame trap and allows the combustion of the fuel-air mixture to take place within the voids of PM. In PMC based combustion devices, the heat energy generated from the combustion process is recirculated internally within the PM and a part of the generated heat energy is utilized for preheating the incoming fuel-air mixture. The heat energy transfer to the load occurs through radiation and convection, in which the contribution of radiation is predominant, and hence it is called “Porous Radiant Burners (PRB)”. CO and NO_x emissions are less in PRBs because of the increased residence time of the fuel-air mixture inside PM and low surface temperature. PRBs can operate at a wide range of power modulation and equivalence ratios and are suitable for operation with high and low energy density fuels. Also, the thermal efficiencies of PRB are comparatively high when compared to FFC based combustion devices, because of the predominance of radiative heat transfer.

Several researchers (Pantangi et al., 2007, 2011; Muthukumar and Shyamkumar, 2013; Mishra et al., 2015, 2018; Devi et al. 2020a; Sunita et al., 2021) at the Indian Institute of Technology Guwahati (IIT Guwahati) have developed PRBs operating on Liquified Petroleum Gas (LPG), that have demonstrated promising outcomes. However, due to the burner's submerged mode of operation, there is a risk of flashback during use, which makes these PRBs impractical for real-

time applications. Additionally, no stability or parametric studies have been conducted on the developed PRBs. This necessitated the need to develop a PRB suitable real-time application which can operate without flashback. Also, Kaushik et al. (2021) developed a cookstove incorporated with a self-aspirated Biogas-PRB (BG-PRB) and demonstrated that it can serve as a substitute for LPG cookstoves in domestic settings. However, the utilization of forced air and pressurized biogas as a fuel source impeded the practicality of the real-time application of the developed BG-PRB.

The following core objectives are considered in the thesis work from the corollaries derived from the literature.

- To develop and test the performance of LPG based Porous Radiant Burner (LPG-PRB) suitable for real-time cooking applications
- To develop and test a Natural Gas based Porous Radiant Burner (NG-PRB)
- To develop a cookstove with self-aspirated Biogas based Porous Radiant Burner (BG-PRB) capable of operating with direct biogas supply from a biogas digester
- To assess the environmental and economic benefits of the developed LPG-PRB, NG-PRB and BG-PRB by performing Lifecycle Assessment (LCA) and Techno-economic Assessment (TEA).

In the present study, LPG-PRB operating in the partially surface-stabilized mode of operation is presented as an improvement of PRB developed by Mishra (2015b). Experimental investigations were performed to assess the performance of the developed LPG-PRB in terms of thermal efficiency and emissions. From the experimental results, it was observed that the developed LPG-PRB showed maximum thermal efficiency of 69.7-63.8% for a power input range of 5-7 kW, which is higher compared to LPG-PRB developed by Mishra (2015b) (55-54%) and Liquefied Petroleum Gas based Conventional Burner (LPG-CB) (54.4-49.7%). Also, an analytical expression has been derived for the air-fuel entrainment ratio in two-layer LPG-PRB. The analytical expression showed that injector exit diameter influences the primary air entrainment in PRB more than any other parameter. To prove the above mentioned hypothesis, experiments were performed to determine primary air entrainment in PRBs operating with different injector exit diameters. Among the LPG-PRBs operating with injector exit diameters of 0.49 mm, 0.63 mm and 0.74 mm, it was observed that the LPG-PRB operating with 0.49 mm injector exit diameter showed the highest thermal efficiency of 69.7%. In addition, stability

analysis was performed to prove the safe operation of the developed LPG-PRB without flashback phenomenon.

The developed LPG-PRB was modified to operate with Natural Gas (NG) and experimental investigations were performed to assess its performance in terms of thermal efficiency and emissions. The thermal efficiency of the developed NG-PRB is in the range of 61.4-52.9% for the power input range of 5-7 kW. In addition, NG-PRB was subjected to thermal mapping to study its thermal behaviour when operated at different power inputs. The developed LPG-PRB and NG-PRB were assessed for their environmental and economic impacts by performing LCA and TEA. From the TEA results, it was observed that LPG-PRB and NG-PRB can lead to maximum annual savings of Rs. 40548.9 /- and Rs. 56033.9 /-, respectively. Also, from LCA results it was observed that LPG-PRB and NG-PRB are environmentally superior to LPG-CB.

Also, a cookstove with BG-PRB suitable for domestic cooking applications was developed as an alternative to conventional biogas burners (BG-CB). The developed BG-PRB was assessed for its thermal efficiency and emissions following IS 8749:2002 prescribed by the Bureau of Indian Standards (BIS). There was an improvement of 7.1% and 10.9% in thermal efficiency at high and low power settings, respectively. Also, CO emissions from BG-PRB at low and high power setting was found to be 447 and 513 ppm, respectively, whereas the same for BG-CB, was found to be 622 and 816 ppm, respectively. Both numerical and experimental investigations were performed on BG-PRB to study its thermal behaviour when operated at high and low power settings. The environmental and economic impacts of the developed BG-PRB were evaluated through LCA and TEA. The TEA results indicated an annual cost savings of Rs. 2375.2 /- and Rs. 4065.4 /- when the BG-PRB was used instead of LPG-CB at low and high power settings, respectively. The LCA results showed that when operated at low power setting, biogas consumption in BG-PRB resulted in significant reductions of 41.7%, 86.5%, and 87.2% in the categories of Human health, Ecosystem quality, and Resource utilization damage. Similarly, the operation of BG-PRB at high power setting, resulted in a reduction of 40%, 86.4%, and 86.8%, respectively, in the same categories.

Nomenclature

η_t	Thermal efficiency (%)
P_i	Power input, kW
ϕ	Equivalence ratio
$\dot{Q}_{useful}$	Useful output energy
$\dot{m}_{fuel}$	Mass flow rate of fuel (kg/s)
LHV_{fuel}	Lower heating value of the fuel (kJ/kg)
T_f and T_i	Final temperature and initial temperature
C_p	Specific heat constant at constant pressure
Q_c	Heat energy released by the combustion process
Q_a	Energy added
H_f and H_O	Enthalpy at the initial and final state
$\dot{q}_{cond}$, $\dot{q}_{conv}$ and $\dot{q}_{rad}$	Conductive, convective and radiative heat flux (W/m^2)
k_{PM}	Thermal conductivity of Porous Medium (W/m.K)
ε_{PM}	Emissivity of Porous Medium
$k_{fuel-air}$	Thermal conductivity of the fuel-air mixture (W/m.K)
$h_{fuel-air}$	Convective heat transfer coefficient between fuel-air mixture and porous medium surface ($W/m^2 \cdot K$),
$T_{fuel-air}$ and T_{PM}	Temperature of the fuel-air mixture and ceramic (K)
σ	Stefan-Boltzmann constant (5.67051×10^{-8} W/m^2K^4)
Re	Reynold's number
Pr	Prandtl number
Pe	peclet number

H_i and H_o	Heat input and heat output
Q_r	Heat recirculated
Q_c	Heat of combustion
$\dot{m}_{LPG}$	Mass flow rate of LPG (g/s)
LCV_{LPG}	Lower Calorific Value of LPG (kJ/kg))
M	Total mass of the pan along with the lid (kg)
m	Mass of water (kg),
C_p	Specific heat of pan (kJ/kg.K)
C_w	Specific heat of Water (kJ/kg.K)
T_1 and T_2	Temperatures of water (°C) at the end and the start of WBT
$\dot{m}_{NG}$	Mass flow rate of NG (g/s)
LCV_{NG}	Lower Calorific Value of NG (kJ/kg))
$\dot{m}_{BG}$	Mass flow rate of biogas (g/s)
LCV_{BG}	Lower Calorific Value of biogas (kJ/kg))

Abbreviations

PMC	Porous Medium Combustion
UN	United Nations
MDG	Millennium Developments Goal
SDG	Sustainable Development Goal
FFC	Free Flame Combustion
PM	Porous Medium
PRB	Porous Radiant Burner
LPG	Liquefied Petroleum Gas
NG	Natural Gas
LPG-PRB	Liquefied Petroleum Gas based Porous Radiant Burner
NG-PRB	Natural Gas based Porous Radiant Burner
BG-PRB	Biogas based Porous Radiant Burner
LPG-CB	Liquefied Petroleum Gas based Conventional Burner
BG-CB	Biogas based Conventional burner
TEA	Techno-Economic Assessment
LCA	Lifecycle Assessment
ppm	Parts per million
ppi	Pores per inch
CL	Combustion Layer
PL	Preheating Layer
MFM	Coriolis Mass Flow Meter
WBT	Water Boiling Test
IS	Indian Standard

Contents

List of Figures

List of Tables

CHAPTER 1

INTRODUCTION TO ENERGY SCENARIO AND COMBUSTION DEVICES

Preface

Energy is a topic of great importance to humankind. People all over the world concentrate on how efficiently energy can be utilized in all sectors. There is a possibility of an energy catastrophe in the years to come since fossil fuels are being used up faster than they are being regenerated. Hence it is important to consume energy efficiently and wisely. The present chapter puts forward the global and Indian energy scenario (sections 1.1 and 1.2). Also, the importance of combustion devices in both industrial and domestic applications is discussed. This thesis presents the development and performance investigation of Porous Medium Combustion (PMC) based burners. Hence a glimpse of combustion devices and their types are discussed in this chapter (section 1.3). Also, a short introduction to PMC and its conceptual background is presented for a better understanding of the technology. Eventually, the motivation and organization of this thesis are presented in sections 1.4 and 1.5, respectively.

1.1 Overview of global energy scenario

In the present scenario, energy is the topic that has gained importance in all discussions and meetings across the globe. It is essential for the world's normal functioning and also, for the survival and evolution of humankind. Sources of energy can be classified into renewable and non-renewable. Fossil fuels, nuclear energy, natural gas, etc., fall under the non-renewable energy source category and solar energy, geothermal energy, biomass energy, wind energy, etc. fall under renewable energy sources. All activities happening worldwide are based on non-renewable energy sources, particularly fossil fuels. In 2021, Fossil fuels accounted for 82% of the world's primary energy and the consumption of the latter increased by 31 EJ when compared to 2020 (bp Statistical Review of World Energy, 2022). Fig. 1.1 shows the energy consumption (Renewable, hydro-electricity, Nuclear energy, Coal, Natural gas and oil) in various regions of the globe. From Fig.1.1, it is understood that there is enormous stress on fossil fuels to meet the primary energy demand across the globe and they are consumed at a rate higher than their rate of generation. If this scenario continues, there will be a huge energy

crisis in the forthcoming future. In addition to that, global warming is a serious issue that is believed to lead to drastic climate change in the forthcoming years. To defend humankind from such a situation, there is a need for sustainable development in all sectors. And now, people have started to think about how efficiently and effectively energy can be utilized.

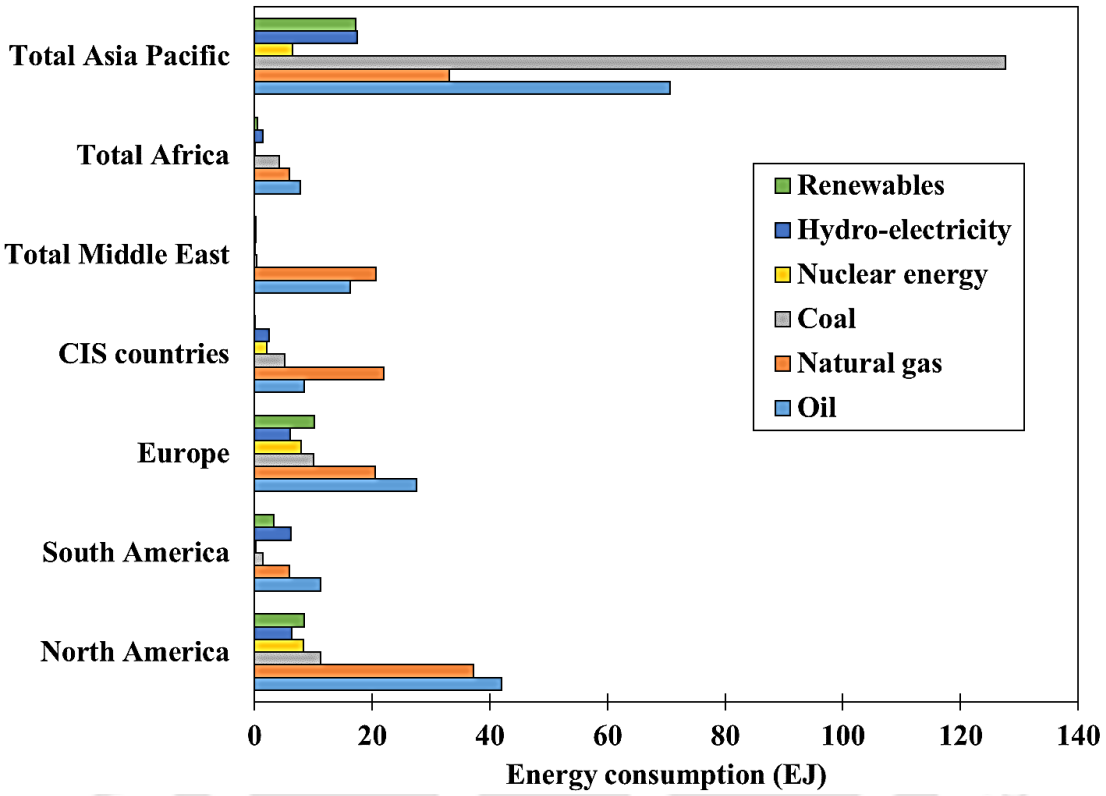

Fig. 1.1. Global energy consumption in 2021 (BP Statistical Review of World Energy, 2022)

In 1992, the United Nations (UN) at the Earth Summit in Rio de Janeiro (Brazil), adopted "Agenda 21" for sustainable development to improve the life of humankind and protect the environment. Later in 2000, at the Millennium Summit held in New York, Eight Millennium Developments Goals (MDG) were put forward to reduce poverty by 2015, but they failed. To compensate for the failure of MDGs, in 2015, the UN announced 17 Sustainable Development Goals (SDGs) at the UN Sustainable Development Summit. Fig. 1.2 shows 17 SDGs of the UN and it is targeted to be accomplished by 2030. Among the SDGs mentioned in Fig. 1.2, SDG-7, 9, 11 and 12 focus mainly on efficient and effective utilization of resources and remedies for climate change.

- SDG-7: Ensure access to affordable, reliable, sustainable and modern energy for all.

- SDG-9: Build resilient infrastructure, promote inclusive and sustainable industrialization and foster innovation.
- SDG-11: Make cities and human settlements inclusive, safe, resilient and sustainable.
- SDG-12: Ensure sustainable consumption and production patterns.
- SDG-13: Take urgent action to combat climate change and its impacts.

Fig. 1.2. 17 Sustainable Development Goals of UN

1.2 Overview of India's energy scenario

In recent years, India has accounted for a notable amount of energy consumption in the world. Being a developing nation, India has been striving very hard to achieve its status as a developed

nation. And therefore, India has increased its exports, commerce, productivity, etc., leading to increased energy consumption and overutilization of resources, manpower, water, etc. Fig. 1.3 represents India's total installed capacity (coal, lignite, gas, diesel, renewables and nuclear energy) in 2023.

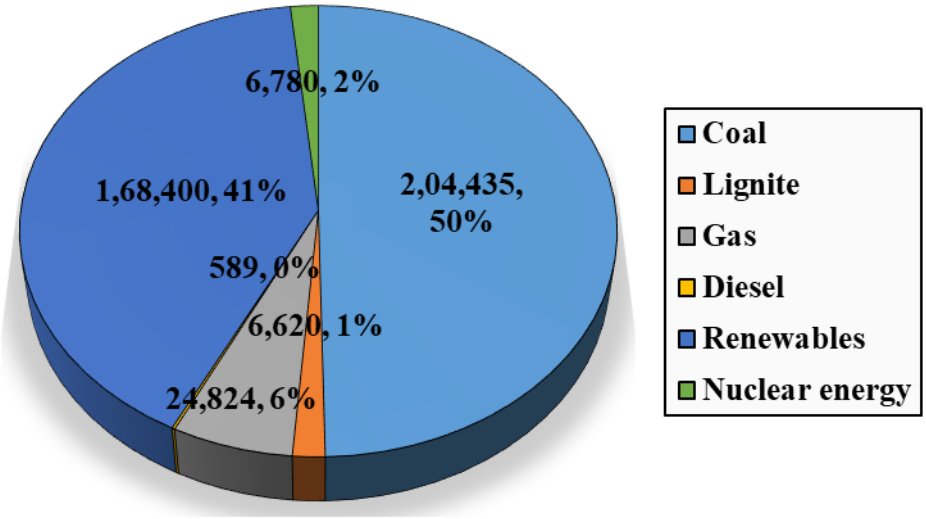

Fig.1.3. India's total installed capacity in 2023 (Ministry of Power, Government of India, 2023)

Fig. 1.3 shows that about 57.4% of the primary energy demand is met by oil, coal and natural gas. This shows that the nation's survival and progress depend on non-renewable energy sources. In the year 2022, India was the world's third-largest energy-consuming country. And the Indian government has propounded many schemes and initiated many programs to transform all sectors to run renewable energy sources and use locally available fuels to meet the energy demands. Yet, the nation still lacks efficient technology and machinery that works on renewables and locally available fuels. And the nation should still depend on fossil fuels, oil and natural gas to meet its energy demands. The government of India has initiated various schemes in adopting sustainable development techniques in almost all sectors of the nation. Also, the Indian government has invested in the development of advanced energy-efficient machinery and modification of the existing machinery to improve its performance. And it should be noted that the majority of the energy is spent on heating applications. In India, most of the heat energy requirements are compensated by combustion devices working on fossil fuel, oil and natural gas. And the nation must have energy-efficient and less polluting combustion devices and systems for effective utilization of the fuels. Combustion devices account for the

largest portion of energy consumption in industrial sectors. The application of combustion devices can be seen in almost all major industries like power plants, metal industries, mining industries, food industries, etc. A detailed description of combustion devices, their working principle and their types will be discussed in the next section.

1.3. Combustion devices and their types

A combustion device is used to convert the chemical energy of fuels (solid, liquid and gases) into heat energy. The process that happens within the combustion device is exothermic, as heat energy is released in the combustion process. Combustion devices play a vital role in almost all thermal-oriented industries and cooking applications. The performance of a combustion device is determined by thermal efficiency (η_t), power input (P_i), equivalence ratio (ϕ) and emissions. Equivalence ratio (ϕ) is defined as the ratio of the stoichiometric air and fuel ratio to the actual air and fuel ratio (Eq. (1.1)). Power input (P_i) is defined as the amount of the energy supplied to the combustion device which mainly depends on the mass flow rate of fuel (Eq. (1.2)). Thermal efficiency (η_t) is an important performance parameter that indicates the performance of the combustion device, as it determines the tendency of the combustion device to convert the input energy (chemical) into useful output energy (heat) ($\dot{Q}_{useful}$)(Eq. (1.3)).

$$\phi = \frac{\left(\frac{A}{F}\right)_{Stoichiometry}}{\left(\frac{A}{F}\right)_{Actual}} \tag{1.1}$$

$$P_i = \dot{m}_{fuel} \times LHV_{fuel} \tag{1.2}$$

$$\eta_t = \frac{Useful\ output\ energy}{Input\ energy(P_i)} = \frac{\dot{Q}_{useful}}{\dot{m}_{fuel} \times LHV_{fuel}} \tag{1.3}$$

Where $\dot{m}_{fuel}$ is the mass flow rate of fuel (kg/s) and LHV_{fuel} is the lower heating value of the fuel (kJ/kg). Combustion devices contribute to a large amount of energy consumption in domestic and industrial applications. Combustion devices generally work on the following two principles:

1. Free Flame Combustion (FFC)
2. Porous Medium Combustion (PMC)

1.3.1 Free Flame Combustion based combustion devices

There are wide varieties of Free Flame Combustion (FFC) based combustion devices available in the market (Fig. 1.4). The conventional combustion devices, in practice, operate in either self-aspiration or forced air supply mode. Self-aspirated combustion devices are commonly used in domestic and small-scale and medium-scale industrial applications. In self-aspirated combustion devices, the air entrains along with the fuel into the combustion chamber by natural draft. Combustion devices operating in forced air supply mode are used in large-scale applications where high power output is needed, in which air is supplied separately into the combustion chamber with the aid of an external device.

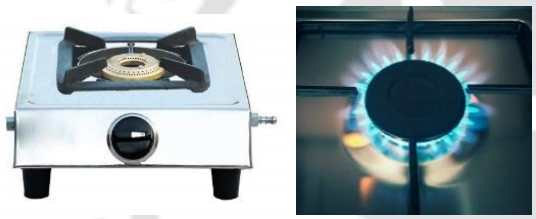

(a) Domestic burners

(b) Industrial burners

(c) Medium-scale commercial burners

Fig. 1.4. FFC based combustion devices

The conventional burners used in all domestic and industrial applications for heating purposes work on the principle of FFC. In FFC based combustion devices, combustion of the fuel-air mixture takes place above the head of the combustion device in the open environment. The main mode of heat transfer from FFC based combustion device to the load is convection. The burnt flue gases from these combustion devices have low thermal conductivity and low emissivity, hence the heat transfer via conduction and radiation is insignificant. Fig. 1.5 illustrates the heat transfer and combustion mechanism occurring in FFC based combustion devices. Preheating the fuel-air mixture can improve the combustion efficiency of the

combustion devices, but in FFC based combustion devices there is no such recirculation of heat energy. Also, these combustion devices emit a large amount of pollutants because of incomplete combustion.

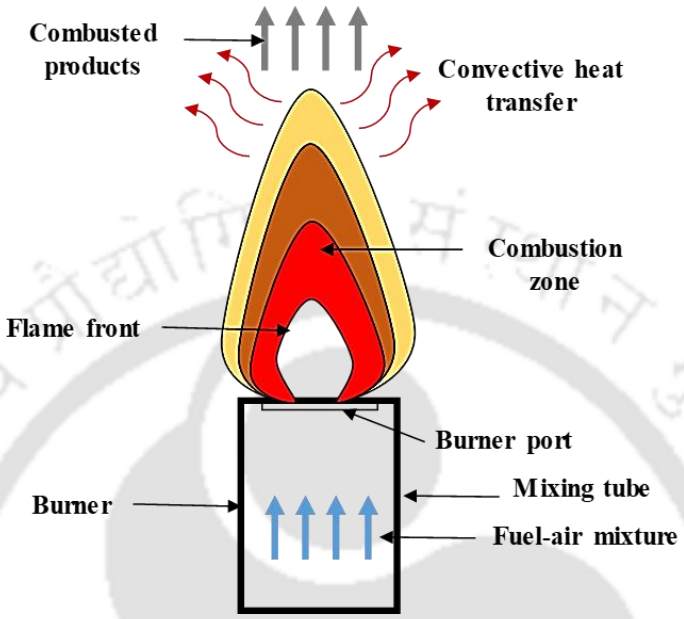

Fig. 1.5. Heat transfer and combustion mechanism of FFC based combustion device

1.3.2 Porous Medium Combustion based combustion devices

Many research works have been carried out worldwide to overcome the shortcomings of the FFC based combustion devices and further increase the efficiency of combustion devices. Researchers are working on developing new technologies for the efficient combustion of fuels. In recent times, Porous Medium Combustion (PMC) based combustion devices are finding attention among researchers as an alternative to FFC based combustion devices. Researchers are very interested in PMC based combustion devices and many works are being carried out across the globe because of their performance, feasibility and effectiveness.

Conceptual background of PMC and its heat transfer mechanism

The operating principle of PMC based combustion device is completely different from that of FFC based combustion devices. As mentioned in section 1.3.1, in FFC based combustion device, the combustion of the fuel-air mixture takes place in the open environment above its head. But in PMC based combustions, the operation is completely different. In PMC based combustion devices, there is heterogeneous interaction between two media in two different phases, usually gas and solid. There are two major design approaches-namely stationary and

transient system approaches, employed in developing a PMC based combustion device (Mujeebu et al., 2009). In the stationary approach, the combustion zone is stabilized in the finite elements of the porous matrix and it is used in radiant burners and surface heaters due to the high radiant emissivity of the solid. In the transient approach, the combustion device operates on the concept of "excess enthalpy flame" theory where the combustion zone is free to shift either in an upstream or downstream direction depending upon the energy flux. In 1971, Weinberg explained the concept of heat recirculating combustion or excess enthalpy recirculation, in which the combustion of the fuel-air mixture takes place within a porous layer of the combustion device, transferring a part of the energy for preheating the incoming fuel-air mixture. The amount of energy recirculated within the porous medium can be given as (Weinberg, 1971):

$$\int_{T_o}^{T_f} C_p dT = Q_C + Q_a = H_f - H_o \tag{1.4}$$

Where, T_f and T_0 are the final and initial temperature, C_p is the specific heat constant at constant pressure, Q_C is the heat energy released by the combustion process, Q_a is the energy added and H_f and H_o are the enthalpy at the initial and final state. Fig. 1.6 illustrates the heat recirculation concept proposed by Weinberg (1971) in PMC based combustion device.

Many researchers across the globe use Porous Medium (PM) for achieving heat recirculation. PM acts as a flame trap and allows the combustion of the fuel-air mixture to take place within the voids of PM. Generally, in combustion devices employing PM, the combustion of the fuel-air mixture occurs either inside (fully submerged mode) or above (surface stabilized mode) the PM, depending on the operating conditions. In a PM based combustion device operating in surface stabilized mode, the combustion of the fuel-air mixture takes on the surface of the porous medium, where the significance of heat recirculation is negligible and a free flame can be seen on the surface of the combustion device. And its operation is similar to a FFC based combustion. Whereas, in a PM based combustion device operating in fully submerged mode, the combustion of the fuel-air mixture takes place within the PM. And it operates on the principle of PMC, where the heat energy generated from the combustion process is recirculated internally within the porous medium and part of the generated heat energy is utilized for preheating the incoming fuel-air mixture. In this type of combustion device, the output heat

energy transfer will be through radiation and convection, in which the contribution of radiation is predominant. And the combustion devices that operate based on the principle of PMC are generally referred to as Porous Radiant Burners (PRB). And from now on, PMC based combustion devices will be termed PRB throughout the thesis.

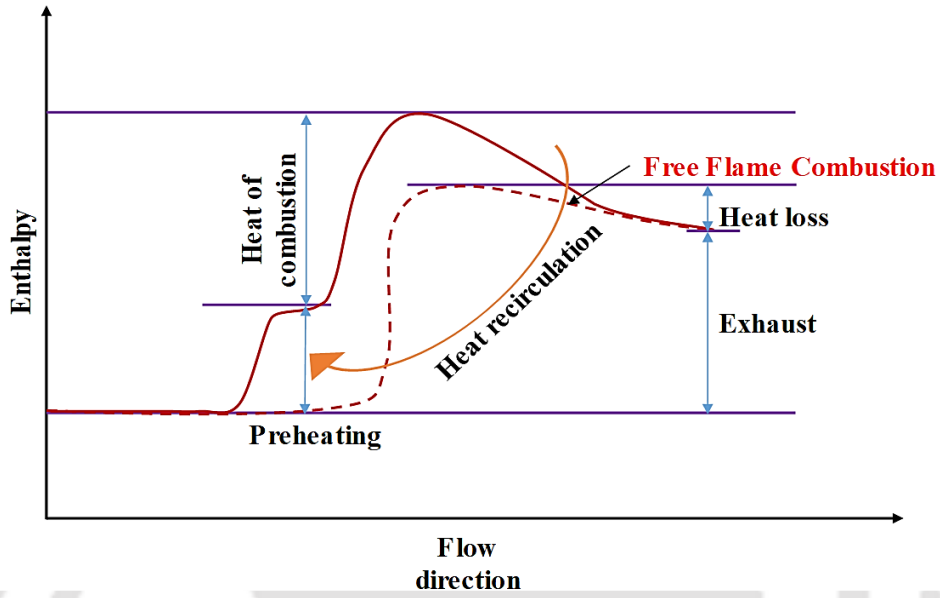

Fig. 1.6: Heat recirculation concept in PMC proposed by Weinberg (1971)

PRB can be classified into single-layer (Fig. 1.7) and multi-layered PRB (Fig. 1.8), based on their arrangement. And it should be noted that double-layered PRB is the most preferred option among multi-layered PRBs all over the world. As shown in Figs. 1.7 and 1.8, the three forms of heat transfer, viz., conduction, convection and radiation, are present in a PMC based combustion device. Conduction, convection and radiation heat transfer in a PMC based combustion device can be estimated by using Eqs. (1.5), (1.6) and (1.7). Also, the coefficient of convective heat transfer can be determined from the Nusselt number (Nu) by using Eq. (1.8).

$$\dot{q}_{cond} = -k_{PM} \frac{dT_{PM}}{dx} \tag{1.5}$$

$$\dot{q}_{conv} = -h_{fuel-air}\left(T_{fuel-air} - T_{PM}\right) \tag{1.6}$$

$$\dot{q}_{rad} = \varepsilon_{PM}\sigma\left(T_{PM}\right)^4 \tag{1.7}$$

$$Nu = \frac{h_{fuel-air} \times l}{k_{fuel-air}} = f(\text{Re}, \text{PR}, \text{Geometry}) \quad (1.8)$$

Where, $\dot{q}_{cond}$, $\dot{q}_{conv}$ and $\dot{q}_{rad}$ are the conductive, convective and radiative heat flux (W/m^2), k_{PM} and ε_{PM} are the thermal conductivity (W/m.K) and emissivity of PM, $k_{fuel-air}$ is the thermal conductivity of the fuel-air mixture (W/m.K) and $\frac{dT_{PM}}{dx}$ is the temperature gradient along the x-direction. $h_{fuel-air}$ is the convective heat transfer coefficient between fuel-air mixture and PM surface (W/m^2.K), $T_{fuel-air}$ and T_{PM} are the temperature of the fuel-air mixture and ceramic (K), respectively, σ is the Stefan-Boltzmann constant (5.67051x10^{-8} W/m^{2}K^4). Re and Pr are Reynolds number and Prandtl number, respectively.

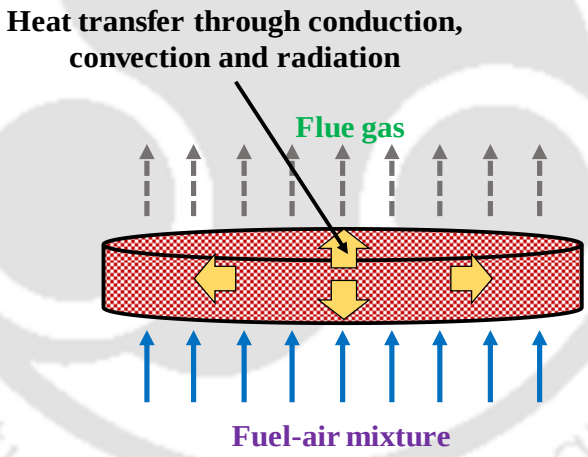

Fig. 1.7: Schematic of single-layer PRB

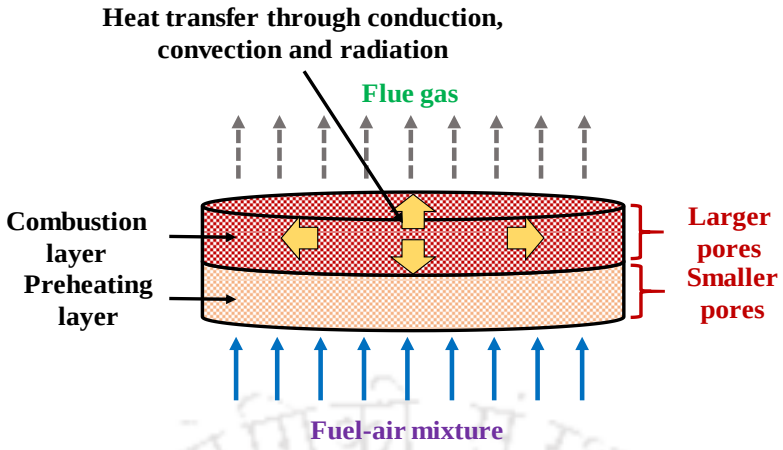

Fig. 1.8: Schematic of multi-layer PRB

Flame stabilization in PMC based combustion devices

In PMC based combustion devices, flame stabilization is of prime importance. The unstable flame within PM may lead to adverse conditions like lift-off or flashback, which ultimately ends the combustion process within the PM and turns off the combustion device. "Flashback" prevails when the incoming fuel-air mixture velocity is not sufficient to resist the flame velocity and allows the flame to propagate upstream towards the incoming reactants. Similarly, when the incoming fuel-air mixture velocity is higher than the flame velocity, the flame travels downstream (out of the burner surface) and this phenomenon is termed "Blow-off". For stable operation of PRB, incoming fuel-air mixture velocity should be equal to flame velocity. Babkin et al. (1991) differentiated the combustion regimes based on flame velocity in PM (for gaseous fuel combustion) (Table. 1.1).

Table 1.1: Steady-state combustion regime and their flame propagation mechanism in PM (for gaseous fuels combustion) (Babkin et al., 1991)

Regimes	Flame velocities (m/s)	Flame propagation mechanism
Low velocities	$0\text{-}10^{-4}$	PM heat conductivity, interphase heat exchange
High velocities	0.1-10	Convective gas movement under constant pressure condition
Sound velocities	100-300	Convective gas movement because of pressure gradient
Low velocities detonation	500-1000	Self-ignition under shock wave interaction with PM
Normal detonation	1500-2000	Detonation under heat and pulse losses

A double-layered PRB, generally consists of two layers, namely combustion layer and preheating layer, in which the flame stabilizes in the combustion layer (CL) as shown in Fig. 1.8. For hydrocarbon fuel, Babkin et al. (1991) proposed a criterion for stabilization of flame within PM based on peclet number (Pe) (Eq. (1.9)), which is the ratio of convective to conductive heat flow. They proposed a limiting condition ($Pe \geq 65$) for flame propagation. Hence for stable operation of double-layered PMC based combustion devices, CL should be designed to have $Pe \geq 65$ and PL should be designed to have $Pe < 65$. Fig. 1.9 shows the schematic representation of the arrangement of double-layer PRB based on peclet number. Later, Dhillon (1999) found out that the criterion for hydrogen fuel combustion in PM is 37.

$$Pe = \frac{S_L d_m c_{fuel-air} \rho_{fuel-air}}{K_{fuel-air}} \tag{1.9}$$

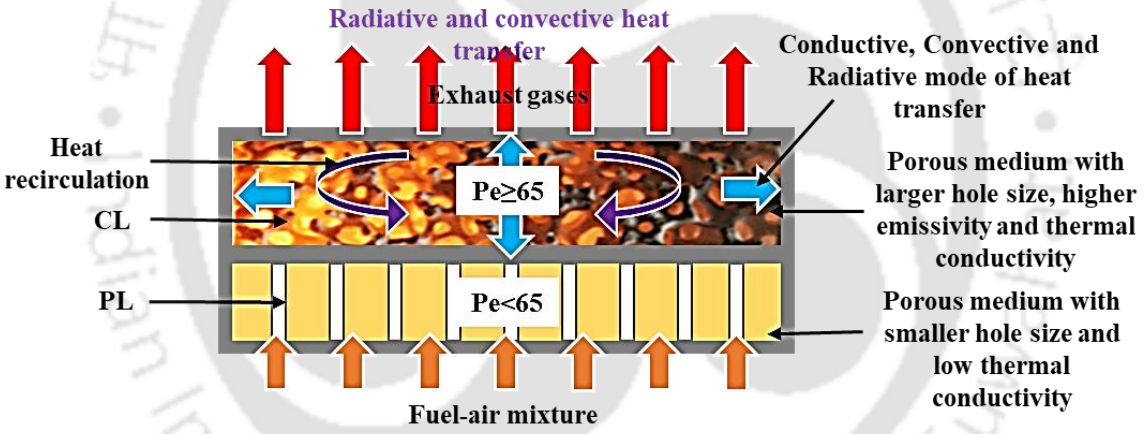

Fig. 1.9: Schematic representation of the arrangement of double-layer PRB based on peclet number

Materials used in PMC based combustion devices

Ceramics (ceramic foam, honeycomb perforated plate, ceramic balls) such as aluminium oxide (Al_2O_3), zirconium dioxide/zirconia (ZrO_2), silicon carbide (SiC), mullite, cordierite, etc. and some metallic materials (metal fibre) such as stainless steel, Fe-Cr-Ni alloy (iron-chromium-nickel), etc. in porous structure are used most commonly used PM in PRB (Fig. 1.10). In recent times, development of PRB is towards employing a ceramic based PM, because of their thermal stability at high temperature and low thermal inertia. There has been a drastic improvement in the structure of PRB in the last few decades, as many research work has been devoted to finding the best material and structure of PM having high durability, which is suitable for practical

applications. And they have also succeeded in finding the best material suitable for PRB. Table 1.2 provides the thermal and radiative properties of the PM used across the globe.

(a) Ceramic foam

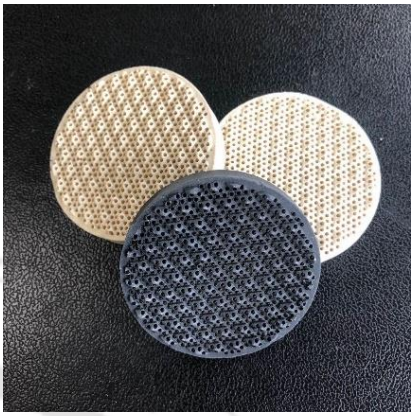

(b) Honeycomb perforated plates

(c) Metal fibre

(d) Ceramic balls

Fig. 1.10: Different types of ceramics

Table 1.2: Ceramic material properties (Sinha et al., 2021)

Material		**A**	**B**	**C**	**D**	**E**	**F**	**G**	**H**	**I**
Maximum temperature resistance (°C)		1600	1900	1800	1400-1750	1380	1700	-	-	-
k_{PM} (W/m.k)		20-50	5-6	2-4	40-120	110-160	80-145	2.6	0.37	0.13
		at (1000°C)			at (20-100°C)					
ε_{PM} at 1727 °C		0.9	0.28	0.31	-	-	-	-	-	0.65
Thermal expansion coefficient 20-1000°C		4-5	7.2	10-13	-	-	-	-	-	-
C_p at 25-800°C		-	1.05	0.59	0.84	0.84	0.84	0.80	-	0.432
Optical thickness (m)	10 ppi	-	-	28.2	-	-	-	-	-	-
	65 ppi			300						

Scattering albedo	10 ppi	0.55-0.88	-	0.87-0.99	-	0.7	-	0.76	0.84	-
Extinction coefficient (m^{-1})	10 ppi 20 ppi 25 ppi 30 ppi	234.1 468.1 585.2 702.2	210 300	234.1	100	178 244	-	270	202	34.1

A: SiC- Silicon carbide; B: Al_2O_3- Aluminium oxide; C: ZrO_2- Zirconium dioxide
D: SSiC- Sintered silicon carbide; E: SiSiC-Silicon infiltrated silicon carbide
F: HPSiC- Hot pressed infiltrated silicon carbide; G: Cordierite; H: Mullite
I: FeCrAl alloy (Iron-Chromium-Aluminium alloy)

Advantages of PMC based combustion devices

The main advantages of PMC are given below;

- Improved heat transfer properties compared to FFC based combustion devices
- Because of the low surface temperature of the combustion device, NO_x emissions from PMC based combustion devices are less
- Owing to the increased residence time of the fuel-air mixture inside PM, the CO emissions from PMC based combustion devices are low
- PMC based combustion devices can operate at a wide range of power modulation and equivalence ratios
- PMC based combustion devices are suitable for operation with high and low energy density fuels
- Thermal efficiencies of PMC based combustion devices are comparatively high when compared to FFC based combustion devices, because of the predominance of radiative heat transfer

Applications of PMC based combustion devices

Some of the featured applications of PMC based combustion devices are as follows:

- Domestic heating and cooking systems
- Automobiles
- Gas turbine and propulsion systems
- Heat exchangers
- Electricity and steam generation systems, etc

1.4 Motivation of the thesis

In recent times, the main topic of interest in discussion is energy and efficiency. Because of the over-utilization of fossil fuels, it is important to concentrate on how efficiently energy can be consumed and search for an alternate fuel to meet the energy demand. For over a decade, the Government of India has been focusing on developing energy-efficient systems and supplying clean fuels for both domestic and industrial applications in the country. The Government of India has invested huge money in subsidies for fuels used in both domestic and industrial applications. In general, fuel is spent in thermal applications via combustion devices. It is important to have an energy-efficient and environment-friendly combustion device. Hence there is a need for improvement in the combustion devices used in domestic and industrial applications. Recently, PRBs are reported to be highly efficient and produce less pollutants compared to FFC based combustion devices. PRBs developed by various researchers at Indian Institute of Technology Guwahati (IIT Guwahati), India showed encouraging results. However, PRBs with lower risk of flashback while in operation have not been developed. Also, there are no parametric studies or stability studies reported on the developed PRBs. Hence in this thesis, chapter 3 is devoted to the development, performance and stability analysis of LPG based PRB (LPG-PRB) operating in a partially surface-stabilized mode of operation. In addition, there is no multi-fuel operated self-aspirated PRB reported so far, hence chapter 4 is focused on the development and performance analysis of self-aspirated Natural Gas based PRB (NG-PRB). Also, the cookstove equipped with Biogas based PRB (BG-PRB) developed by Kaushik et al. (2021) proved to be an alternative to LPG cookstoves for domestic applications. But the operation of PRB with forced air supply and pressurized biogas hindered its real-time application. Hence, chapter 5 of this thesis is devoted to the design and development of self-aspirated BG-PRB which can operate with direct biogas from a biogas digester.

1.5 Organization of the thesis

This thesis contains seven chapters and the contents presented in each chapter are discussed in this section.

Chapter 1 presents the global and Indian energy scenario along with the SDGs proposed by the UN. A glimpse of combustion devices and their types are discussed in this chapter. Also, a short introduction to Porous Medium Combustion (PMC) and its conceptual background is

presented for a better understanding of the technology. Later motivation and organization of this thesis are presented.

Chapter 2 presents a literature survey on PMC, providing a comprehensive insight into the technology. And a detailed literature survey on PRB (operating on hydrocarbon fuels) that motivated the work disclosed in chapter 3 and 4 is presented, and works carried out on PRB at IIT Guwahati is also presented. Later, a literature survey on biogas cookstoves that motivated the work disclosed in chapter 5 is presented. This chapter ends with concluding remarks on the literature survey and then presents the objectives of the present thesis.

Chapter 3 deals with the development of self-aspirated LPG-PRB operating in a partially surface-stabilized mode of operation. An analytic model for a self-aspirated LPG-PRB is presented. From the analytical model developed, it was observed that the primary air entrainment depends on various design parameters. The performance of the self-aspirated LPG-PRB is examined by varying the injector diameter in terms of thermal efficiency and CO and NO_x emissions. Also, the stability of self-aspirated LPG-PRB operating in a partially surface-stabilized mode of operation is studied to prove its feasibility for its application in real-time situations.

Chapter 4 presents the development of self-aspirated NG-PRB operating in a partially surface-stabilized mode of operation. The developed self-aspirated NG-PRB is assessed for its performance in terms of thermal efficiency and CO and NO_x emissions. Also, the developed NG-PRB is studied for its temperature distribution to understand the behavior of PRB when operated at different power inputs. Further, Techno-Economic Assessment (TEA) and Lifecycle Assessment (LCA) were performed for the developed LPG-PRB and NG-PRB and compared with LPG based Conventional Burner (LPG-CB) to prove their economic and environmental superiority.

Later in Chapter 5, the development of self-aspirated BG-PRB operating with direct biogas supply from a digester for domestic application is presented. The developed self-aspirated BG-PRB is assessed for its performance in terms of thermal efficiency and CO and NO_x emissions. Also, the thermal behavior of the developed self-aspirated BG-PRB is studied experimentally (by thermal mapping using k-type thermocouples) and numerically (using ANSYS 17.2 FLUENT software). Also, TEA and LCA were performed for the developed BG-PRB and compared with LPG-CB to prove their economic and environmental superiority.

Conclusions and future work are presented in chapter 6.

Fig. 1.11 represents a flowchart that provides insight into the overall structure of the thesis and an overview of the work reported in the thesis.

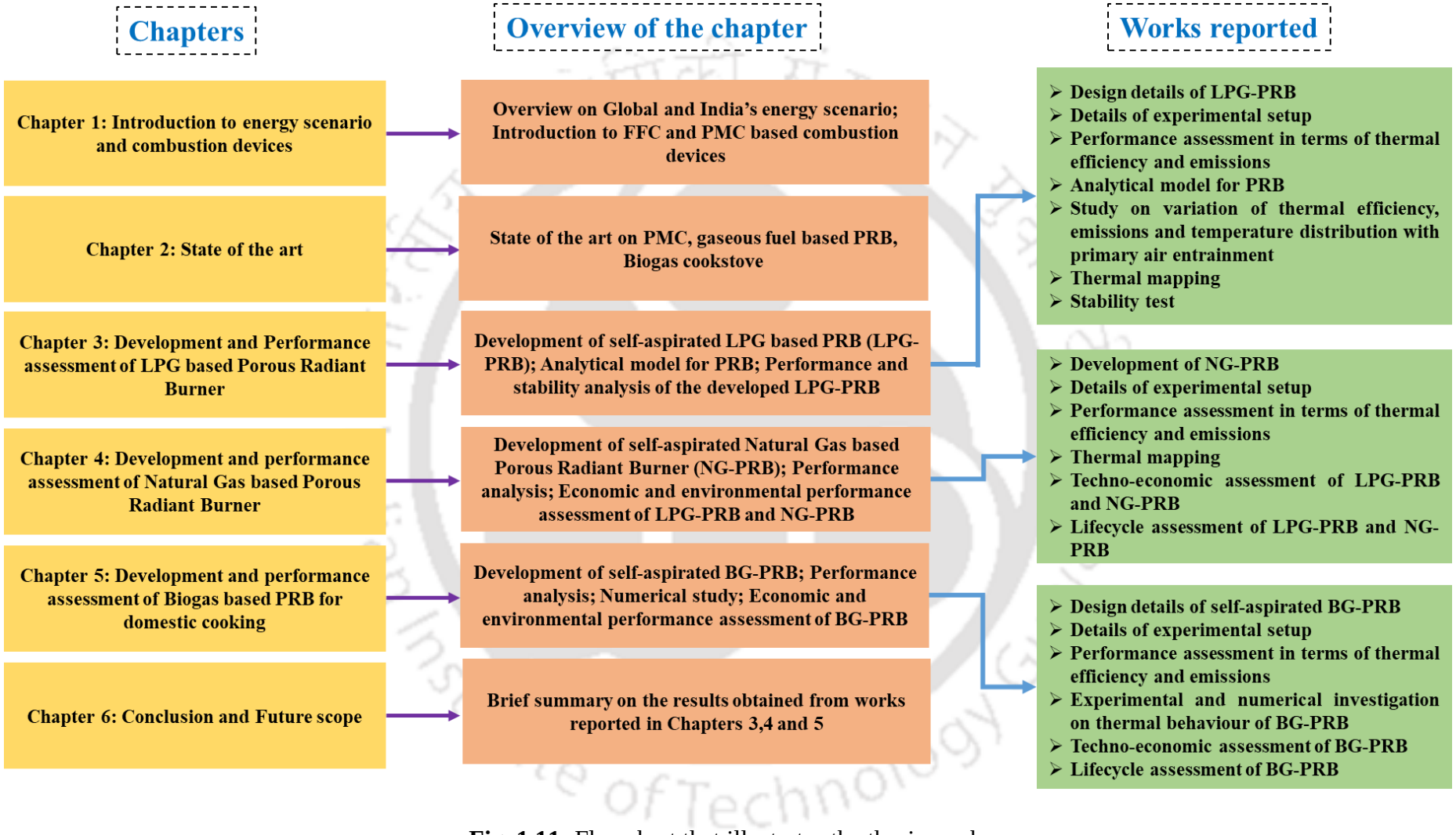

Fig. 1.11: Flowchart that illustrates the thesis work.

CHAPTER 2

STATE OF THE ART

Preface

In this chapter, literature supporting the development and performance assessment of Porous Radiant Burners (PRB) based on Porous Medium Combustion (PMC) is presented. Porous Medium Combustion (PMC) is an interesting technology that has gained importance in the last few decades. For a better understanding of the readers, this section starts with section 2.1, in which the literature related to the advent of PMC technology is discussed. Subsection 2.2 presents the literature on the development and performance assessment of gaseous fuel-based PRB. Later, subsection 2.3 presents literature related to the development and performance assessment of Biogas cookstoves. At the end of this section, various corollaries and literature gaps observed from the literature survey and the objectives of the present thesis work are presented.

2.1 Historical background of Porous Medium Combustion

In the late 18th century, Sir Humphry Davy was the first to work on Porous Medium Combustion (PMC). He revealed that combustion cannot occur in tubes below a certain radius because of the local cooling of the flame and radical termination. He defined the quenching distance, showed that the gas can be burnt below its ignition temperature without a flame and proposed the new term “flameless combustion”. Weinberg (1971) proposed the concept of excess enthalpy flames while investigating the combustion of a lean fuel-air mixture which led to the concept of recirculating the flame within the combustion system. Later, Hardesty and Weinberg (1973) analyzed the combustion systems operating based on the concept of heat recirculation in terms of flammability limits, pollutant emissions, maximum burning rate, fuel saving, etc. Fig. 2.1 (a) and 2.1 (b) show the combustion of the fuel-air mixture in the combustion system without heat recirculation and with heat recirculation, respectively.

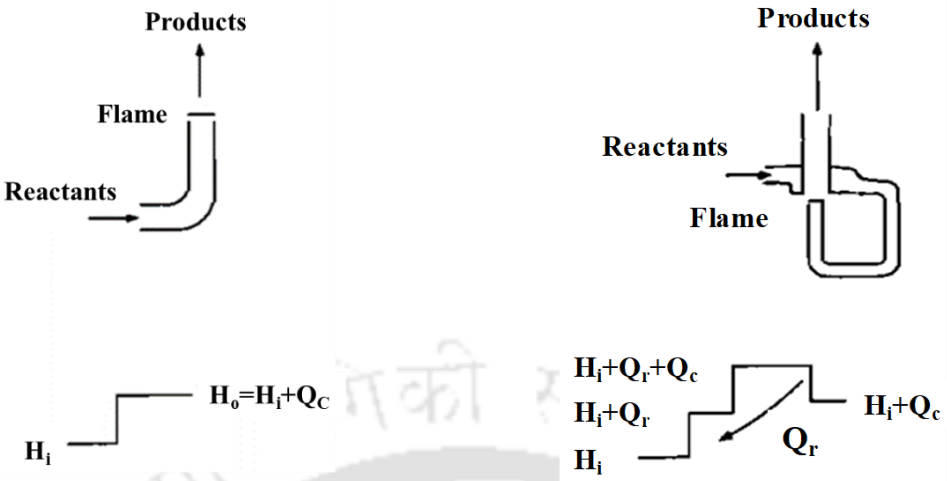

H_i - Heat input; H_o - Heat output; Q_r - Heat recirculated; Q_c - Heat of combustion

(a) **(b)**

Fig. 2.1: Principle of combustion in combustion systems (a) without heat recirculation and (b) with heat recirculation (Hardesty and Weinberg, 1973)

Takeno and Sato (1979) were the first to propose a model to generate excess enthalpy flame using a porous insert of high thermal conductivity on the fuel-air mixture path. They proved that this type of combustion system can be used to combust fuels with low energy content effectively. Deshaies and Joulin (1980) did an analytical study of the same model proposed by Takeno and Sato (1979). They confirmed the model's capability and proposed that a high temperature can be achieved within the reaction zone. Kotani and Takeno (1982) conducted an experimental study on the model proposed by Takeno and Sato (1979) to burn a fuel-air mixture with low heat content. They reported that the degree of heat recirculation, fuel flow rate and equivalence ratio are the key factors that decide the combustion system's stability. In another breakthrough, Durst et al. (1996) introduced a double-layered PRB, where the two layers of PM were used; (i) the upper layer with higher porosity such that the value of the Peclet Number (Pe) is more than 65 and supports combustion and (ii) the lower layer having low porosity where combustion is restricted and the Pe is lower than 65. They also reported three distinct behaviour of the flame in the combustion system- stable flame, flashback and blow-off. Also, researchers focused on different aspects of PMC namely flame stabilization (Babkin et al.,1991; Min and Shin, 1991; Mital et al., 1997; Dhillon, 1999), emissions (Goeckner et al., 1992; Xiong et al., 1995; Hoffman et al., 1997; Mital et al., 1997; Suzukuwa et al., 1997;

Bouma and Goey, 1999) and heat transfer characteristics (Yoshida et al., 1990; Tong et al., 1990; Hsu et al., 1993; Hackert et al., 1999).

In the early 21st century, researchers focused on developing efficient PMC based combustion devices called Porous Radiant Burners (PRB) for commercial applications like cooking, heating metals, drying food products, etc. Researchers developed and assessed the performance of different PRBs working on gaseous and liquid fuels. Researchers believed PRB could be an alternative to conventional Free Flame Combustion (FFC) based burners. As per the context of the thesis, literature supporting the development and performance assessment of gaseous fuel-based PRB are presented in the forthcoming subsections.

2.2 Development and Performance Assessment of Gaseous fuel based PRB

The development of PRB started in the late 20th century. The first PRB for the cooking application was developed by Jugjai and Sanitjai (1996). They developed a gaseous fuel based burner called Porous Radiant Recirculated Burner (PRRB) employing Porous Medium (PM) (Fig. 2.2(a)). They fabricated PRRB using PM made of stainless steel wire mesh (40 meshes/inch) placed in layers and housed inside two layers of stainless steel sheet. They observed that the efficiency of PRRB was 10% higher than the standard Conventional Burner (CB) because of the highly emissive porous medium. Later, Jugjai and Rungsimuntuchart (2002) further upgraded PRRB and developed two PRRBs, operating in conventional radial flow mode-PRRB(CB) and swirling central flow mode-PRRB(SB) (Fig. 2.2(b)). PRRB(CB) was found to have about 12% higher thermal efficiency than CB. Further improvement in thermal efficiency was found in PRRB(SB), with a maximum thermal efficiency of 60%. The CO and NO_x emissions from PRRB(SB) were found to be higher when compared to PRRB(CB) because of low aeration, which leads to incomplete combustion. Makmool et al. (2007) investigated 400 burners operating in self-aspirated mode from 13 local manufacturers in Thailand, in which they also investigated a single-layer PRB (Fig. 2.2(c)). They have not mentioned the description of the burner in their article. They reported that the maximum thermal efficiency observed in the tested PRB was about 47%. Avdic et al. (2010) developed a gas Porous Medium Burner (PMB) coupled with a heat exchanger incorporated into an electro-fossil system used for space and domestic water heating in a family house (Fig. 2.2(d)). They developed PMB to operate in forced aeration mode with a capacity of 1-8 kW. The maximum CO and NO_x emission observed from the developed PMB was 48 mg/kWh and 45 mg/kWh.

Mujeebu et al. (2011) developed porous burners employing alumina foam and alumina spheres operating in submerged (MSB) and surface combustion modes (SSB), respectively (Fig. 2.2(e)). They observed that MSB and SSB showed NO_x reduction of 76% and 75%, respectively, compared with the CB. The thermal efficiencies of CB, MSB and SSB are 47%, 59% and 71%, respectively, at a thermal load of 0.62 kW. A Self-aspirated Porous Medium Burner (SPMB) with a firing rate ranging from 23 to 61 kW was developed by Yoksenakul and Jugjai (2011) for heating applications in small and medium-sized enterprises in Thailand (Fig. 2.2(f)). They reported an output radiation efficiency of up to 23% and a comparatively high turn-down ratio of 2.65. Additionally, they stated that emissions of CO and NO_x from SPMB were below 200 parts per million (ppm) and 98 ppm, respectively, which was less when compared to CB. Ismail et al. (2013) investigated the application of a Porous Medium Burner (PMB) embedded with thermoelectric cells for domestic cooking applications shown in Fig. 2.2(g). The thermoelectric cells use the heat released during fuel combustion inside the porous medium to generate electricity. In their study, they found that for a flow rate of 0.25 L/min, the average surface temperature was 544.8 °C. They developed a 9.3 V total output voltage, which decreased to 7 V during discharge. Wu et al. (2014) developed a flat flame burner employing a porous metal medium for domestic cooking applications and compared its performance with CB (Fig. 2.2(h)). From the experimental investigation, they observed that the developed flat flame burner is superior to CB. They reported that, in contrast to CBs, flat flame burner's efficiency and pollutant emissions are not significantly affected by the distance between the load and the burner exit. Iral and amell (2015) presented a natural gas based PRB operating in the submerged mode of operation and forced aspiration (air supply) mode (Fig. 2.2(i)). They investigated PRBs with different honeycomb thicknesses (7 mm, 15 mm and 20 mm). They reported that PRB having a honeycomb of thickness 15 mm showed a maximum thermal efficiency near 50% for a heat flux of 370 kW/m^2 and a radiation efficiency of 27%. For all PRB configurations examined, the primary aeration rate ranged from 0.65 to 0.7.

Herrera et al. (2015) developed a PRB operating in forced aeration mode suitable for domestic applications, where the preheater material was uniquely chosen from alumina grinding wastes and CZ comprised of SiSiC ceramic foam (Fig. 2.2(j)). Experiments were conducted for a specific heat input rate of 98.5 kW/m^2 to 244 kW/m^2. CO emissions were lower than 25 ppm for a specific heat input rate lower than 154 kW/m^2. They reported that a critical rise in CO emissions was observed when the burner worked at a higher heat input rate due to a moderate

lift-off and quenching on the surface of the burner. Their PRB showed a thermal efficiency improvement between 7% and 14%. Pradhan and Mishra (2018) developed a self-aspirated two-layered PRB using firebrick and steel balls in combustion and preheating layer, respectively, with an operating range of 0.5-2 kW (Fig. 2.2(k)). They investigated the performance of the developed PRB and compared it with CB. They also studied the effect of burner geometry on thermal performance and emissions. They observed that the circular-shaped PRB showed slightly higher thermal efficiency than the square-shaped PRB. The circular-shaped PRB showed a maximum thermal efficiency of 71.78% at a flow rate (V) of 2.0 m/s. The CO and NO_x emissions for both circular-shaped PRB and square-shaped PRB were found to be 44-52 ppm and 12-32 ppm, and 44-54 ppm and 12-40 ppm, respectively. Corresponding values for CB were found as 125-228 ppm and 73-101 ppm. Chaelek et al. (2019) developed a self-aspirating Annular Porous Medium Burner (APMB) with Porous Radiant Recirculated Heater (PRRH) using a packed bed of alumina spheres (Fig. 2.2(l)). PRRH was integrated into the APMB to obtain an elevated air temperature. Experiments were performed for a power range of 21-44 kW, and they observed an evaluated air temperature of 136–252 °C. APMB integrated with PRRH yielded maximum temperatures more significant than the adiabatic flame temperature. APMB integrated with PRRH generated the highest thermal efficiency of 51%, and their energy consumption dropped by 28.6% compared to CB. Fig. 2.2 presents various PMC based burners developed by various researchers across the globe and a detailed description of the burners is presented in Table 2.1.

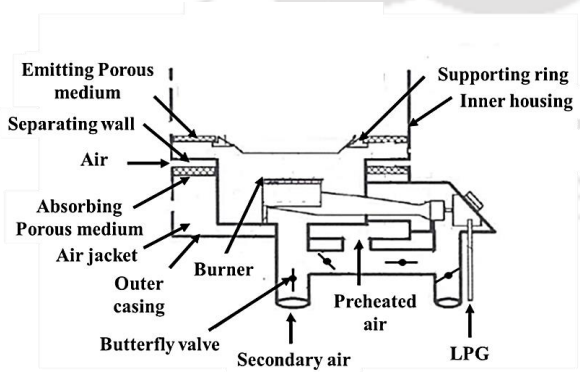

(a) PRRB developed by Jugjai and Sanitjai (1996)

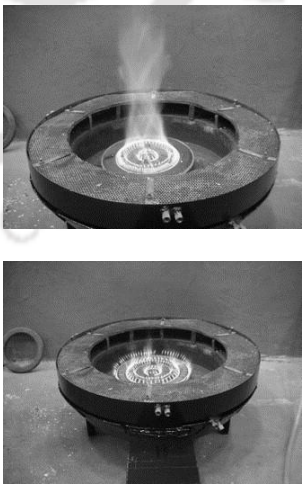

(b) PRRB(CB) and PRRB(SB) developed by Jugjai and Rungsimuntuchart (2002)

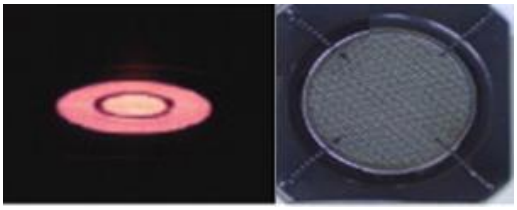

(c) Single-layer PRB investigated by Makmool et al. (2007)

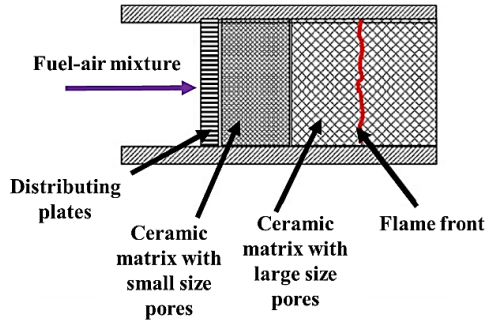

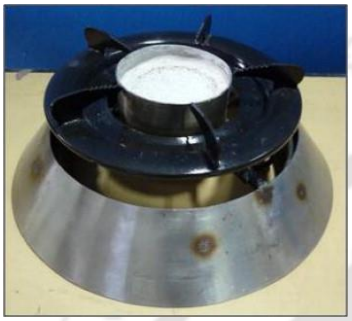

(e) Porous burner developed by Mujeebu et al. (2011)

(d) PMB developed by Avdic et al. (2010)

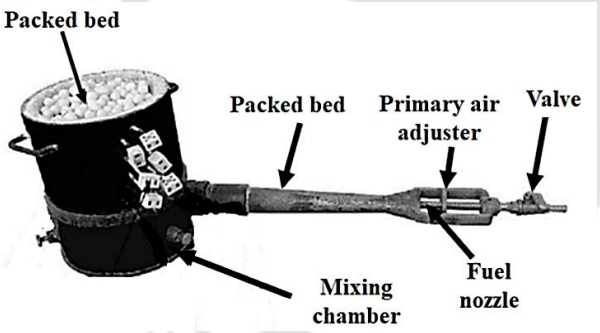

(f) SPMB developed by Yoksenakul and Jugjai (2011)

(g) PMB embedded with thermoelectric cells developed by Ismail et al. (2013)

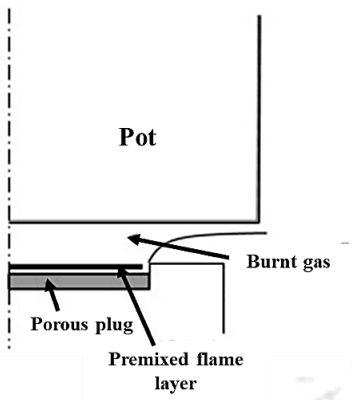

(h) Flat flame burner developed by Wu et al. (2014)

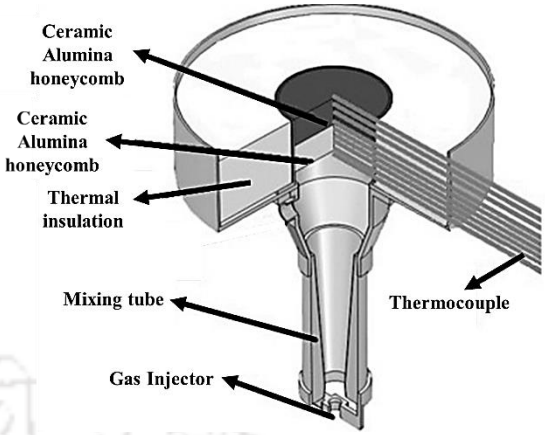

(i) Natural gas based PRB developed by Iral and amell (2015)

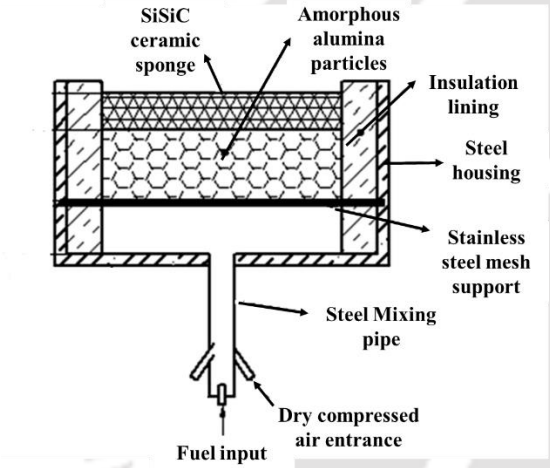

(j) PRB developed by Herrera et al. (2015)

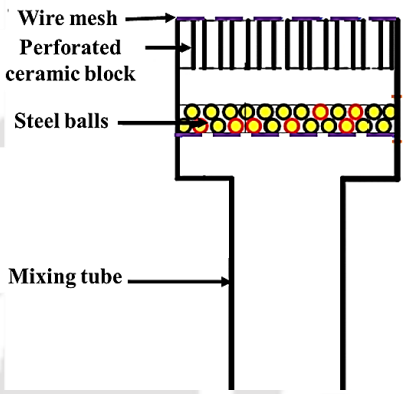

(k) Two-layered PRB developed by Pradhan and Mishra (2018)

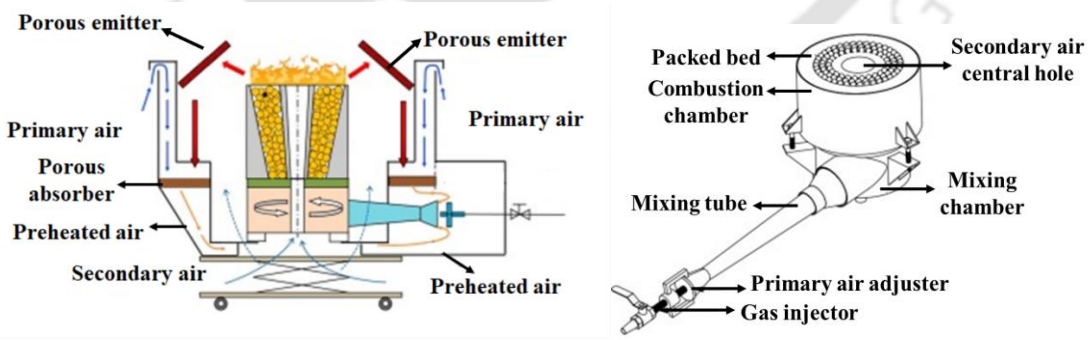

(l) APMB integrated with PRRH developed by Chaelek et al. (2019)

Fig.2.2: Different types of PMC based burners developed by various researchers

Table 2.1: Description of PMC based burners presented in Fig.2.2.

Fig. No.	Design details	Ref.
2.2 (a)	• Fuel: LPG • Inner and outer casing material: Stainless steel • Porous Medium: Stainless steel wire mesh (40 meshes/inch) placed in layers	Jugjai and Sanitjai (1996)
2.2 (b)	• Fuel: LPG PRRB(CB) • Flow type: Radial • Number of port: Inner ring-108 (54 ports (1 mm diameter); 54 ports (2.5 mm diameter)); outer ring-234 (117 ports (1 mm diameter); 117 ports (2.5 mm diameter)) • Total port area: 974 mm^2 PRRB(SB) • Flow type: Swirl • Number of port: Inner ring-108 (54 ports (1 mm diameter); 54 ports ((2.5 mm diameter)); outer ring-104 ((2.5 mm diameter)) • Total port area: 818 mm^2	Jugjai and Rungsimuntuchart (2002)
2.2 (c)	• Fuel: LPG • Type: Single-layer PRB • Porous medium: Honeycomb ceramic matrix	Makmool et al. (2007)
2.2 (d)	• Maximum power input: 8 kW • Porous Medium: Upstream layer- ZrO2 foam (Porosity-0.95); Downstram layer- Al_2O_3 fiber wavy lamellae structure (8 mm height, 20 mm length) • Air supply: Forced aeration	Avdic et al. (2010)
2.2 (e)	• Fuel: LPG • Power input: 0.62 kW • Surface Stabilized Burner (SSB): Preheating Layer- Alumina (Al_2O_3) foams (26 ppcm, 12.7 mm thick, porosity 86%); Combustion layer- Al_2O_3 foams (8 ppcm, 12.7 mm thick, porosity 84%) • Matrix Stabilized Burner (MSB): Preheating Layer- Porcelain form (18 ppcm and 15 mm thickness); Combustion layer- Al_2O_3 spheres of (30 mm diameter) • Body material: Stainless steel body (3 mm thickness)	Mujeebu et al. (2011)
2.2 (f)	• Fuel: LPG • Porous medium: Al_2O_3 spheres (15 mm diameter) • Injector diameter: 1.6 mm • Casing: High-temperature cement	Yoksenakul and Jugjai (2011)
2.2 (g)	• Fuel: Butane • Casing: Stainless steel (3 mm thickness) • Porous medium: Preheating Layer- Al_2O_3 foam (24 ppcm, 4.2 mm pore diameter); Combustion layer-	Ismail et al. (2013)

	Al_2O_3 foam (8 ppcm, 12.5 mm pore diameter) • Number of Thermoelectric cells: 6 (30 mm width, 30 mm length and 3.7 mm height, Each)	
2.2 (h)	• Fuel: LPG • Power input: 1 kW, • Porous medium: Bronze pellet with a diameter of 0.5 mm which forms a plug (50.8 mm diameter; 3 mm thickness) having a porosity of 0.237	Wu et al. (2014)
2.2 (i)	• Fuel: Natural gas • Porous Medium: Preheating layer- Al_2O_3 honeycomb (400 ppi, 64 mm diameter and 15 mm thickness); Combustion layer- SiC foam (90% porosity, 64 mm diameter and 20 mm thickness) • Injector diameter: 0.71 mm	Iral and amell (2015)
2.2 (j)	• Fue: LPG • LPG supply pressure: 0.023 bar • Air pressure: Dry air at 0.7 bar • Combustion rate: 98.5 – 244 kW/m2 • Porous medium: Preheating layer- A bed of amorphous Al_2O_3 particles (11 mm diameter) resulting from grinding wastes (85 mm in height); Combustion layer- SiSiC ceramic foam disks (20 ppi, 15 mm height and 160 mm diameter) • Casing: Steel housing	Herrera et al. (2015)
2.2 (k)	• Fuel: LPG • Shape: Circular • Casing: Mild steel (3 mm thickness) • Porous Medium: Preheating layer- Steel balls (5-3 mm diameter); Combustion layer- Firebrick material (20 mm thickness)	Pradhan and Mishra (2018)
2.2 (l)	• Fuel: LPG • Porous Medium: packed bed of alumina spheres with a diameter of 10 mm • Casing: Steel (3 mm thickness) • Mixing tube length: 323 mm • Throat diameter: 22 mm. • Injector diameter: 1.2 mm	Chaelek et al. (2019)

A group of researchers from Indian Institute of Technology Guwahati (IIT Guwahati), India developed various PRBs (Pantangi et al., 2007, 2011; Muthukumar and Shyamkumar, 2013; Mishra et al., 2015, 2018; Devi et al. 2020a; Sunita et al., 2021) for domestic and commercial applications. Pantangi et al. (2007) carried out earlier works at IIT Guwahati. They developed double-layered porous burners employing porous medium (Metal balls, pebbles and metal chips) for domestic cooking applications (Fig. 2.3(a)). They observed a maximum thermal efficiency of 73% in the porous burner with pebbles as the preheating layer and metal chips as

the combustion layer. Later, Pantangi et al. (2011) improved the burner design by employing ceramic materials. They developed a two-layered PRB consisting of SiC foam and alumina balls as shown in Fig. 2.3 (b). Experiments were performed to investigate the thermal efficiency and emissions of PRB of different diameters for different equivalence ratios and power inputs. They carried out the Water Boiling Test (WBT) following Indian Standard (IS) 4246:2002, prescribed by the Bureau of Indian Standards. They reported a maximum thermal efficiency of 68% in 80 mm diameter PRB, which was 3% higher than CB. The CO and NO_x emissions from the tested PRBs were in the range of 25-350 mg/m^3 and 12-25 mg/m^3, which are much lower than the corresponding values of CB (CO: 400-1050 mg/m^3 and NO_x: 162-216 mg/m^3) used for domestic cooking applications.

Muthukumar et al. (2011) further investigated the PRB proposed by Pantangi et al. (2011). They found that the thermal efficiency increased to 71% at a power input of 1.24 kW and an equivalence ratio of 0.68. Muthukumar and Shyamkumar (2013) modified the PRB developed by Pantangi et al. (2011) by replacing the alumina balls with a ceramic matrix, as shown in Fig. 2.3 (c). The developed PRB with SiC foam as the combustion layer and ceramic matrix as the preheating layer. They performed experiments with PRBs having SiC foam of different porosities viz. 80%, 85% and 90% for a power input range of 1.3-1.7 kW. PRB having SiC foam of 90% porosity, showed a maximum thermal efficiency of 75% at a power input of 1.3 kW and an equivalence ratio of 0.54. Later, The PRB developed by Muthukumar and Shyamkumar (2013) was scaled up to a power capacity range of 5–10 kW by Mishra et al. (2013). They used SiC foam of 90% porosity and ceramic block of 40% porosity in the combustion and preheating layer, respectively (Fig. 2.3 (d)). They compared the performance of the developed PRB with commercially available burners. They reported a maximum thermal efficiency of 50% at a power input of 5 kW and an improvement of 34.3% in thermal efficiency at a power input of 10 kW. Further, the same PRB was investigated by Mishra et al. (2015a) for its thermal performance in terms of thermal efficiency, emissions and temperature distribution at different power inputs and equivalence ratios. They reported that the developed PRB showed a maximum thermal efficiency of 58% at a power input of 5 kW and an equivalence ratio of 0.56. Mishra (2015b) developed a self-aspirated PRB operating in a submerged mode of operation using a mixing pipe with four feeder pipes for fuel-air inlet (Fig. 2.3(e)). The author reported a maximum thermal efficiency of 55%. Panigrahy and Mishra (2016a) numerically analyzed the combustion of Liquefied Petroleum Gas (LPG) and methane

in PRB. They found that the radiative heat flux from the combustion of LPG in PRB was higher compared to that of methane. Additionally, they reported that the lowest equivalence ratios for the combustion of LPG and methane were 0.399 and 0.43, respectively. Later Panigrahy et al. (2016b) experimentally and numerically investigated the combustion of LPG in PRB with SiC foam and alumina balls as the combustion and preheating layer, respectively. They also investigated the impact of varying the thickness of SiC foam. They reported that PRB with SiC foam of 15 mm thickness showed a maximum thermal efficiency of ~71% and CO emissions were below the standard limits permitted by the World Health Organisation (WHO).

Mishra and Muthukumar (2018) developed a self-aspirated two-layered PRB consisting of SiC foam and alumina ceramic block for domestic cooking applications (Fig. 2.3(f)). They performed WBT following the standards prescribed by IS 4246:2002 for a power range of 1-3 kW. They achieved a maximum thermal efficiency of 75.1% at 1 kW in PRB with a port diameter of 21 mm and an orifice diameter of 0.35 mm. The corresponding CO and NO_x emissions were in the range of 30-140 ppm and 0.2-3.2 ppm, respectively. Later, Devi et al. (2020a) developed biogas based Sideway Faced Porous Radiant Burner (SFPRB) using SiC foam and alumina porous structure (Fig. 2.3(g)). The developed SFPRB was stable within an equivalence ratio range of 0.75-0.97 for a power input range of 5-10 kW. They reported a maximum radiation efficiency of 33% at a power input of 5 kW and an equivalence ratio of 0.97. Sunita and Muthukumar (2021) developed an LPG-based cluster PRB (CPRB) operating in forced aeration mode, as shown in Fig. 2.3(h). They performed experiments with CPRBs of different configurations and compared their performance with commercially available CBs. They reported that CPRB having an individual burner diameter of 80 mm, showed a maximum thermal efficiency improvement of 27% and maximum CO and NO_x emission reduction of 85.3% and 83.3%, respectively. Later, Sunita et al. (2021) experimentally and numerically investigated the thermal performance of the same CPRB. They reported that the developed CPRB was found to operate under the stable submerged combustion mode for the power input range of 8–20 kW. Fig. 2.3 presents various PMC based burners developed in IIT Guwahati and a detailed description of the burners is presented in Table 2.2.

(a) Porous burners with metal balls and metal chips developed by Pantangi et al. (2007)

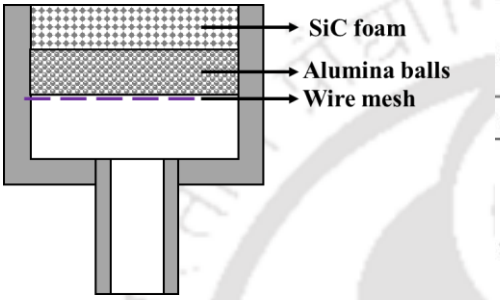

(b) Double-layered PRB developed by Pantangi et al. (2011)

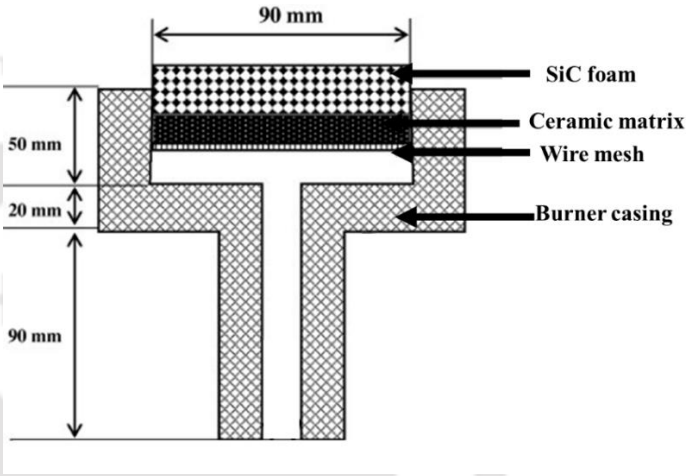

(c) PRB developed by Muthukumar and Shyamkumar (2013)

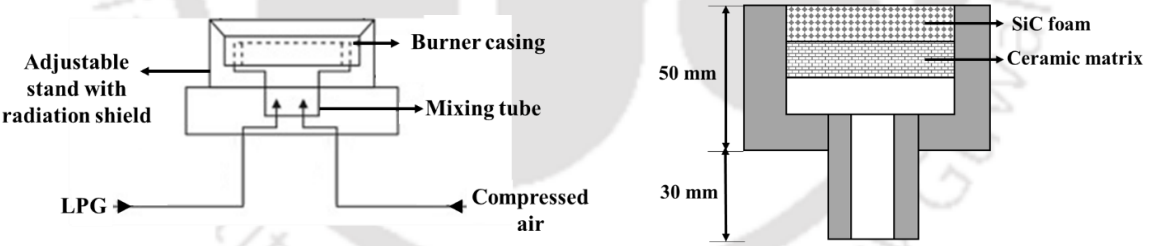

(d) Medium-scale PRB developed by Mishra et al. (2013)

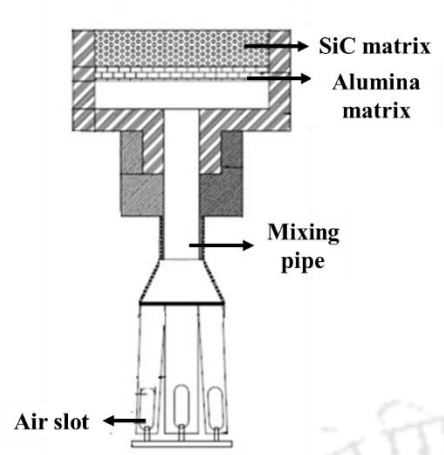

(e) Self-aspirated PRB developed by Mishra et al. (2015b)

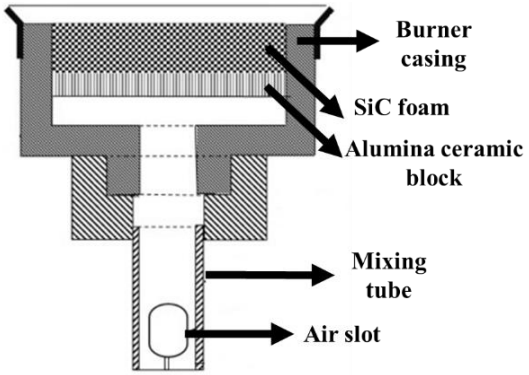

(f) Self-aspirated PRB developed by Mishra and Muthukumar (2018) for domestic applications

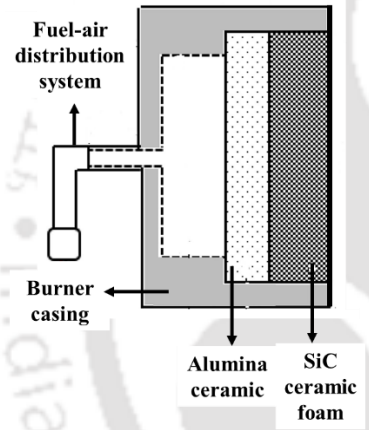

(g) Biogas based SFPRB developed by Devi et al. (2020a)

(h) CPRB developed by Deb and Muthukumar (2021)

Fig. 2.3: PMC based combustion devices developed in IIT Guwahati

Table 2.2: Description of PMC based burners presented in Fig.2.3.

Fig. No.	Design details	Ref.
2.2 (a)	• Fuel: LPG Porous burner with metal balls • Porous medium: Preheating Layer- Metal balls (3 mm diameter); Combustion layer- Metal balls (8 mm diameter) Porous burner with metal balls-metal chips • Porous medium: Preheating Layer- Metal balls (3-4 mm diameter); Combustion layer- Metal chips (8 mm diameter) • Air supply: Self-aspiration	Pantangi et al. (2007)
2.2 (b)	• Fuel: LPG • Porous medium: Preheating Layer- Al_2O_3 balls (5 mm	Pantangi et al. (2011)

	diameter); Combustion layer- SiC porous matrix (90% porosity, 80 mm diameter and 15-20 mm thickness) • Air supply: Forced aeration	
2.2 (c)	• Fuel: LPG • Porous medium: Preheating Layer- Al_2O_3 matrix (40% porosity, 90 mm diameter and 10 mm thickness); Combustion layer- SiC (90% porosity, 90 mm diameter and 20 mm thickness) • Air supply: Forced aeration	Muthukumar and Shyamkumar (2013)
2.2 (d)	• Fuel: LPG • Porous medium: Preheating Layer- Al_2O_3 porous matrix (40% porosity and 120 mm diameter); Combustion layer- SiC (90% porosity and 120 mm diameter) • Air supply: Forced aeration	Mishra et al. (2013)
2.2 (e)	• Fuel: LPG • Porous medium: Preheating Layer- Al_2O_3 matrix (1.5 mm pore size, 120 mm diameter and 10 mm thickness); Combustion layer- SiC matrix (120 mm diameter and 25 mm thickness) • Air supply: Self-aspiration • Number of feeder pipes: 4 • Port diameter: 21 mm • Injector diameter: 0.25 mm	Mishra et al. (2015b)
2.2 (f)	• Fuel: LPG • Porous medium: Preheating Layer- Al_2O_3 porous matrix (7% porosity, 80 mm diameter and 10 mm thickness); Combustion layer- SiC (90% porosity, 80 mm diameter and 20 mm thickness) • Air supply: Self-aspiration • Injector diameter: 0.35 mm	Mishra and Muthukumar (2018)
2.2 (g)	• Fuel: Biogas • Casing: High-temperature resistant cement • Porous medium: Preheating Layer- Al_2O_3 Ceramic (7% porosity, 120 mm diameter and 15 mm thickness); Combustion layer- SiC ceramic foam (90% porosity, 120 mm diameter and 20 mm thickness) • Air supply: Forced aeration	Devi et al. (2020a)
2.2 (h)	• Fuel: LPG • Power input: 12.6 kW, • Porous medium: Preheating Layer- Al_2O_3 porous matrix (7% porosity, 80 mm diameter and 10 mm thickness); Combustion layer- SiC foam (90% porosity, 80 mm diameter and 20 mm thickness) • Number of PRB: 3 • Casing: Refractory cement • Casing wall thickness: 10 mm	Deb and Muthukumar (2021)

- Air supply: Forced aeration

2.3 Development and performance assessment of Biogas Cookstoves

Biogas based cookstove technology has been widely implemented in several countries such as India (Ministry of New & Renewable Energy, 2022), China (Giwa et al., 2020), Bangladesh (Bangladesh National Biogas Program Monitoring Services, 2022), and Pakistan (Yasmin and Grundmann, 2019) with subsidization of biogas plants. These cookstoves are similar to the traditional LPG-based cookstoves working on FFC or PMC. A biogas cookstove usually has a single or double-layer burner with varying power input (Domestic burners: 1.2 to 5.5 kW, Commercial burners: 5.5 to 17 kW) (Fulford, 1996). The burner itself has several parts viz., Jet (Injector orifice), air intake holes, mixing tube (diffuser), flame port, baffle, burner manifold, frame and brackets welded on the top of it. There are two types of FFC based biogas cookstove designs: one is a modified design of the existing LPG cookstoves and the other is an original design based on the properties of biogas (Sasse et al., 1991). In the early 90s, Chandra et al. (1991a) presented a hydrodynamical model of a biogas cookstove with analytical expressions for the design parameters of a biogas burner. With the help of the analytical expressions, for a given biogas pressure and pressure drop across the nozzle orifice, the design parameters of a biogas burner such as orifice, interspace between orifice and the mixing tube for aspiration of primary air, burner head area, and port number could easily be selected. Chandra et al. (1991b) tested the biogas cookstoves of 14 brands available in the Indian market. Efficiencies of these cookstoves varied between 32 to 49% and 37 to 54% for the tests carried out under unsteady-state and steady-state conditions, respectively. Further, they studied the effects of the input pressure, pan size, and pan position over the burner. The results showed that for optimal utilization of the heat available from the cookstove, optimization of all the three above-mentioned parameters is very essential. Fulford (1996) presented a detailed design equation for biogas cookstoves consistent with the scientific and technical criteria for low-pressure burners. They also presented a typical design calculation for a DCS cookstove to supply about 1.5 kW for cooking. Smith et al. (2000) studied the domestic biogas cookstoves (operating at ~1.4 kW) available in India and estimated the nominal combustion efficiency, heat transfer efficiency, and overall energy efficiency as 99.5%, 57.7%, and 57.4%, respectively. The Center for Energy Studies, Nepal, reported an efficiency of ~49.5% for biogas cookstoves in Nepal and it was

~45% for India (A study report on efficiency measurement of biogas, kerosene and LPG stoves, 2001).

Analogous designs of domestic cookstoves can be found in the literature (Kandpal et al., 1995; Itodo et al., 2007; Kurchania et al., 2010; Kurchania et al., 2011; Syamsuri et al., 2015; Mulugeta et al., 2017; Decker et al., 2018; Petro et al., 2020; Awulu et al., 2020). Kandpal et al. (1995) investigated the indoor air pollutants during biogas combustion in the KVIC model biogas based cookstove. They reported that the Suspended Particulate Matter (SPM) and concentration of benzo[a]pyrene in the kitchen breathing level were within 250 µg/m^3 and 0.044 µg/m^3, respectively. Itodo et al. (2007) designed a biogas based cookstove operating with biogas from a 3 m^3 continuous flow Indian-type biogas plant. They performed experiments to test the performance of the cookstove by boiling water (1 L) and cooking 146.6 g of rice and 123.3 g of beans. They found that the cooking rate was 0.14 L/min,5.13 g/min and 2.55 g/min, respectively for all three mentioned quantities and biogas consumption rate was 0.69 m^3/min, 2.87 m^3/min, and 4.87 m^3/min, respectively. The efficiency of the cookstove for boiling water and cooking rice and beans was 20%, 56%, and 53%, respectively. A report by Netherlands Development Organization (SNV) pointed out the problems associated with the poor design of Asian and African biogas cookstoves (Khandelwal and Gupta, 2009). Using three different test standards viz. Chengdu Energy Environment International Cooperation (CEEIC), China, Department of Renewable Energy Sources (DRES), India, and Kiwa Gastec Certification (GASTEC), Apeldoorn, performance was assessed. Later, Kurchania et al. (2010) developed a community-scale biogas cookstove using the design principles proposed by Fulford (1996). They reported that the developed biogas cookstove yielded a cooking efficiency of 44% for fuel consumption of 1 m^3/h. Kurchania et al. (2011) developed a biogas based cookstove with a fuel consumption of 0.375 m^3/h. They reported that the developed biogas based cookstoves showed a thermal efficiency of ~60 % and CO_2 emission of ~150–180 ppm. A burner for injera baking application with an operating power of 5.7 kW and biogas consumption of 0.93 m^3/h was developed by Kebede and Kiflu (2014). They reported that the thermal efficiency of the burner was only 25%.

Obada et al. (2014) designed a biogas based burner for residential cooking. They reported that the thermal efficiency recorded by WBT was 21% at a fuel consumption rate of 0.47 m^3/h, while the thermal efficiency recorded by cooking rice was 60% at 2.87 m^3/h. Tumwesige et al. (2014) studied various biogas stoves available in the market of Sub-Saharan Africa and the

average thermal efficiency of the tested stoves (KEJS, Reo, Tusk, Bremen, Ideal, Psem, Double, Psem L) ranged between 19.8 and 25.7% with input power in the range of 5.1-13 kW. Syamsuri et al. (2015) studied the impact of burner shape (regular and cyclone) on the thermal efficiency of the burner. Two cyclone-shaped burners (Cyclone-1 and Cyclone-2) were used for the experiments and compared with the baseline standard burner. The cyclone-2 model produced a maximum thermal efficiency of 58.4% at 1.53 kW. Decker et al. (2018) found a higher thermal efficiency of 56.8% (at 1.1 kW) with the optimized design (4 mm diameter circular ports) of the biogas stove; the CO and total HC emissions were 1.103 g/MJ and 0.071 g, respectively. Petro et al. (2020) achieved a thermal efficiency of 67% (obtained in the simmering phase at a consumption rate of 8.18 g/min), which was higher than the efficiency of the locally available burners. The specific fuel consumption (for boiling 1 litre of water) of the developed burner was 736 g/L, whereas the same was 920 g/L for CARMARTEC and 833 g/L for Simgas. Awulu et al. (2020) measured the meantime for boiling water, cooking rice, yam and beans and obtained 5 min, 34.33 min, 34.66 min, and 49.33 min with biogas consumption of 0.474 m^3, 3.254 m^3, 3.285 m^3, and 4.778 m^3, respectively. And the corresponding efficiency values were 42%, 63%, 61% and 30%, respectively. By using the PMC principle, Kaushik et al. (2021) developed a domestic double-layer PRB cookstove for biogas following the design of Mishra et al. (2015) meant for LPG. They estimated the thermal efficiency of developed PRB (using IS 8749: 2002) to be in the range of 51–62% for a biogas flow rate of 177-530 L/h, and its maximum was observed at 0.75 equivalence ratio and 0.177 m^3/h flow rate of biogas. The CO and NO_x emissions were 29–80 ppm and less than 4 ppm, respectively.

The various biogas cookstove designs are illustrated in Fig. 2.4, and their basic design specifications are listed in Table 2.3.

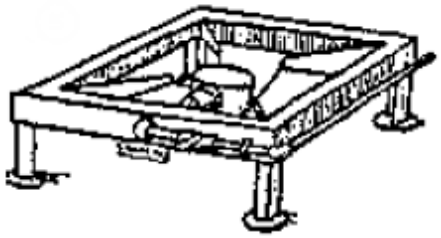

(a) Biogas cookstove developed by CAMARTEC (Sasse et al., 1991)

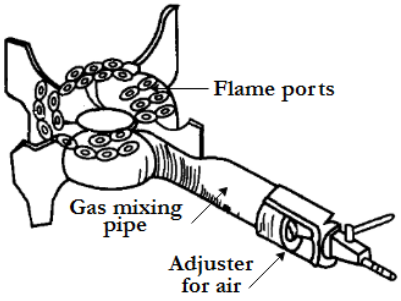

(b) Biogas stove-KVIC model (Kandpal et al., 1995)

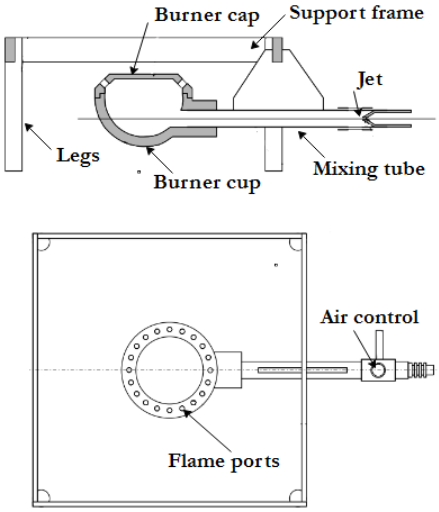

(c) DCS burner used in Nepal (Fulford, 1996)

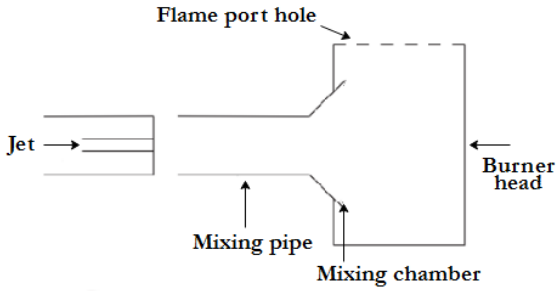

(d) Biogas stove designed by Itodo et al. (2007)

(e) Biogas stove for baking developed by Kurchania et al. (2010)

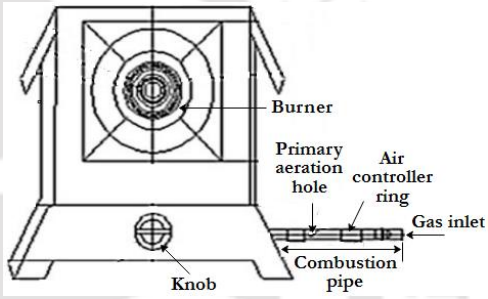

(f) Domestic biogas stove developed by Kurchania et al. (2011)

(g) 1.) Regular-shaped burner, 2.) Cyclone 1-shaped burner, 3.) Cyclone 2-shaped burner (Syamsuri et al., 2015)

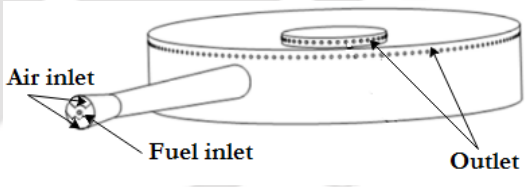

(h) Biogas Injera baking burner (Mulugeta et al., 2017)

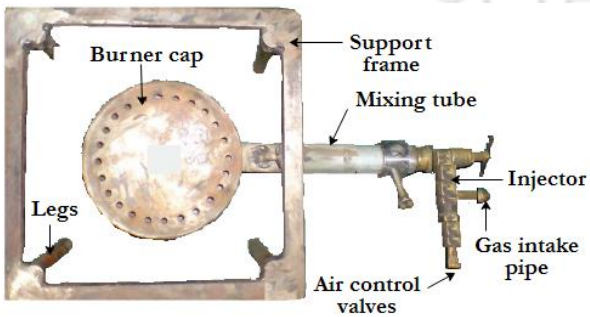

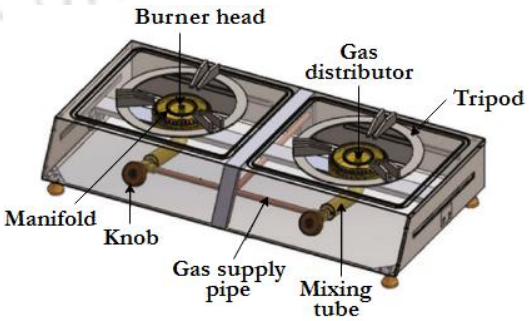

(i) Biogas burner (Stove) developed by Awulu et al. (2020)

(j) Biogas burner developed by Petro et al. (2020)

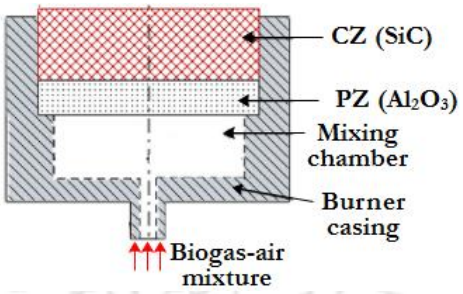

(k) Biogas operated porous radiant burner developed by Kaushik et al. (2021)

Fig. 2.4: Biogas cookstoves.

Table 2.3: Design features of biogas cookstoves.

Fig. No.	Design details	Ref.
2.4 (a)	• Materials: High-quality steel or cast iron • Air-intake holes of the mixing pipe: Two drillings of 8 mm diameter	Sasse et al. (1991)
2.4 (b)	• KVIC model	Kandpal et al. (1995)
2.4 (c)	• Biogas supply pressure: 0.01bar • Biogas flow rate: 0.471 m^3/h • Injector size: 2.1 mm • Port hole: 20 holes of 5 mm diameter (total burner port area = 390 mm^2) • Materials: cast iron, aluminium, mild steel, ceramics	Fulford (1996)
2.4 (d)	• Jet diameter: (d_o) 16 mm • Diameter of mixing pipe: (d) 97 mm • Length of air intake hole (Max., Min.): (L_{max}, L_{min}) 679, 131 mm • Diameter of mixing chamber: (D) 126 mm • Length of mixing chamber: (L) 146 mm • Number of ports: (n) 35 • Diameter of flame port: (d_H) 2.5 mm	Itodo et al. (2007)
2.4 (e)	• Length of gas and air mixing tube: 960 mm • Inner diameter of tube: 19 mm • Number of air holes for primary aeration: 16 • Diameter of air holes for primary aeration: 18 mm • Number of perforated tubes for burner: 2 • Number of ports: 56	Kurchania et al. (2010)

	• Diameter of each port: 2.5 mm • Distance between pan and burner: 35 mm • Orifice diameter: 3 mm	
2.4 (f)	• Length of the gas and air mixing tube: 850 mm • Inner diameter of tube: 14 mm • Number of air holes for primary aeration: 4 • Diameter of air holes for primary aeration: 4 mm • Number of ports: 49 • Diameter of each port: 2 mm • Distance between pan and burner: 35 mm • Orifice diameter: 2 mm • Crown diameter: 80 mm	Kurchania et al. (2011)
2.4 (g)	• Biogas burner head (1.) Regular shaped, (2.) Cyclone-1 shaped (3.) Cyclone-2 shaped	Syamsuri et al. (2015)
2.4 (h)	• Material: Sheet metal (2 mm thickness) • Jet diameter: 2.3 mm • Primary air inlet: No of holes- 2, Area of holes- 96 mm^2 • Gas air mixing tube: Length 158 mm, Throat dia. 15.63 mm • Port: No. of port- 180, Dia. of port- 2 mm • Manifold: Cylindrical shape, 260 mm external dia.	Mulugeta et al. (2017)
2.4 (i)	• Estimated gas flow rate: 5.69 m^3/h • Jet diameter: 11 mm • Diameter of mixing pipe: 66 mm • Maximum length of air intake hole: 462 mm • Minimum length of air intake hole: 89.1mm • Diameter of mixing chamber: 86 mm • Length of mixing chamber: 99 mm • Number of holes: 24 • Diameter of flame port hole: 2.5 mm	Awulu et al. (2020)
2.4 (j)	• Injector diameter: 2.5 mm • Internal throat diameter: 18 mm • Number of burner ports: 71 • Mixing tube length: 170 mm • Internal manifold diameter: 100 mm • Flame port diameter: 2.5 mm • Air inlet diameter: 5.0 mm	Petro et al. (2020)

2.4 (k)	• Porous medium: PZ (Al_2O_3 ceramic) - 90 mm diameter thickness 20 mm and porosity 31%; CZ (SiC foam) - diameter 90 mm and thickness 20 mm and porosity 90%). • Body Materials: Casing: high-temperature–resistant castable cement • Biogas supply pressure: 1.2 bar	Kaushik et al. (2021)

Table 2.4 summarizes the performances of various biogas cookstoves presented in the literature, from which one can easily observe a considerable discrepancy between measured performances. This implies that certain standardized tests are required to estimate the performances of these cookstoves.

Table 2.4. Summary of literature on the performance tests of biogas cookstove carried out in the laboratory

<table>
<tr><th>S. No.</th><th>Thermal and Emission Performances</th><th>Ref.</th></tr>
<tr><td>1.</td><td>Thermal efficiency: 55%</td><td>Sasse et al. (1991)</td></tr>
<tr><td>2.</td><td>Thermal efficiency: 32 to 49% (unsteady state), 37 to 54% (steady state)</td><td>Chandra et al. (1991)</td></tr>
<tr><td>3.</td><td>Thermal efficiency: 67% (Biogas consumption rate: 8.18 g/min)</td><td>Petro et al. (2020)</td></tr>
<tr><td>4.</td><td><table><tr><th>Activities performed</th><th>Efficiency (%)</th><th>Biogas Consumption rate (m^3/min)</th></tr><tr><td>Boiling water (1 L)</td><td>20%</td><td>0.69</td></tr><tr><td>Cooking rice (146.6 g)</td><td>56%</td><td>4.87</td></tr><tr><td>Cooking beans (123.3 g)</td><td>53%</td><td>4.87</td></tr></table></td><td>Itodo et al. (2007)</td></tr>
<tr><td>5.</td><td>Cooking efficiency: 43.96% (Biogas consumption rate: 1 m^3/h)</td><td>Kurchania et al. (2010)</td></tr>
<tr><td>6.</td><td>Thermal efficiency: ~60 % (Biogas consumption rate: 375 L/h)
Emissions: CO – ~150–180 ppm</td><td>Kurchania et al. (2011)</td></tr>
<tr><td>7.</td><td>Thermal efficiency: 56.8%
Emissions: CO – 1.103 g/MJ
Total HC – 0.071 g</td><td>Decker et al. (2018)</td></tr>
<tr><td>8.</td><td>Thermal efficiency: 51–62% (Biogas flow rate: 177-530 L/h)
Emissions: CO – 29–80 ppm
NO_x – < 4 ppm</td><td>Kaushik et al. (2021)</td></tr>
</table>

	Country	Gas consumption (L/h), Thermal efficiency (%) and CO emission (ppm)	CEEIC	DRES	GASTEC	
9.	Bangladesh	L/h	474.5	211	500	Khandelwal and Gupta (2009)
		%	57	64.5	52.1	
		ppm	>1180	5300	2800	
	Cambodia	L/h	762	489	808	
		%	55	48.1	45.6	
		ppm	>1180	2200	1700	
	Ethiopia	L/h	252.5	537	633	
		%	53	40.5	41.2	
		ppm	>1180	4350	4463	
	India	L/h	597	400	261	
		%	57	54.5	89.9	
		ppm	>1180	2840	85	
	Lesotho	L/h	270.5	217	354	
		%	41	45.1	45	
		ppm	28	4350	8	
	Nepal	L/h	565.5	453	536	
		%	55	42.1	42.2	
		ppm	>1180	4350	2140	
	Rwanda	L/h	340	285	336	
		%	60	53.8	54.6	
		ppm	>1180	2250	2200	
	Vietnam	L/h	758	620	1039	
		%	39	21.2	31.5	
		ppm	>1180	4350	1100	

2.4 Corollaries derived from literature

Important corollaries derived from the literature review on Gaseous fuel-based PRB:

i. Heat recirculation within the PM is an essential fact behind the improved performance of PRBs
ii. Gaseous fuel based PRBs show improved performance compared to their conventional counterparts, making them viable for application in the cooking sector
iii. The emissions from PRB are comparatively less when compared to their conventional counterparts, which proves its environmental superiority
iv. PRB is suitable for all gaseous fuels irrespective of their calorific values
v. Ceramic materials are the best-suited material for the construction of PRB
vi. The porosity of the combustion layer should be higher when compared to that of the preheating layer

But no PRB has been developed for real-time application, which is safe for operation without any flashback. Also, no literature on the analytical model is available to determine the primary air entrainment in PRB. Further, there is no work reported on the field trial of PRB for cooking applications.

Important corollaries derived from the literature review on Biogas cookstoves:

i. The performance of Biogas cookstoves depends on their geometrical aspects
ii. The construction of Biogas cookstoves is similar to that of a commercial LPG cookstove
iii. Less aeration is needed for biogas cookstoves because of the CO_2 content in the biogas
iv. Kaushik et al. (2021) proved that Biogas based PRB showed improved performance when compared to conventional biogas cookstoves.

From the literature, it is observed that there is no biogas cookstove with PRB developed for real-time application that can operate in self-aspirated mode and with direct biogas from a biogas digester. Also, no literature on the numerical modeling of biogas cookstoves is available.

2.5 Objectives of the thesis

From the corollaries derived from the literature, the following are the core objectives of the thesis:

- To develop an LPG-PRB suitable for real-time cooking applications, using the PRB model proposed by Mishra (2015b) as a reference. The detailed sub-objectives are as follows;
  - To experimentally assess the performance of LPG-PRB in terms of thermal efficiency and CO and NOx emissions
  - To develop an analytical model for predicting the primary air entrainment in PRB
  - To study the primary air entrainment and thermal behavior in LPG-PRB
  - To check the stability of the developed LPG-PRB
- To develop and test a Natural Gas based PRB (NG-PRB)

  - To assess the performance of NG-PRB in terms of thermal efficiency and emissions
- To develop a cookstove with Biogas based PRB (BG-PRB) operating in self-aspirated mode and with direct biogas supply from a biogas digester
  - To assess the performance of BG-PRB in terms of thermal efficiency and emissions
  - To perform numerical simulations and compare the results with the experimental results
- To assess the economic benefits of the developed LPG-PRB, NG-PRB and BG-PRB by performing Techno-Economic Assessment (TEA)
- To assess the economic benefits of the developed LPG-PRB, NG-PRB and BG-PRB by performing Lifecycle Assessment (LCA)

CHAPTER 3

DEVELOPMENT AND PERFORMANCE ASSESSMENT OF LPG BASED POROUS RADIANT BURNER

Preface

Chapter 3 presents a Liquefied Petroleum Gas (LPG) based Porous Radiant Burner (LPG-PRB) operating in a partially surface-stabilized mode of operation, i.e., with blue flame above the burner surface of LPG-PRB as an improvement over the PRB developed by Mishra (2015b). The specifications of LPG-PRB developed by Mishra (2015b) are presented in section 3.1. The developed LPG-PRB operates in a self-aspirated mode without the aid of an air supply unit and its specifications are presented in section 3.2. Sections 3.3 and 3.4 presents the experimental methodology and results obtained from the experiments. Also, an analytical model was developed to determine the factors affecting primary air entrainment in the developed LPG-PRB (section 3.5). Parameters influencing the primary air entrainment are defined based on the expression derived from the analytical model. The performance of LPG-PRB was assessed by varying a significant parameter that influences the primary air entrainment. Results obtained from the experimental results are presented and the reason for such results are presented in section 3.6. Finally, section 3.7 presents the summary that concludes this chapter.

3.1 Improved Porous Radiant Burner operating in partially surface-stabilized mode of operation

The main objective of the present work is to develop a Liquefied Petroleum Gas (LPG) based Porous Radiant Burner (LPG-PRB) feasible for real-time cooking applications. LPG-PRB developed by Mishra (2015b) operates in a submerged mode of operation. In the present work, an LPG-PRB operating in a partially surface-stabilized mode of operation, i.e., with blue flame above the burner surface is developed as an improvement over LPG-PRB developed by Mishra (2015b). LPG-PRB developed by Mishra (2015b) is susceptible to flashback because of enormous heat recirculation within the Porous Medium (PM), leading to overheating of the burner parts in the upstream direction. Fig. 3.1 and 3.2 shows the schematic of LPG-PRB developed by Mishra (2015b) and various components used in its construction.

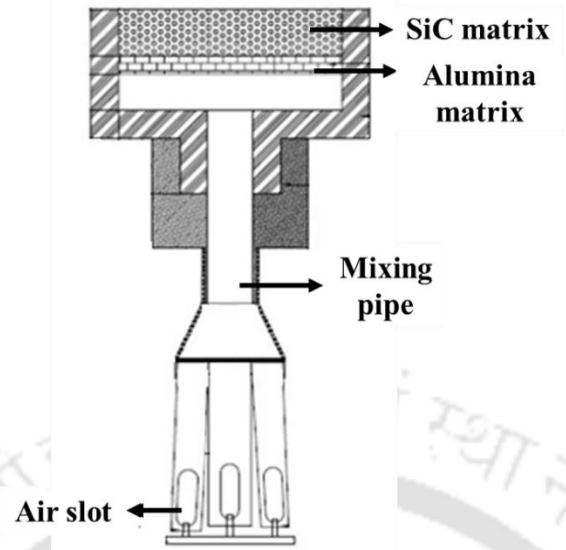

Fig. 3.1: Schematic of LPG-PRB developed by Mishra (2015b)

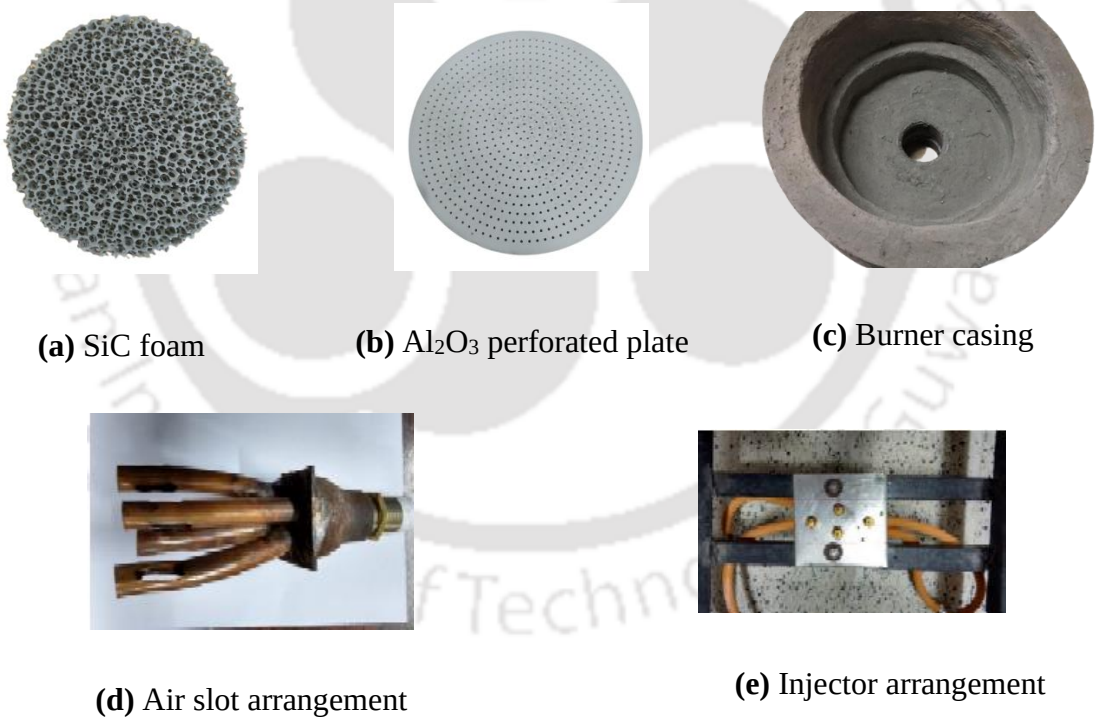

(a) SiC foam **(b)** Al_2O_3 perforated plate **(c)** Burner casing

(d) Air slot arrangement **(e)** Injector arrangement

Fig. 3.2: Components used in LPG-PRB developed by Mishra (2015b)

In the area of research on Porous Medium Combustion (PMC) for cooking applications, the development trend is toward self-aspirated PRBs. LPG-PRB developed by Mishra (2015b) is an excellent finding which is highly efficient with a low level of emissions which makes it superior to FFC based burner. The improved performance of the LPG-PRB developed by

Mishra (2015b) is mainly due to the better efficient heat transfer from the burnt gases to the incoming unburnt fuel-air mixture. However, it also makes the fuel-air mixture susceptible to getting overheated (above the self-ignition temperature of fuel), while entering the preheat layer. After a period of stable operation, PM reaches high temperatures, which leads to the ignition of the incoming fuel-air mixture ahead of the preheat layer itself, thus resulting in a flashback. The literature reviewed in section 2.2 shows the capability of PRBs as a potential alternative to FFC based burners. However, flashback during their operation remains a very challenging issue. Therefore, in the present work, self-aspirated LPG-PRB operating in a partially surface-stabilized mode of operation is presented as an improvement of the LPG-PRB developed by Mishra (2015b).

3.2 Description of construction and working of LPG-PRB

The developed LPG-PRB consists of SiC foam and Al_2O_3 perforated plate housed inside a high-temperature resistant refractory casing. SiC foam and Al_2O_3 perforated plate act as Combustion Layer (CL) and Preheating Layer (PL), respectively. The high-temperature resistant refractory casing prevents heat loss to the surroundings. LPG is supplied to the burner by an injector through a mixing pipe having slots for air aspiration. LPG enters at high pressure from the injector and enters the mixing pipe. Because of the venturi effect, the high-velocity LPG jet creates a low static pressure near the air slot, which in turn causes the suction of primary air through the air slots. The fuel-air mixture gets properly mixed in the mixing chamber above the mixing pipe before reaching PL. The fuel-air mixture enters the Al_2O_3 perforated plate through the holes, where it is preheated and evenly distributed to SiC foam. SiC foam acts as a flame trap, thereby combusting almost most of the combustible fuel-air mixture percentage and allowing intermediate products like hydrogen and carbon monoxide to combust above the foam. Fig. 3.3 shows the schematic of the developed LPG-PRB and Table 3.1 presents its specification.

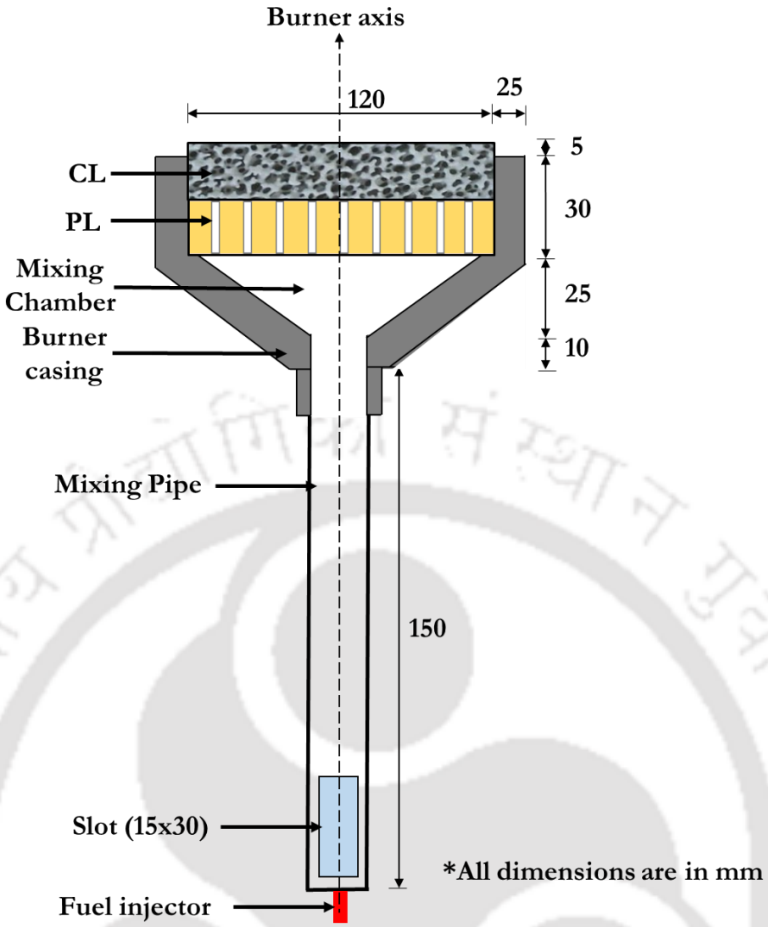

Fig. 3.3: Schematic of the developed LPG-PRB

Table 3.1: Specification of the developed LPG-PRB

Components	Details	Pictorial view
CL	Material: SiC foam Porosity: 45-55% (10 ppi) Thickness: 20 mm Diameter: 120 mm	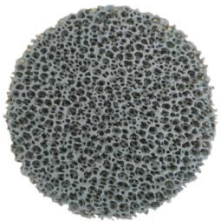
PL	Material: Al_2O_3 perforated plate Porosity: 7% Thickness: 15 mm Diameter: 120 mm	

Casing	Material: Alumina-based high-temperature resistant refractory Thickness: 25 mm	
Mixing pipe	Material: MS threaded pipe Inner diameter: 26 mm Outer diameter: 31 mm Length: 150 mm	
Injector	Injector exit diameter: 0.49 mm	

3.3 Experimental methodology

3.3.1 Experimental setup

The schematic for the experimental setup used for the present investigation is shown in Fig. 3.4. The fuel supply system consists of a 19 kg commercial LPG (Propane: 40% and Butane: 60%) cylinder, an unreduced LPG regulator, and a control valve. The flow rate of LPG ($\dot{m}_{LPG}$) is monitored through a Coriolis Mass Flow Meter (MFM) having accuracy ± 0.001 g. For particular power input ($\dot{m}_{LPG} \times LCV_{LPG}$), the mass flow rate of LPG ($\dot{m}_{LPG}$) is adjusted by the control valve connected between the LPG cylinder and MFM. The experiments were conducted for a $\dot{m}_{LPG}$ range of 0.11 g/s to 0.15 g/s, equivalent to 5 to 7 kW power input.

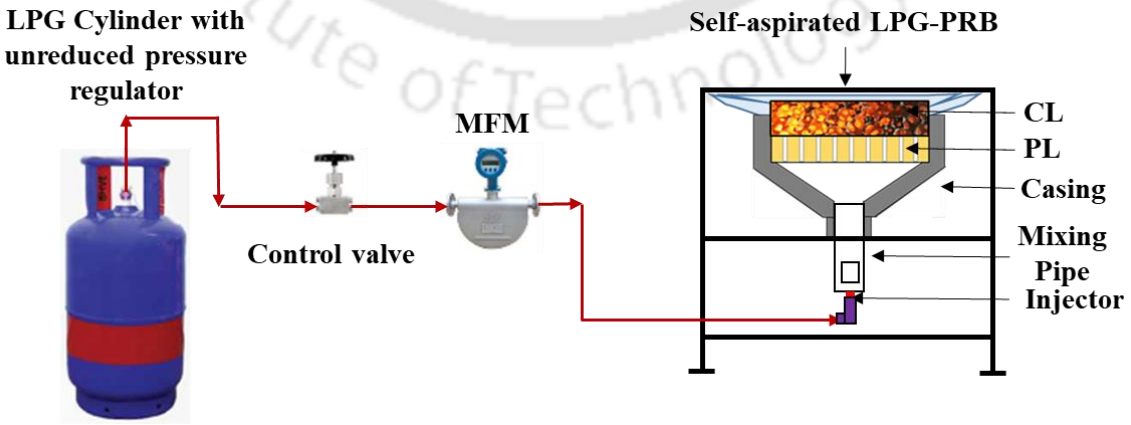

Fig. 3.4: Schematic of the experimental setup

3.3.2 Performance testing

Thermal efficiency

In general, the efficiency of any system is defined as the tendency of that particular system to convert the input energy to output energy. In the present work, it is necessary to calculate the thermal efficiency (η_t) of the burner, as it shows the tendency of the burner to convert the energy content of the fuel into usable heat output and transfer the usable heat output to the load, i.e., pan in the present case. η_t of the burner was determined by conducting the Water Boiling Test (WBT) as per Indian Standard (IS) 14612:1999 (Prescribed by the Bureau of Indian Standards). Fig. 3.5 shows the schematic of the arrangement used for WBT. WBT for LPG-PRB and LPG based Conventional Burner (LPG-CB) was conducted once the burner reached its stable state condition and continued until the temperature of water reached 90 °C. The aluminium pan of diameter 300 mm and height 150 mm was used for WBT. The total mass of the aluminium pan along with the lid was 1.078 kg. The aluminium pan was filled with 9 kg of water and inserted with a stirrer. Mass and temperature measurements were done by weighing balance (accuracy ± 0.001 g) and mercury-in-glass thermometer (accuracy ± 0.5°C), respectively. It was ensured that $\dot{m}_{LPG}$ was kept constant throughout WBT. The amount of LPG consumed during the test was measured using MFM. WBT was performed thrice, and the average of the results obtained from these three tests was considered for estimating the η_t. Eq. (3.1) is used for the calculation of η_t.

$$\eta_t = \frac{\left(M \times C_p + m \times C_w\right) \times \left(T_2 - T_1\right)}{m_{LPG} \times LCV_{LPG}} \tag{3.1}$$

Where M is the total mass of the pan along with the lid (kg), m is the mass of water (kg), C is specific heat (kJ/kg-k, p : pan and w : water), T_2 and T_1 are the temperatures of water (°C) at the end and the start of WBT, m_{LPG} is the mass of LPG consumed (kg) to raise water temperature from T_1 to T_2 and LCV_{LPG} is the Lower Calorific Value of LPG (kJ/kg). The properties of LPG used for the present study are given in Appendix-I.

For the present case, no IS standard is available. In the case of LPG, IS 4246:2002 and IS 14612:1999 are available for burners operating in the power input range of 0-2.5 kW and 12.67-

44.35 kW, respectively. Details of pan size and mass of water prescribed by IS 4246:2002 and IS 14612:1999 are presented in Appendix–II. But in IS 14612:1999, it is mentioned that for any LPG commercial burners of different burning rates, the criteria for selection of vessel size and water quantity is based on identical testing time, which is approximately 17 mins. The ratio of total water quantity to gas burning rate shall be 17±0.5 as per IS 14612:1999. From this criteria, the mass of water and pan size is selected for the present investigation.

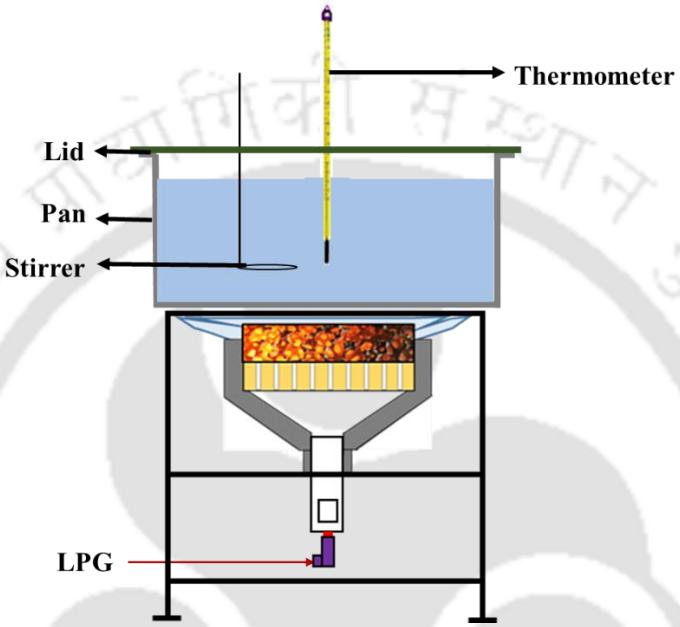

Fig. 3.5: Arrangement for WBT

Emissions analysis

Emission analysis was performed as prescribed by IS 14612:1999. Testo 350 flue gas analyzer was used to measure the emissions in LPG-PRB and LPG-CB. Figs. 3.6 and 3.7 present the arrangement used for emission analysis and the hood used for the analysis. The analyzer unit consists of a stainless steel probe used for collecting samples from determined space. For measuring CO and NO_x emissions, a hood was used to collect the flue gas from the burner. The sampling probe is inserted in the vent pipe of the hood. In the present study, CO and NO_x emissions referred to dry-basis measurement, with the correction to 3% fixed O_2 level is considered.

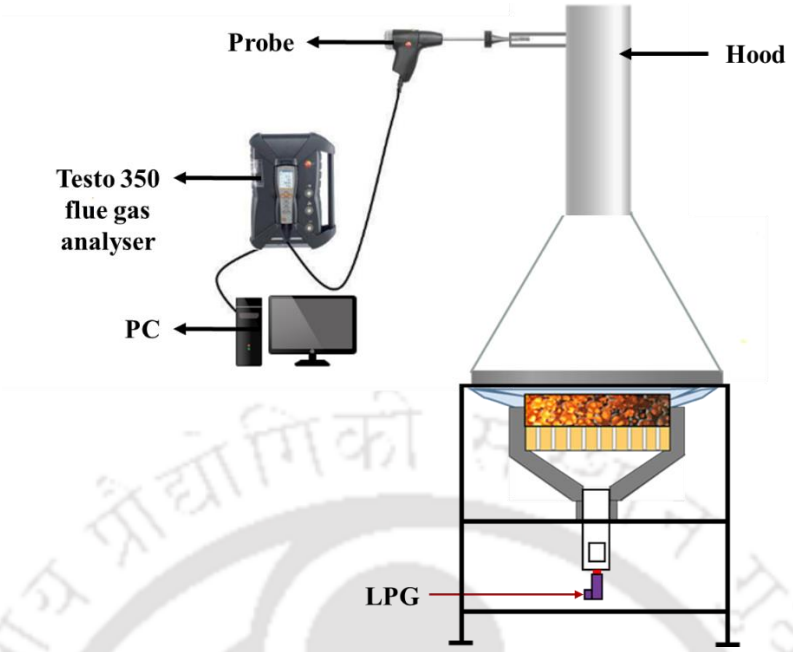

Fig. 3.6: Arrangement for emission analysis

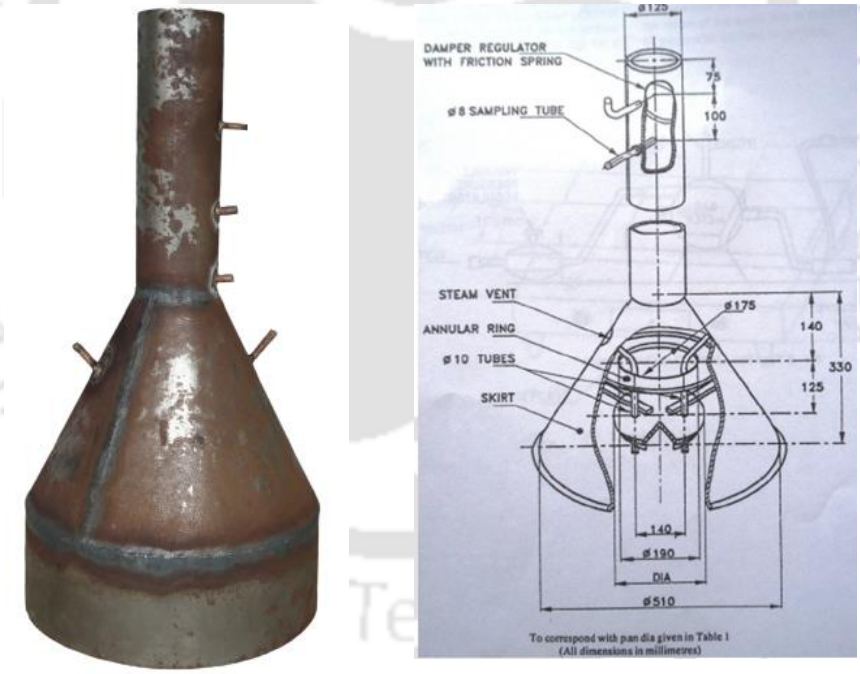

(a) Pictorial view **(b)** Schematic view

Fig. 3.7: Pictorial and Schematic view of the hood used for emission analysis

Experimental uncertainty

It is important to determine the uncertainty in the calculation of dependent parameters. The calculated values of η_t depend on the values obtained from the instruments used to measure

parameters like temperature, mass of LPG consumed and mass of pan and water. Using Eq. (3.2), the uncertainty in the estimation of η_t is calculated (Moffat, 1988).

$$\delta\eta_t = \sqrt{\left(\frac{\delta\eta_t}{\delta M}\Delta M\right)^2 + \left(\frac{\delta\eta_t}{\delta m}\Delta m\right)^2 + \left(\frac{\delta\eta_t}{\delta(\Delta T)}\Delta(\Delta T)\right)^2 + \left(\frac{\delta\eta_t}{\delta m_{LPG}}\Delta m_{LPG}\right)^2} \quad (3.2)$$

The uncertainty in the measurement of the mass of water and pan, the mass of LPG consumed and temperature are ±0.1 g, ±0.001 g and ±0.5 °C, respectively.

3.4 Results and discussion on thermal efficiency and emissions

For the LPG-PRB operating in partially surface-stabilized mode of operation, the flame was found to be partially stabilized above the red hot radiating surface, resulting in an efficient energy transfer by radiation and convection to the load. The heat transfer predominantly occurs through radiation because of the SiC foam's high emissivity, which results in relatively high radiant efficiencies. At a 5-7 kW power input range, the PRB yields η_t in the range of 63.8-69.7 %. An increase in power input, increases the surface temperature but also significantly increases the heat loss from the burner casing. As a result, an increase in temperature could not be able to entirely compensate for the effect of heat loss, which lowers η_t at higher power input. The viability of LPG-PRB operating in partially surface-stabilized mode of operation, as an alternative to FFC based LPG-CB was assessed by comparing its η_t and concentrations of CO and NO_x in the flue gas. The specification of LPG-CB is given in Appendix-III. Within an operating range of 5-7 kW, η_t for LPG-PRB varied between 69.7-63.8%, whereas the same was 54.4-49.7% for LPG-CB.

The emission characteristics of LPG-PRB were found to be far better than LPG-CB. Concentrations of CO and NO_x for LPG-PRB ranged between 29-34 ppm and 2-5 ppm, respectively, whereas the same for CB was 98-205 ppm and 11-19 ppm, respectively. LPG-PRB showed maximum CO and NO_x percentage reductions of 83.9% (at a power input of 7 kW) and 81.8% (at a power input of 5 kW) compared to FFC-CB. In all the compared factors LPG-PRB outperformed the FFC-CB and presented itself as a strong alternative. Fig. 3.8 presents the η_t values of LPG-PRB developed in this work, LPG-PRB developed by Mishra (2015b) and LPG-CB for a power input range of 5-7 kW. The emission indices of CO and NO_x

for the studied LPG-PRB are plotted in Fig. 3.9 as a function of power input. The combustion process in the partially surface-stabilized mode of operation was found to be highly efficient, with substantial heat transfer to the solid matrix, which is indicated by the low CO and the NO_x emissions (CO: 29-34 ppm, NO_x: 2-5 ppm). Both CO and NO_x emissions were found to increase with burner capacity. The increasing trend of CO with escalating power input is mainly due to reduced residence time in the porous layer, which in turn leads to higher unconverted CO. The NO_x emission shows a similar trend of variation as that of the CO (Fig. 3.9). The impact of the burner capacity of 5-7 kW is of meagre importance in NO_x concentrations.

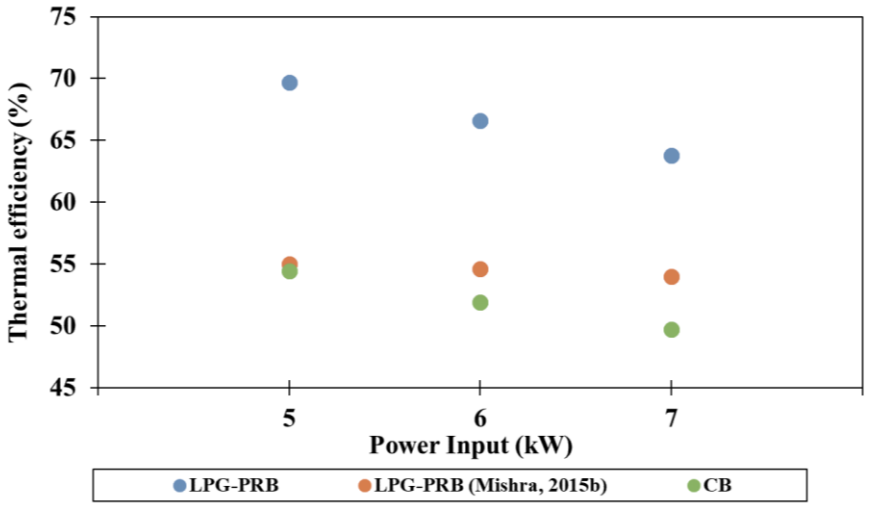

Fig. 3.8: Thermal efficiency for a power input range of 5-7 kW

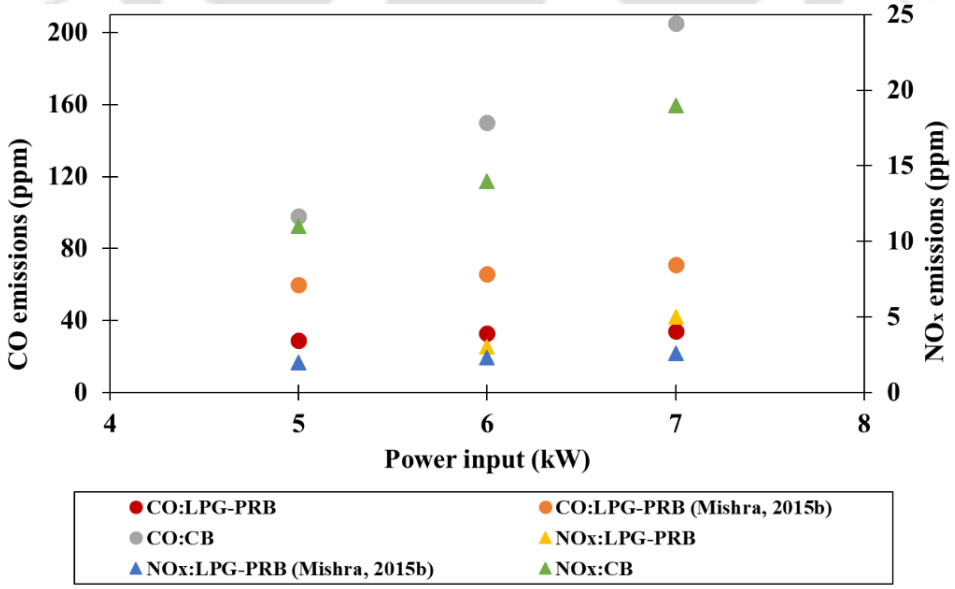

Fig. 3.9: CO and NO_x emissions for a power input range of 5-7 kW

In order to prove the effectiveness and novelty of the present work, a comparison with notable literature is needed. Various researchers have developed burners suitable for various applications operating with different fuels and at different power inputs. Here, η_t and CO and NO_x concentrations in the flue gas of the burners developed by various researchers have been presented in Table.3.2 for comparison.

Table 3.2: Comparison of thermal performance of LPG-PRB with notable literature

Authors	Burner Description	Performance characteristics
Mujeebu et al. (2011)	• Fuel: LPG **Surface Stabilized Burner (SSB)** • Double layer burner (0.62 kW) • PL: 12.7 mm thick Al_2O_3 foam with 26 ppcm and 86% porosity • CL: 12.7 mm thick Al_2O_3 foam with 8 ppcm and 84% porosity **Matrix Stabilized Burner (MSB)** • Double layer burner (0.62 kW) • PL: 15 mm thick porcelain foam with 18 ppcm • CL: Al_2O_3 balls of 30 mm diameter	**SSB** • η_t : 71% • CO: 36 ppm • NO_x: 10 ppm **MSB** • η_t : 59% • CO: 21 ppm • NO_x: 7 ppm
Mishra et al. (2015b)	• Fuel: LPG • Double layer burner (120 mm in diameter) (5-10 kW) • PL: 10 mm thick Al_2O_3 matrix • CL: 25 mm thick SiC	• η_t : 58% (maximum) • CO: ~35-90 ppm • NO_x: ~3- 9 ppm
Chaelek et al. (2019)	• Fuel: LPG • Single layer burner (21-44 kW) with porous radiant re-circulated heater. • Al_2O_3 balls of 10 mm in diameter.	• η_t : 51% (maximum) • CO: ~1165-5738 ppm • NO_x: ~25-46 ppm
Present study	• Fuel: LPG • Double layer burner operating in Partially surface-stabilized mode (5-7 kW) • PL: 20 mm thick Al_2O_3 perforated plate with 7% porosity • CL: 20 mm thick SiC foam with 45-55% porosity and 10 ppi.	• η_t : 69.7-63.8% • CO: 29-33 ppm • NO_x: 2-5 ppm

3.5 Derivation of an analytical expression for primary air entrainment in LPG-PRB

For any self-aspirated burner, primary air entrainment is essential for its stable operation and Pritchard et al. (1977) developed an analytical expression for primary air entrainment in FFC based burner. Based on this expression, any FFC based burner can be designed. Hence, in the present case, an analytical expression for primary air entrainment in PRB is developed.

The design of the self-aspirated PRB relies on the same parameters as that of an FFC-CB, i.e., pressure drop across the burner and specifications of burner geometry. In this section, the expression for primary air entrainment in naturally-aspirating PRB is derived using the methodology followed by Pritchard et al. (1977). Simple momentum and energy conservation principles are implied to study the primary air entrainment characteristics of a self-aspirated PRB. The flow is considered in a one-dimensional direction (1-D) and it is assumed to be incompressible, non-reacting, and isothermal for simplifying the formulation. Fig. 3.10 shows the two-layer PRB model considered for the formulation. A fuel jet from the injector at specific pressure entering the mixing tube is considered. Before reaching the exit of PRB, the fuel jet passes through the mixing chamber, Al_2O_3 perforated plate and SiC foam, where it undergoes a pressure drop at each stage.

In the injector, the potential energy of the fuel supplied at high pressure is converted into the kinetic energy of an emerging fuel jet. Therefore, by the law of conservation of energy, the possible maximum heat input can be written as (Pritchard et al., 1977),

$$q = 12.78 A_j W C_{dj} \sqrt{P_j} \tag{3.3}$$

And one obtains,

$$A_j = \frac{q}{12.78 W C_{dj} \sqrt{P_j}} \tag{3.4}$$

where, A_j is the cross-sectional area of the injector exit, q is the heat input supplied by fuel, W is Wobbe number, C_{dj} is the discharge coefficient of the injector, and P_j is the fuel supply pressure. It can be understood from Eq. (3.4), A_j depends on q, W, C_{dj} and P_j.

At specified q and P_j, A_j decides the possible maximum velocity of the fuel jet from the injector.

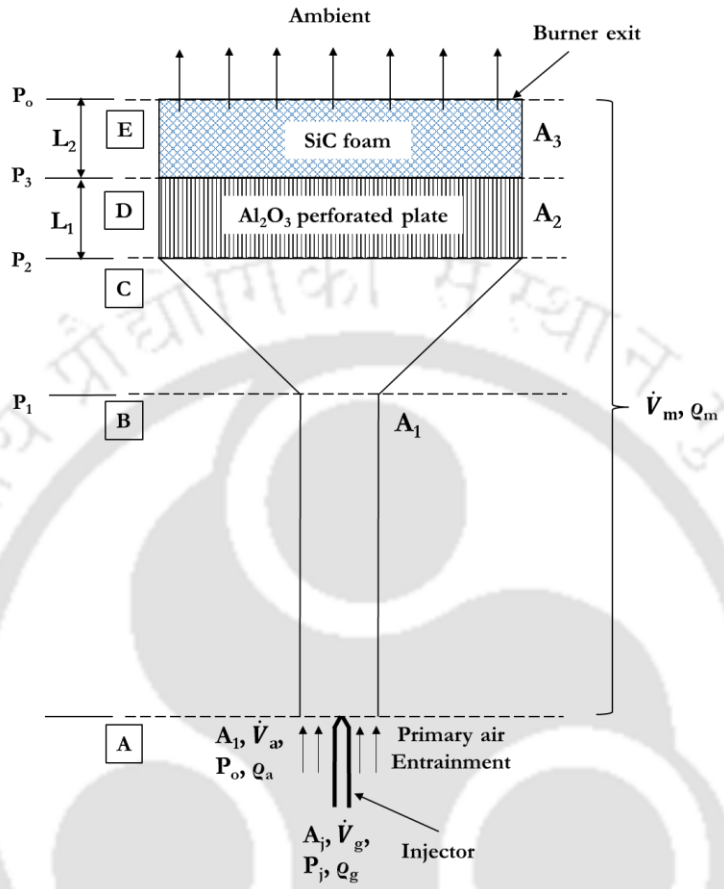

Fig. 3.10: Self-aspirated PRB model

As the fuel jet enters the mixing tube from the injector exit, it undergoes a pressure drop. Because of this pressure drop, primary air entrains along with the fuel jet and gets mixed up in the mixing tube. Assuming $A_j << A_1$, the force-momentum balance between sections A and B can be written as (Pritchard et al., 1977),

$$(P_1 - P_0)A_1 = \frac{\rho_g \dot{V}_g^{\,2}}{A_j} - \frac{\rho_m \dot{V}_m^{\,2}}{A_1} \tag{3.5}$$

$$P_1 - P_0 = \frac{\rho_g \dot{V}_g^{\,2}}{A_j A_1} - \frac{\rho_m \dot{V}_m^{\,2}}{A_1^{\,2}} \tag{3.6}$$

The energy balance between B and C can be written as (Pritchard et al., 1977),

$$P_2 - P_1 = \frac{\rho_m \dot{V}_m^{\,2}}{2A_1^{\,2}}\left(1 - C_L\right) \tag{3.7}$$

Where C_L is the loss coefficient for the mixing chamber.

The mass flow rate of the air-fuel mixture in Al_2O_3 perforated plate (Smith and Winkle, 1958),

$$\dot{m}_m = k_a A_2 \sqrt{\frac{2\rho_m (P_3 - P_2)}{\left(1 - \left(\frac{A_2}{A_s}\right)^2\right)}} \tag{3.8}$$

In general, $\dot{m}_m = \rho_m u_{f1} A_s$, where u_{f1} is the superficial velocity of the air-fuel mixture in Al_2O_3 perforated plate ($u_{f1} = \frac{\dot{V}_m}{A_s}$) and A_s is the total surface area of the perforated plate. By combining $\dot{m}_m = \rho_m u_{f1} A_s$ and Eq. (3.8), the pressure difference between sections C and D can be written as,

$$P_3 - P_2 = \frac{\rho_m \dot{V}_m^{\,2}}{2A_2^{\,2}}\left(C_a\right) \tag{3.9}$$

The pressure difference between sections D and E Dietrich et al. (2019) can be written as,

$$\frac{P_3 - P_0}{L_2} = 110\frac{\mu_m}{\in_{SiC} d_h^{\,2}} u_{f2} + 1.45\frac{\rho_m}{\in_{SiC}^{\,2} d_h} u_{f2}^{\,2} \tag{3.10}$$

Where, $C_a = \frac{1}{k_a^{\,2}}\left(1 - \left(\frac{A_2}{A_s}\right)^2\right)$, in which k_a is a coefficient for various hole diameter to plate thickness ratio, A_2 is the total area of the holes, μ_m is the Dynamic viscosity (Kinematic viscosity (υ_m) x Density (ρ_m)), $\in_{SiC}$ is the porosity of the SiC foam, d_h is the hydraulic diameter of the SiC foam, u_{f2} is the superficial velocity of the air-fuel mixture in SiC foam (

$u_{f2} = \frac{\dot{V}_m}{A_3}$), A_3 is the total cross-sectional area of SiC foam and L_2 is the thickness of the SiC foam. Assign $k_2 = \left(110 \frac{\upsilon_m}{\in_{SiC} d_h^2 u_{f2}} + 1.45 \frac{1}{\in_{SiC}^2 d_h} \right) L_2$,

$$P_3 - P_0 = k_2 \frac{\rho_m \dot{V}_m^2}{A_3^2} \tag{3.11}$$

Solving Eqs. (3.6) and (3.7),

$$P_2 - P_0 = \frac{\rho_g \dot{V}_g^2}{A_j A_1} - \frac{\rho_m \dot{V}_m^2}{2A_1^2}\left(1 + C_L\right) \tag{3.12}$$

Pressure efficiency (η_p) is defined as the ratio of the static pressure at the upstream of Al_2O_3 perforated plate to the dynamic pressure of the fuel jet from the injector exit. Hence, η_p in this case can be written as (Pritchard et al., 1977),

$$\eta_p = \frac{P_2 - P_0}{\left(\frac{\rho_g \dot{V}_g^2}{2A_j^2} \right)} \tag{3.13}$$

$$\eta_p = \left(P_2 - P_0\right)\left(\frac{2A_j^2}{\rho_g \dot{V}_g^2} \right) \tag{3.14}$$

Substitute Eq. (3.12) in Eq. (3.14) and assign $\theta = \frac{A_j}{A_1}$ and $\lambda = \frac{\rho_m \dot{V}_m^2}{\rho_g \dot{V}_g^2}$, Eq. (3.14) becomes,

$$\eta_p = 2\theta - \lambda\theta^2 \tag{3.15}$$

The performance of the self-aspirated PRB is considered to be optimum at the maximum value of η_p $\left(\frac{d\eta_p}{d\theta} = 0 \right)$.

From Eq.(3.14), it is clear that η_p is maximum when

$$\theta|_{\eta_{p\max}} = \left(\frac{A_j}{A_1}\right)_{\eta_{p\max}} = \frac{\rho_g \dot{V}_g^{\,2}}{\rho_m \dot{V}_m^{\,2}\left(1+C_L\right)} \tag{3.16}$$

Here, $R = \frac{\dot{V}_a}{\dot{V}_g}$, $\dot{V}_m = \dot{V}_g + \dot{V}_a = \dot{V}_g\left(1+R\right)$ and $\rho_m = \frac{\rho_g \dot{V}_g^{\,2} + \rho_a \dot{V}_a^{\,2}}{\dot{V}_m} = \frac{\rho_g\left(\sigma+R\right)}{\sigma\left(1+R\right)}$, where, σ is the relative density of the fuel.

Substitute $\dot{V}_m = \dot{V}_g\left(1+R\right)$ and $\rho_m = \frac{\rho_g\left(\sigma+R\right)}{\sigma\left(1+R\right)}$ in Eq. (3.16),

$$\theta|_{\eta_{p\max}} = \left(\frac{A_j}{A_1}\right)_{\eta_{p\max}} = \frac{\sigma}{\left(\sigma+R\right)\left(1+R\right)\left(1+C_L\right)} \tag{3.17}$$

Solving Eqs. (3.9) and (3.11) and substituting $\dot{V}_m = \dot{V}_g\left(1+R\right)$ and $\rho_m = \frac{\rho_g\left(\sigma+R\right)}{\sigma\left(1+R\right)}$,

$$P_2 - P_0 = \frac{\rho_g \dot{V}_g^{\,2}}{2}\left(\frac{\left(\sigma+R\right)\left(1+R\right)}{\sigma}\right)\left(\frac{2K_2}{A_3^{\,2}} - \frac{C_a}{A_2^{\,2}}\right) \tag{3.18}$$

Now substituting $\dot{V}_m = \dot{V}_g\left(1+R\right)$ and $\rho_m = \frac{\rho_g\left(\sigma+R\right)}{\sigma\left(1+R\right)}$ in Eq. (3.12),

$$P_2 - P_0 = \frac{\rho_g \dot{V}_g^{\,2}}{A_1^{\,2}}\left(\frac{A_1}{A_j} - \frac{\left(\sigma+R\right)\left(1+R\right)\left(1+C_L\right)}{2\sigma}\right) \tag{3.19}$$

Substituting Eq. (3.17) in Eq. (3.19),

$$P_2 - P_0 = \frac{\rho_g \dot{V}_g^{\,2}}{2A_1^{\,2}}\left(\frac{\left(\sigma+R\right)\left(1+R\right)\left(1+C_L\right)}{\sigma}\right) \tag{3.20}$$

Equating Eqs. (3.18) and (3.20), we get

$$A_1 = \sqrt{\frac{\left(1+C_L\right)}{\left(\frac{2K_2}{A_3^{\,2}} - \frac{C_a}{A_2^{\,2}}\right)}} \tag{3.21}$$

Substitute Eq. (3.21) in Eq. (3.17),

$$A_j = \frac{\sigma}{(\sigma+R)(1+R)\sqrt{(1+C_L)}}\sqrt{\frac{1}{\left(\frac{2K_2}{A_3^2}-\frac{C_a}{A_2^2}\right)}} \tag{3.22}$$

From Eq. (3.17) an expression for entrainment ratio, R is obtained:

$$R|_{\eta p_{\max}} = \frac{-(1+\sigma)\pm\sqrt{(1-\sigma)^2-\frac{4\sigma A_1}{A_j(1+C_L)}}}{2} \tag{3.23}$$

By assuming $(1-\sigma)^2 << \frac{4\sigma A_1}{A_j(1+C_L)}$, Eq. (3.23) becomes

$$R|_{\eta p_{\max}} = \frac{-(1+\sigma)}{2}+\sqrt{\frac{\sigma A_1}{A_j(1+C_L)}} \tag{3.24}$$

Now substitute Eqs. (3.4) and (3.21) in Eq. (3.24),

$$R|_{\eta p_{\max}} = \frac{-(1+\sigma)}{2}+\sqrt{\frac{12.78\sigma W C_{dj}\sqrt{P_j}}{q\sqrt{(1+C_L)\left(\frac{2K_2}{A_3^2}-\frac{C_a}{A_2^2}\right)}}} \tag{3.25}$$

From Eqs. (3.24) and (3.25), it can be observed that R is a function of the type of fuel used, fuel supply pressure, and geometry of injector, mixing chamber, Al_2O_3 perforated plate, and SiC foam. It should be noted that for flame stabilization in PRB, irrespective of the mode of operation, the pore size of the CL (SiC foam) should be larger and for PL (Al_2O_3 perforated plate), it should be smaller (Trimis, 2000). Also, from Eq. (3.16), it was found that A_1 is dependent on A_j. Hence it can be understood that when the fuel type is specified and the geometries of the mixing tube, mixing chamber, Al_2O_3 perforated plate, and SiC foam are constant, the geometry of the injector is the key parameter that influences R. Therefore, in this

work, A_j is changed in PRB to obtain the necessary air entrainment while keeping the geometries of the mixing chamber, Al_2O_3 perforated plate, and SiC foam constant for a specific fuel (LPG). Injectors with exit diameters of 0.49 mm, 0.63 mm, and 0.74 mm are used in the present investigation. LPG-PRB operating with injectors having exit diameters of 0.49 mm, 0.63 mm, and 0.74 mm are termed LPG-PRB:D1, LPG-PRB:D2 and LPG-PRB:D3, respectively.

3.6 Results and discussion on the performance of LPG-PRB with variation in injector exit diameter

3.6.1 Effect of injector diameter on primary air entrainment

Testo 350 flue gas analyser was used to detect the oxygen concentration in LPG-PRB. For determining oxygen concentration in the LPG-air mixture, the sampling probe is fitted below PL in the mixing chamber, in both cold (absence of combustion of LPG-air mixture) and hot states (presence of combustion of LPG-air mixture). The raw data of oxygen percentage in the LPG-air mixture is then converted into a percentage of primary air entrainment ($\%PAE$). The following chemical reaction is considered for the calculation of $\%PAE$ (Laphirattanakul et al., 2016):

$$0.4C_3H_8 + 0.6C_4H_{10} + x\left(O_2 + 3.76N_2\right) \rightarrow products$$

$$x = \frac{Y_{O_2}}{1 - 4.76Y_{O_2}} \tag{3.26}$$

Where Y_{O_2} is the mole fraction of O_2 in the fuel-air mixture in the mixing chamber.

Therefore, the percentage of primary air entrainment ($\%PAE$) can be calculated from:

$$\%PAE = \frac{4.76x\left(\frac{MW_{air}}{MW_{LPG}}\right)}{\left(\frac{A}{F}\right)_{stoi}} \times 100 \tag{3.27}$$

Where, MW_{air} and MW_{LPG} are the molecular weight of air and LPG (g) and $\left(\frac{A}{F}\right)_{stoi}$ is the stoichiometric air-fuel ratio.

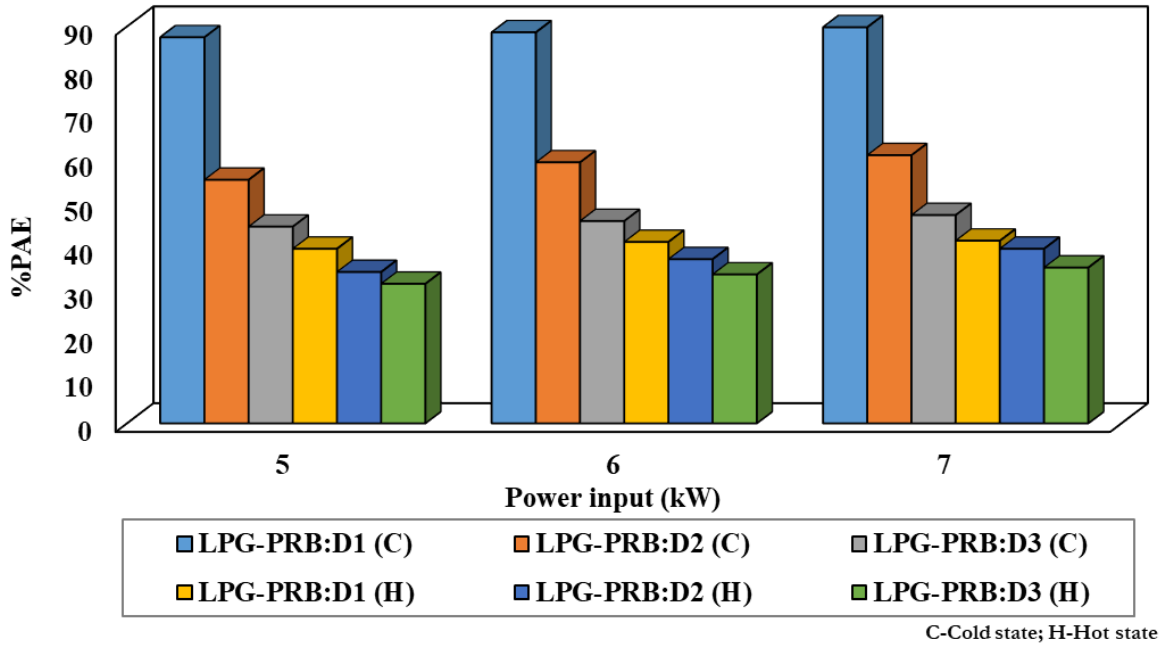

Fig. 3.11: Variation of %PAE in LPG-PRB with injector exit diameters

The experiments were carried out in both hot and cold state conditions. It was observed that in LPG-PRB, there was a variation in % PAE with a change in injector exit diameter and between cold and hot states. Fig. 3.11 shows % PAE in LPG-PRB operated with injectors having exit diameters of 0.49 mm (LPG-PRB:D1), 0.63 mm (LPG-PRB:D2) and 0.74 mm (LPG-PRB:D3) for different power inputs in both cold and hot states. It was observed that LPG-PRB:D1 had the highest %PAE for the studied power input range. And % PAE decreased with an increase in the exit diameter of the injector, which is in accordance with Eq. (3.24). LPG-PRB showed a reduction in %PAE when operated in a hot state compared to a cold state. This variation in %PAE at similar power input in hot and cold states is due to the preheating effect caused by the combustion of the LPG-air mixture in the LPG-PRB. Also, an increase in %PAE is observed with an increase in power input. Such an increase in %PAE is mainly due to an increased pressure drop in the mixing tube with an increase in the momentum of the fuel. A maximum %PAE of 89% and 41% was observed in LPG-PRB:D1 operating at 7 kW (0.15 g/s) in cold and hot states, respectively.

3.6.2 Temperature distribution on the burner surface

For the determination of temperature distribution on the surface of the burner, temperatures were recorded at various radial positions on the top of CL (Fig. 3.12). The temperature

measurements were done using K-type thermocouples (accuracy ± 1°C) connected to data acquisition system (Agilent make) and computer system.

The radial temperature distributions on LPG-PRB surface operating with injectors having different exit diameters at different power inputs are shown in Figs. 3.13. In LPG-PRB, the temperature is measured on the burner surface radially to ensure uniform flame stabilization within CL. The temperature at the centre of the burner surface was observed to be high and decreased towards the periphery. The reason behind the variation of temperature from the centre to the periphery of the burner surface is the heat loss from CL to the burner casing. Maximum radial temperature of 870 ºC, 911 ºC and 930 ºC for 5, 6 and 7 kW, respectively, were observed in LPG-PRB:D1. The burner surface temperature decreased with the increase in injector exit diameter. Also, the variation in temperature from the centre to the periphery of LPG-PRB:D1 surface was less than 100 ºC for all power inputs.

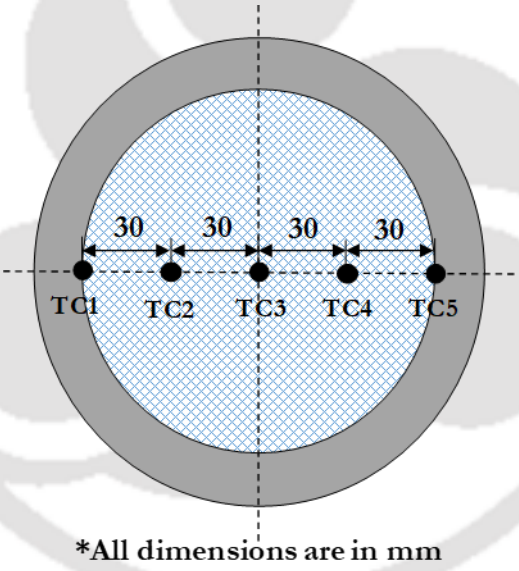

Fig. 3.12: Thermocouple arrangement for radial temperature measurement

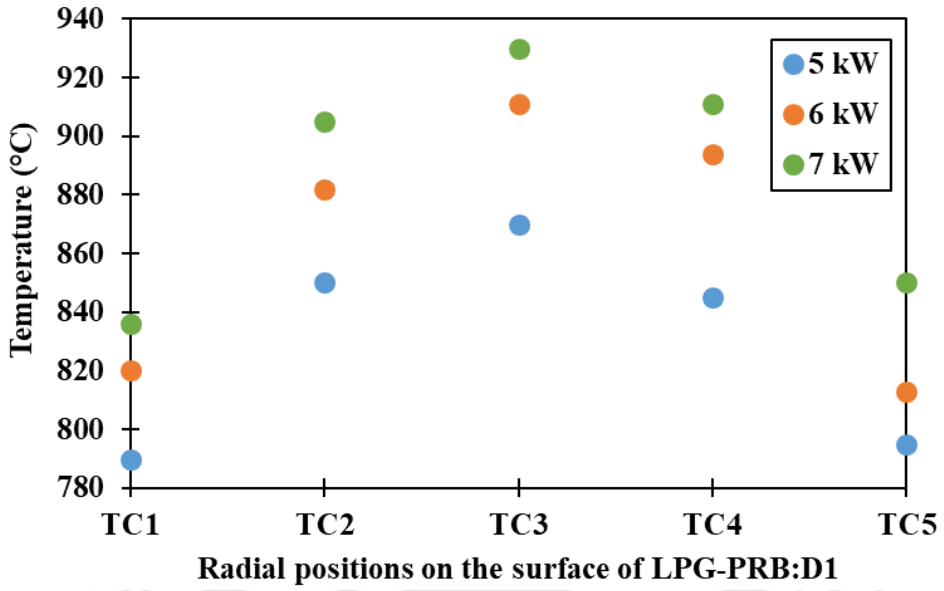

(a) Radial temperature distribution on the surface of LPG-PRB:D1

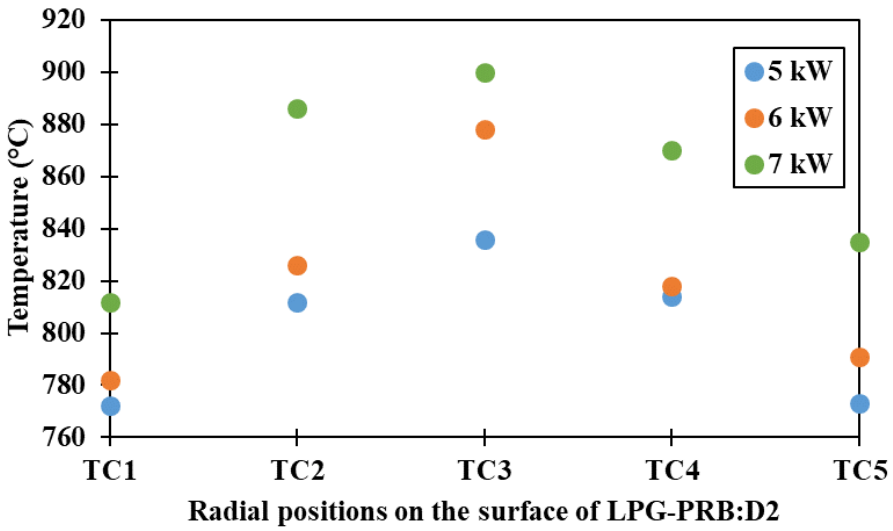

(b) Radial temperature distribution on the surface of LPG-PRB:D2

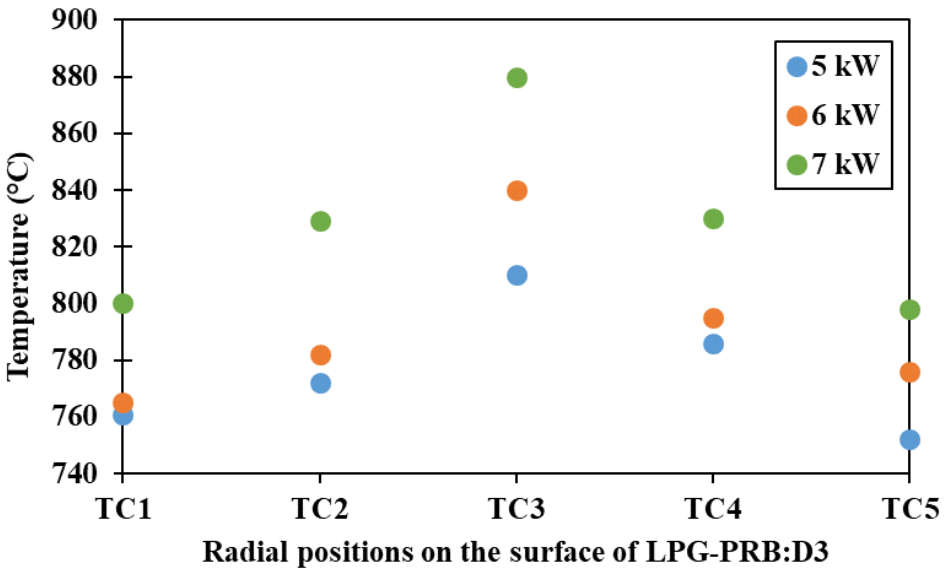

(c) Radial temperature distribution on the surface of LPG-PRB:D3

Fig. 3.13: Radial thermal mapping on the surface of LPG-PRBs operating with different injector exit diameters

3.6.3 Operation of LPG-PRB and its combustion regime

K-type thermocouples were located at a radial distance of 30 mm from the periphery, as shown in Fig. 3.14. The temperature variation from the bottom of PL to the top surface of CL was recorded to understand the flame stabilization mechanism within LPG-PRB and the preheating effect on the incoming LPG-air mixture.

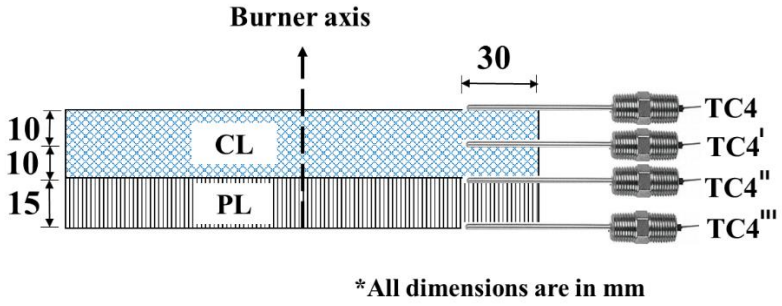

Fig. 3.14: Thermocouple arrangement for axial temperature measurement

Temperatures were measured for LPG-PRB operating with injectors having different exit diameters. It was observed from Fig. 3.15 that the temperature at the interface of CL and PL is maximum, which indicates the reaction zone. And the temperature gradually decreases towards the burner surface. A maximum temperature of 1208 ºC, 1256 ºC and 1289 ºC (at 5, 6 and 7 kW, respectively) was recorded at the interface of CL and PL for LPG-PRB:D1. And the

temperature at the interface of CL and PL decreased with an increase in the injector exit diameter. Also, it was observed that in LPG-PRB:D3, the temperature at the interface of CL and PL were almost close to each other. This indicates that a further increase in injector exit diameter can lead to flame-lift (unstable condition). From the temperature mapping on both the surface and axial positions, it can be understood that LPG-PRB:D1 showed higher temperatures than LPG-PRB:D2 and LPG-PRB:D3.

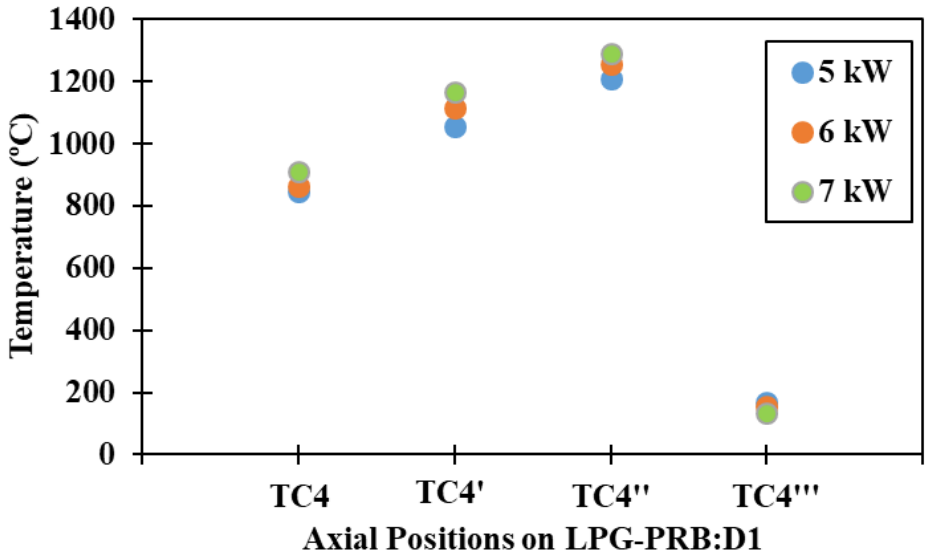

(a) Axial temperature distribution in LPG-PRB:D1

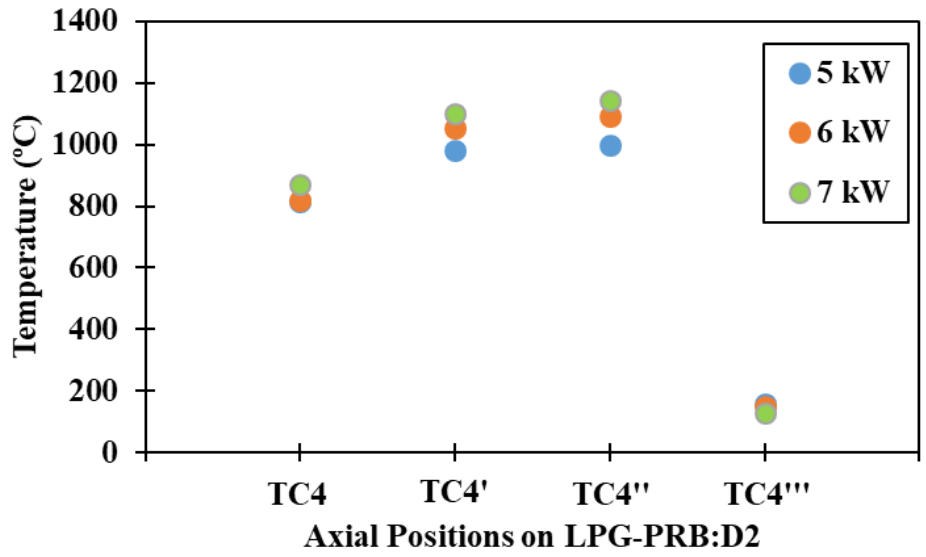

(b) Axial temperature distribution in LPG-PRB:D2

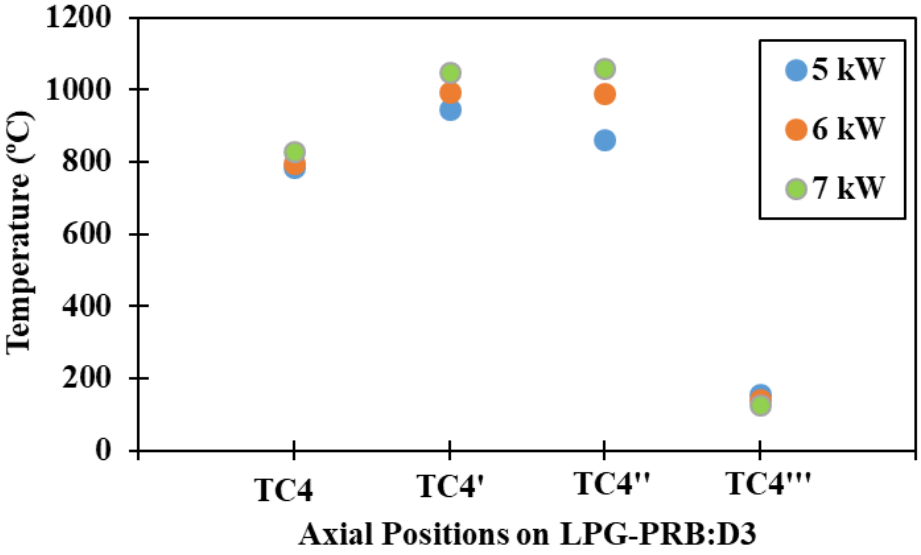

(c) Axial temperature distribution in LPG-PRB:D3

Fig. 3.15: Axial thermal mapping on LPG-PRB with different injector exit diameters

With the same arrangement of thermocouples as shown in Fig. 3.14, temperature mapping was done with respect to time (transient) for LPG-PRB:D1 operating at 5, 6 and 7 kW to prove the stability of PRB operating in partially surface-stabilized mode. The burner was considered stable when temperature fluctuation remained within 10°C, for at least 10 min. The stable burner operation signifies the absence of flashback. As per the changes observed in the temperature recorded by the thermocouple, the time taken for stabilization of combustion waves at different power inputs was recorded. If there is an abrupt rise in the TC_4''' temperature with simultaneous fall of TC_4 temperature, the burner was considered unstable (i.e., flashback has occurred). LPG-PRB showed stable operation throughout the testing process and Fig. 3.16 is presented as proof to show the stability of the developed PRB for the examined power input. It was observed that the LPG-PRB surface attains its steady temperature state between 100 to 150 s for all the examined power inputs. Since the burner loses a lot of heat in the downstream direction, the heat recirculation within the PM was found to be less, preventing overheating of PL and thereby ensuring that the incoming LPG-air mixture doesn't get ignited and result in flashback. Stable operation highlights that the partially surface-stabilized mode provides better heat balance between the radiative and convective heat transfer in studied self-aspirated LPG-PRB.

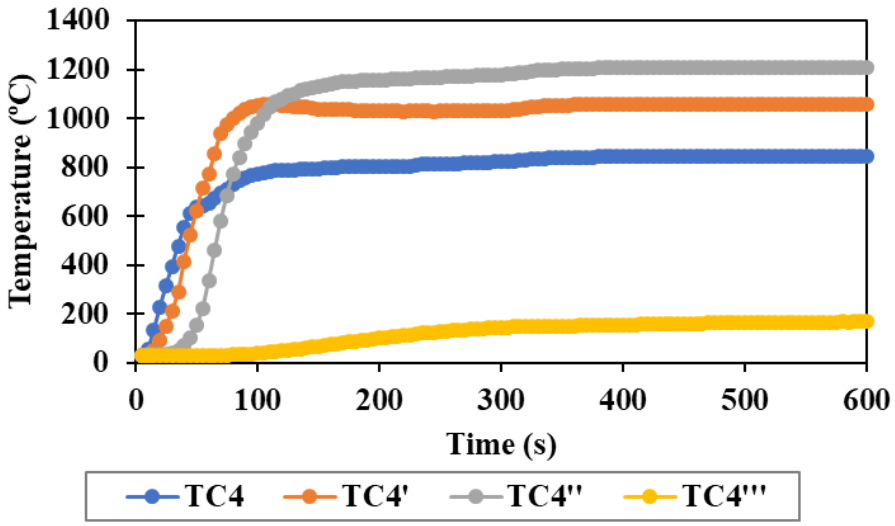

(a) Transient temperature plot at 5 kW

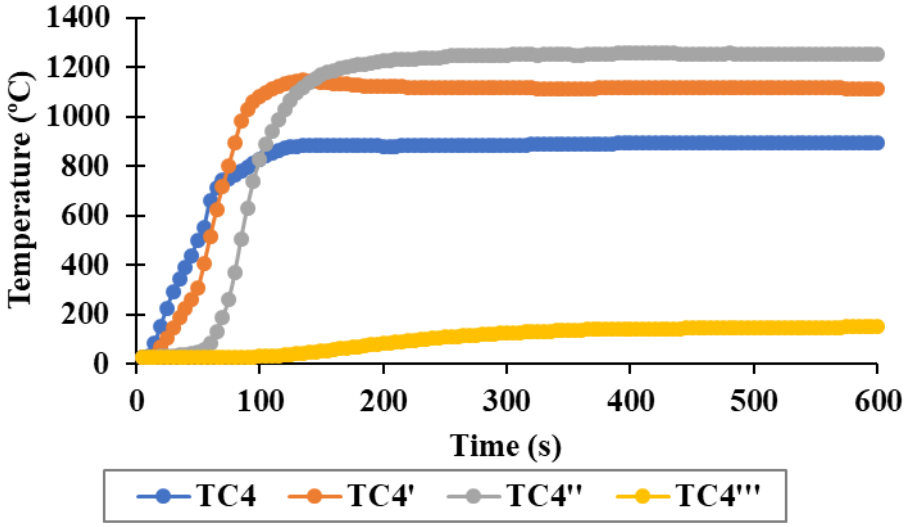

(b) Transient temperature plot at 6 kW

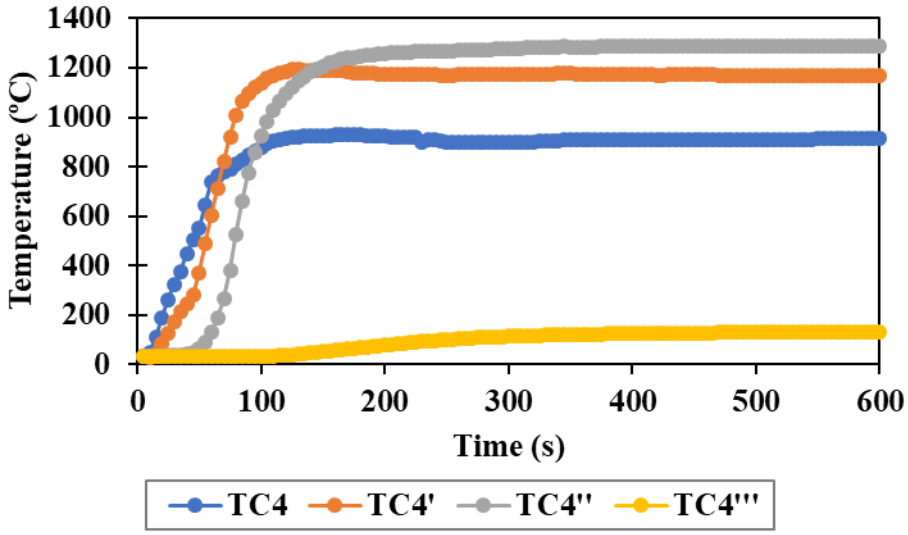

(c) Transient temperature plot at 7 kW

Fig. 3.16: Axial temperature mapping (transient) on LPG-PRB:D1 operating at 5,6 and 7 kW

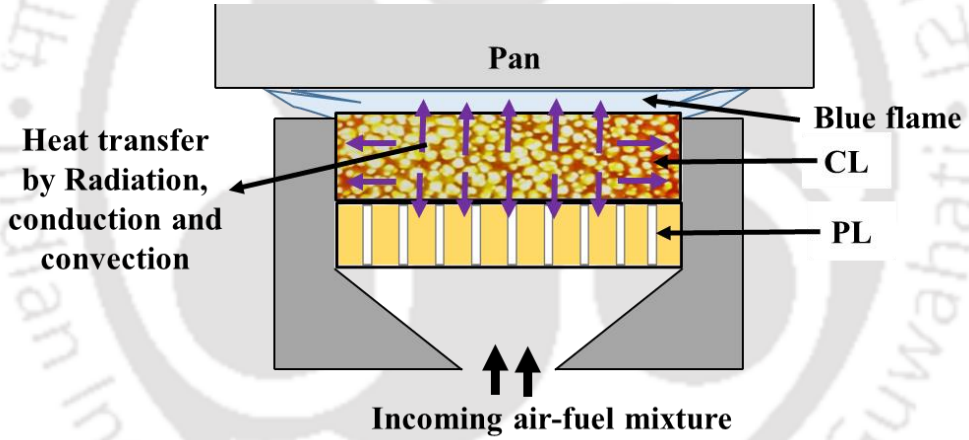

Fig. 3.17: Combustion regime

The schematic representation of the combustion regime in LPG-PRB shown in Fig. 3.17 presents the heat transfer by conduction, convection and radiation in the form of arrows. And among the three modes of heat transfer, radiation is predominant in all directions. For the studied range of power input, LPG-PRB was found to operate in partially surface-stabilized mode with a secondary blue flame above CL. The occurrence of blue flame above CL is mainly due to the combustion of intermediate products such as H_2 and CO that escaped from CL. Observation revealed that in LPG-PRB operating in a partially surface-stabilized mode of operation, the incoming LPG-air mixture from the mixing pipe utilizes the primary air for combustion inside CL and secondary air for combustion above CL. Stabilized flame in CL and

secondary flame above CL due to left-over combustible mixture are important features of burner performance as they enhance the heat transfer pattern while cooking.

3.6.4 Effect of injector diameter on thermal efficiency

Fig. 3.18 shows η_t of LPG-PRB operating with different injector exit diameters at different power inputs. In WBT, because of the combined effect of convective heat transfer from blue flame and radiative heat transfer from the surface of LPG-PRB, there is enhanced heat transfer from LPG-PRB to the pan (load). It was observed that η_t was maximum at lower power input and it decreased with an increase in power input in all LPG-PRBs operating with different injector exit diameters. Such a decrease in η_t is due to the increase in radiative and convective heat loss to the ambient environment at higher power input. LPG-PRB:D1 showed the maximum η_t of 69.7% at 5 kW power input. And at similar power inputs, LPG-PRB: D2 and LPG-PRB:D3 showed η_t of 69% and 68.5%, respectively. It was observed that η_t for specific power input increases with a decrease in the injector exit diameter. This is mainly due to improved primary air entrainment, which in turn leads to better combustion. This shows that the injector diameter is a major factor that affects the primary air entrainment, thereby influencing the η_t. The maximum relative uncertainty in η_t was estimated as ±0.83% at M = 1.078 kg, m = 9 kg, ΔT or T_2 and T_1 = 60°C and m_{LPG} = 0.073 kg.

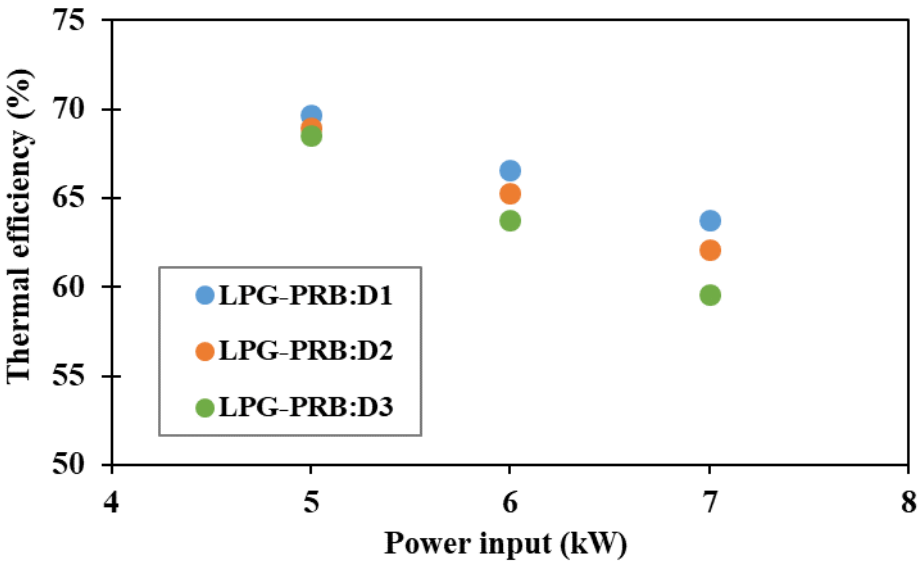

Fig. 3.18: Thermal efficiency of LPG-PRB operating with different injector exit diameters

3.6.5 Effect of injector diameter on emissions

For a power input range of 5–7 kW, CO and NO_x concentrations in the flue gas from LPG-PRB with different injector diameters were investigated. At specific power input, the CO concentration decreased with a decrease in injector exit diameter. With decreasing injector exit diameter, the amount of air entrained is more and hence, the availability of air is sufficient for complete combustion to take place. Consequently, this fact leads to a reduction in the CO concentration in the flue gas from LPG-PRB. Also, due to the lower surface temperature (at the top surface of SiC foam), the NO_x concentration in the flue gas is much less in all cases. Among the LPG-PRB operating with different injector exit diameters, LPG-PRB:D1 produces lower concentrations of CO (29–34 ppm). And the CO concentrations in flue gas from PRB-LPG-PRB:D2 and LPG-PRB:D3 were in the range of 31-37 ppm and 33-43 ppm, respectively. NO_x concentration was less than 5 ppm for all cases. It has been found that CO concentration in the flue gas increases with an increase in the injector exit diameter. Also, it was observed that the CO concentration in the flue gas from LPG-PRB increases with an increase in input power because of the decrease in residence time.

Combustion efficiency (η_{comb}) is defined as the ratio of the concentration of CO_2 in the flue gas to the total concentration of CO and CO_2 in the flue gas. η_{comb} indicates the quality of combustion of the fuel in a burner system. From the results obtained, it was observed that the CO concentration in the flue gas produced is very low compared to the amount of CO_2 in the flue gas and hence, the η_{comb} was more than 99% in all cases.

3.7 Summary

Experimental investigation on the performance characteristics of a two-layered self-aspirated LPG-PRB (5–7 kW) has been carried out in terms of thermal efficiency and emissions. The developed LPG-PRB showed improved η_t and stable operation compared to LPG-PRB developed by Mishra (2015b). LPG-PRB showed η_t in the range of 69.7-63.8% for a power input range of 5-7 kW, which is higher compared to LPG-PRB developed by Mishra (2015b) (55-54%) and LPG-CB (54.4-49.7%). Also, CO and NO_x concentrations ranged between 29-34 ppm and 2-5 ppm, respectively. An analytical expression for the air-fuel entrainment ratio in double-layer LPG-PRB has been derived. From the derived expression, it was understood

that the entrainment ratio is a function of the type of fuel used, fuel supply pressure, and geometry of injector, mixing tube, mixing chamber, Al_2O_3 perforated plate, and SiC foam. Investigation of LPG-PRB operating with various injector exit diameters proved that with a decrease in injector exit diameter, there is an increase in %PAE in both hot and cold states. Also, from the transient temperature mapping, it was understood that LPG-PRB was stable in operation for the studied range of power input. It was observed among the LPG-PRBs operating with injector exit diameters of 0.49 mm, 0.63 mm and 0.74 mm, the LPG-PRB operating with 0.49 mm injector exit diameter showed the highest thermal efficiency of 69.7%. It was found that with the decrease in injector exit diameter, thermal efficiency increases. Compared to its conventional counterpart, the LPG-PRB yields a maximum efficiency improvement of 28.1% (at a power input of 5 kW) and gives almost a clean combustion. Furthermore, the highest percentage reduction in CO and NO_x emissions in LPG-PRB against LPG-CB was found to be 83.9% at a power input of 7 kW and 81.8% at a power input of 5 kW, respectively. The overall performance of LPG-PRB highlights it as a viable alternative to the exiting conventional burners.

CHAPTER 4

DEVELOPMENT AND PERFORMANCE ASSESSMENT OF NATURAL GAS BASED POROUS RADIANT BURNER

Preface

Chapter 4 presents a Natural Gas (NG) based Porous Radiant Burner (NG-PRB) operating in a partially surface-stabilized mode of operation, i.e., with blue flame above the burner surface of NG-PRB by modifying LPG-PRB presented in chapter 3. The specifications of the developed NG-PRB are presented in section 4.1. Sections 4.2 and 4.3 presents the experimental methodology and results obtained from the experiments. Further, Techno-Economic Assessment (TEA) for the developed LPG-PRB and NG-PRB is performed to predict their economic performance (section 4.4). Results obtained from TEA are presented in section 4.5. Also, Lifecycle Assessment (LCA) is performed on the developed LPG-PRB and NG-PRB to predict their environmental impacts (section 4.5). Section 4.6 presents the results obtained from LCA study. Finally, section 4.7 presents the summary that concludes this chapter.

4.1 Description of construction and working of NG-PRB

The developed NG-PRB consists of SiC foam and Al_2O_3 perforated plate housed inside a high-temperature resistant refractory casing similar to LPG-PRB presented in chapter 3. In NG-PRB, SiC foam and Al_2O_3 perforated plate act as Combustion Layer (CL) and Preheating Layer (PL), respectively. NG is supplied to the burner by an injector through a mixing pipe having no slots but with a distance between the mixing pipe entry and injector for air aspiration. NG enters at high pressure from the injector and enters the mixing pipe. Because of the venturi effect, the high-velocity NG jet creates low static pressure in the space between the mixing pipe entry and injector, which in turn causes the suction of primary air through the mixing pipe. The fuel-air mixture gets properly mixed in the mixing chamber above the mixing pipe before reaching Al_2O_3 perforated plate. The fuel-air mixture enters the Al_2O_3 perforated plate through the holes, where it is preheated and evenly distributed to SiC foam. SiC foam acts as a flame trap, thereby combusting almost most of the combustible fuel-air mixture percentage and allowing intermediate products like hydrogen and carbon monoxide to combust above the

foam. Fig. 4.1 shows the schematic of the developed NG-PRB and Table 4.1 presents its specification.

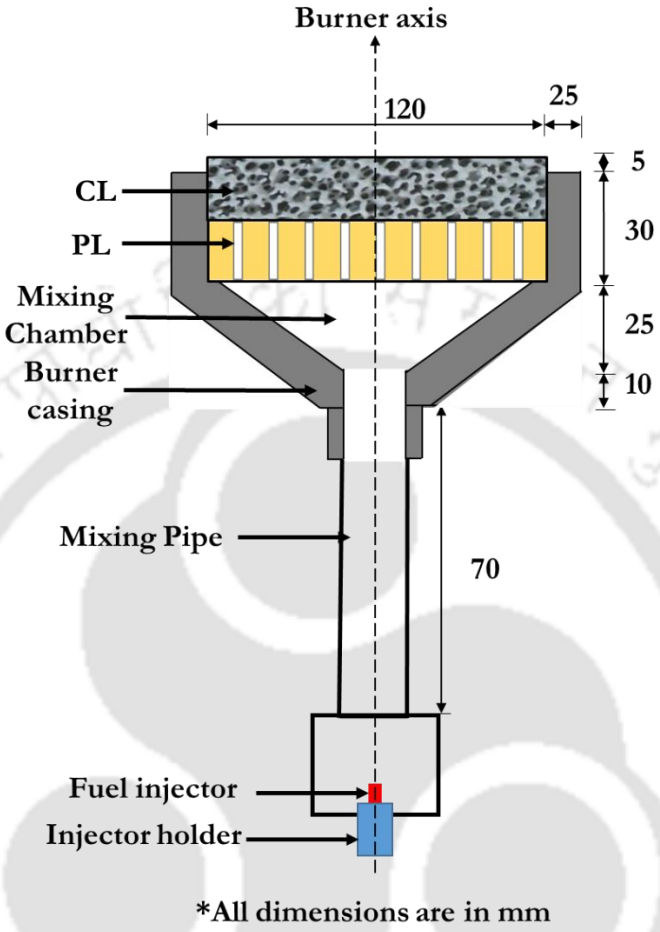

Fig. 4.1: Schematic of the developed NG-PRB

Table 4.1: Specification of the developed NG-PRB

Components	Details	Pictorial view
CL	Material: SiC foam Porosity: 45-55% (10 ppi) Thickness: 20 mm Diameter: 120 mm	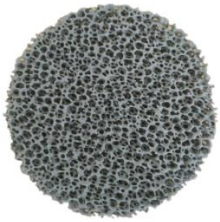

PL	Material: Al_2O_3 perforated plate Porosity: 7% Thickness: 15 mm Diameter: 120 mm	
Casing	Material: Alumina-based high-temperature resistant refractory Thickness: 25 mm	
Mixing pipe	Material: MS threaded pipe Inner diameter: 26 mm Outer diameter: 31 mm Length: 70 mm	
Injector	Injector exit diamter: 0.63 mm	

4.2 Experimental methodology

4.2.1 Experimental setup

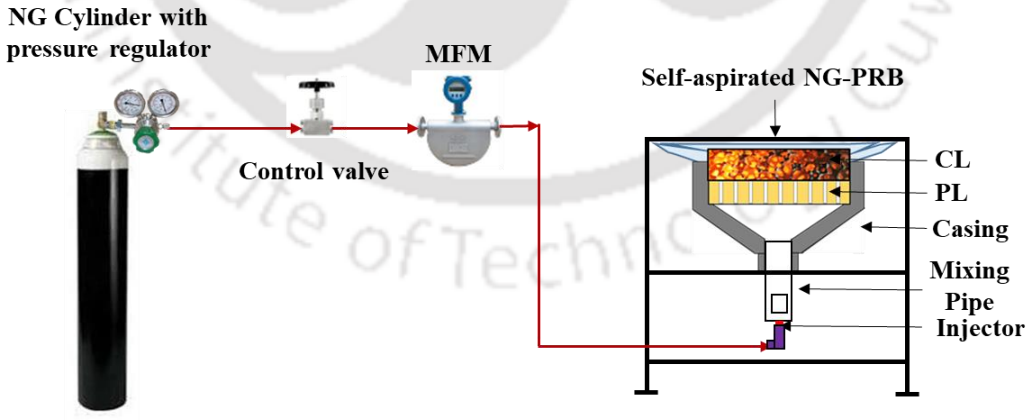

Fig. 4.2: Schematic of the experimental setup

The schematic for the experimental setup used for the present investigation is shown in Fig. 4.2. The fuel supply system consists of a cylinder containing NG, a pressure regulator, and a control valve. The flow rate of NG ($\dot{m}_{NG}$) is monitored through a Coriolis Mass Flow Meter

(MFM) having accuracy ± 0.001 g. MFM is fitted in between the fuel supply system and NG-PRB. For particular power input ($\dot{m}_{NG} \times LCV_{NG}$), the mass flow rate of NG ($\dot{m}_{NG}$) is adjusted by the control valve connected between the cylinder and MFM. The experiments were conducted for a $\dot{m}_{NG}$ range of 0.12 g/s to 0.17 g/s, equivalent to 5 to 7 kW input power.

4.2.2 Performance testing

Thermal efficiency and Emission analysis

Thermal efficiency (η_t) of NG-PRB was determined by conducting the Water Boiling Test (WBT) as per Indian Standard (IS) 14612:1999 (Prescribed by Bureau of Indian Standards). The water mass and pan dimensions employed in the present case are the same as those used for carrying out WBT in LPG-PRB. WBT for NG-PRB was conducted once the burner reached its stable state condition and continued until the temperature of water reached 90 °C. The aluminium pan of diameter 300 mm and height 150 mm was used for WBT. The total mass of the aluminium pan along with the lid was 1.078 kg. The aluminium pan was filled with 9 kg of water and inserted with a stirrer. Mass and temperature measurements were done by weighing balance (accuracy ± 0.001 g) and mercury-in-glass thermometer (accuracy ± 0.5°C), respectively. It was ensured that $\dot{m}_{NG}$ was kept constant throughout WBT. The amount of NG consumed during the test was measured using MFM. WBT was performed thrice, and the average obtained from these three test results was considered for estimating the η_t. Eq. (4.1) is used for the calculation of η_t.

$$\eta_t = \frac{\left(M \times C_p + m \times C_w\right) \times \left(T_2 - T_1\right)}{m_{NG} \times LCV_{NG}} \tag{4.1}$$

Where M is the total mass of the pan along with the lid (kg), m is the mass of water (kg), C is specific heat (kJ/kg-k, p : pan and w : water), T_2 and T_1 are the temperatures of water (°C) at the end and the start of WBT, m_{NG} is the mass of NG consumed (kg) to raise water temperature from T_1 to T_2 and LCV_{NG} is the Lower Calorific Value of NG (kJ/kg). The properties of NG used for the present study are given in Appendix-I.

Emission analysis was performed on the developed NG-PRB as prescribed by IS 14612:1999 and it was conducted as per the procedure mentioned in section 3.3.2. Figs. 3.6 and 3.7 present the arrangement used for emission analysis and the hood used for the emission analysis.

Experimental uncertainty

It is important to determine the uncertainty in the calculation of dependent parameters. The calculated values of η_t depend on the values obtained from the instruments used to measure parameters like temperature, mass of NG consumed and mass of pan and water. Using Eq. (3.2), the uncertainty in the estimation of η_t is calculated (Moffat, 1988).

$$\delta\eta_t = \sqrt{\left(\frac{\delta\eta_t}{\delta M}\Delta M\right)^2 + \left(\frac{\delta\eta_t}{\delta m}\Delta m\right)^2 + \left(\frac{\delta\eta_t}{\delta(\Delta T)}\Delta(\Delta T)\right)^2 + \left(\frac{\delta\eta_t}{\delta m_{NG}}\Delta m_{NG}\right)^2} \quad (3.2)$$

The uncertainty in the measurement of the mass of water and pan, the mass of NG consumed and temperature are ±0.1 g, ±0.001 g and ±0.5 °C, respectively.

Temperature distribution

For the determination of temperature distribution on the surface of the burner, temperatures were recorded at various radial positions on the top of CL (Fig. 4.3). The temperature measurements were done using K-type thermocouples (accuracy ± 1°C) connected to data acquisition system (Agilent make) and computer system.

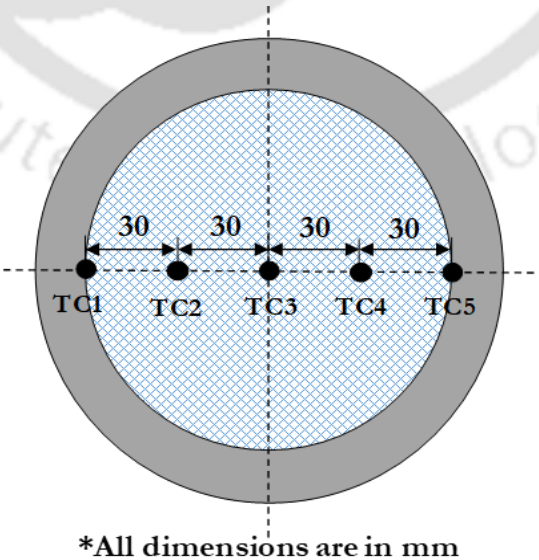

Fig. 4.3: Thermocouple arrangement for Radial temperature measurement

4.3 Results and discussion on performance testing

As explained in section 3.4, the developed NG-PRB also operates in a partially surface-stabilized mode of operation, the flame was found to be partially stabilized above CL, resulting in an efficient energy transfer by radiation and convection to the load. At 5-7 kW power input range, NG-PRB yields η_t in the range of 61.4-52.9%. An increase in power input increases the surface temperature but also significantly increases the heat loss from the burner casing. Therefore, an increment in the temperature could not necessarily overcome the effect of heat loss, which results in lower η_t at higher power input. Within an operating range of 5-7 kW, η_t for LPG-PRB varied between 69.7-63.8%, whereas the same was 61.4-52.9 % for NG-PRB. This is because LCV_{NG} is less when compared to LCV_{LPG} and presence of CO_2 in the composition of NG. Fig. 4.4 presents the η_t values of the developed NG-PRB for a power input range of 5-7 kW and its comparison with LPG-PRB.

The emission characteristics of NG-PRB were found to be the same as that of LPG-PRB. Concentrations of CO and NO_x for NG-PRB ranged between 30-43 ppm and 2.35-6 ppm, respectively. The emission indices of CO and NO_x for the studied NG-PRB are plotted in Fig. 4.5 as a function of power input. The combustion process in the partially surface-stabilized mode of operation was found to be highly efficient, with substantial heat transfer to the solid matrix, which is indicated by the low CO and the NO_x emissions. Both CO and NO_x emissions were found to increase with power input. The increasing trend of CO with escalating power input is mainly due to reduced residence time in the porous layer, which in turn leads to higher unconverted CO. The NO_x emission shows a similar trend of variation as that of the CO (Fig. 4.5).

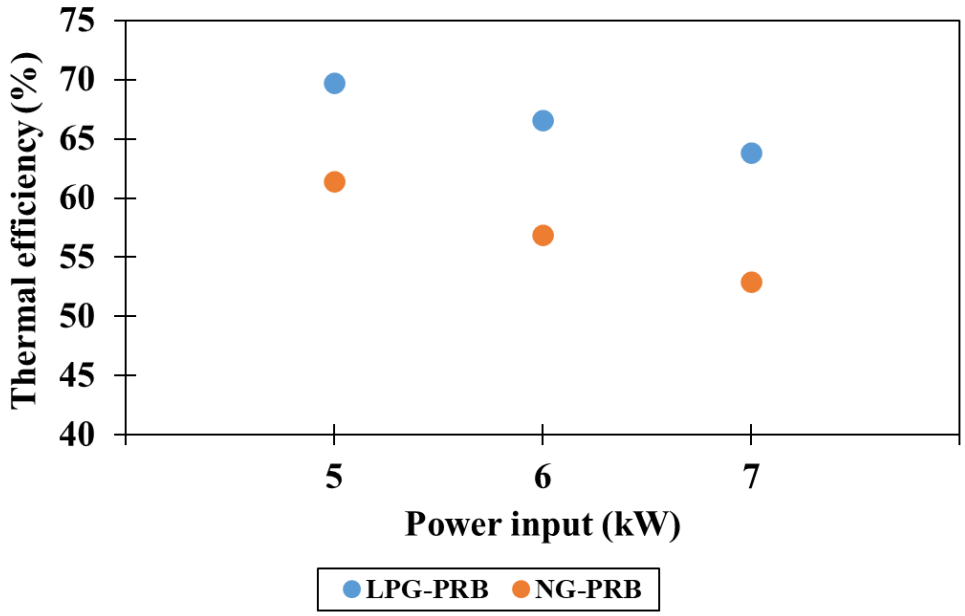

Fig. 4.4: Thermal efficiency for a power input range of 5-7 kW

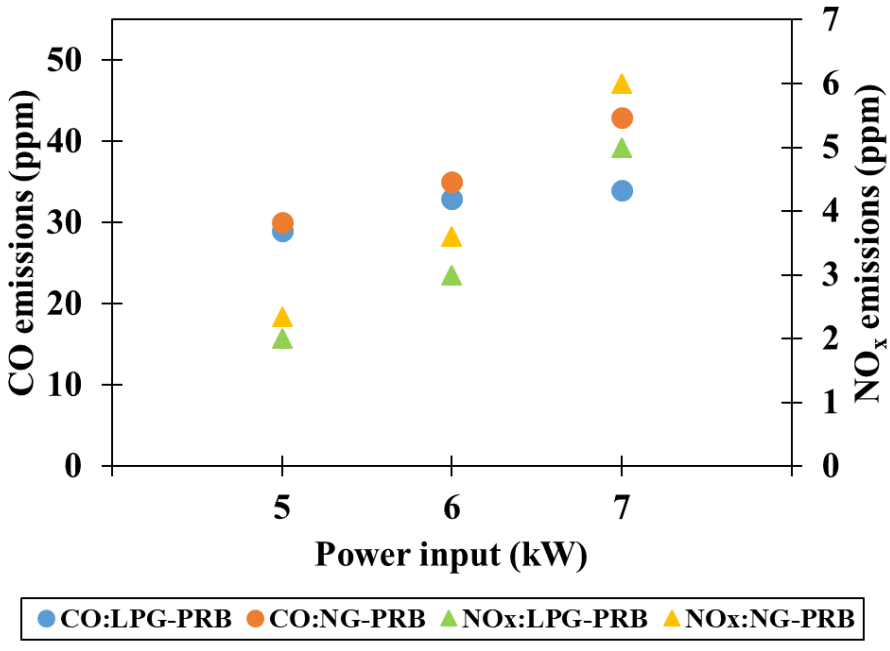

Fig. 4.5: CO and NO_x emissions for a power input range of 5-7 kW

The radial temperature distributions on the NG-PRB surface at different power inputs are shown in Fig. 4.6. In NG-PRB, the temperature is measured on the burner surface radially to ensure uniform flame stabilization within CL. It was observed that the temperature at the centre of the burner surface is high and decreases towards the periphery. The reason behind the variation of temperature from the centre to the periphery of the burner surface is the heat loss from CL to the burner casing. Maximum radial temperatures of 820 ºC, 880 ºC and 906 ºC

were observed in NG-PRB when operated at power input of 5, 6 and 7 kW, respectively. Also, the variation in temperature from the centre to the periphery of NG-PRB surface was less than 100 ºC for all power inputs.

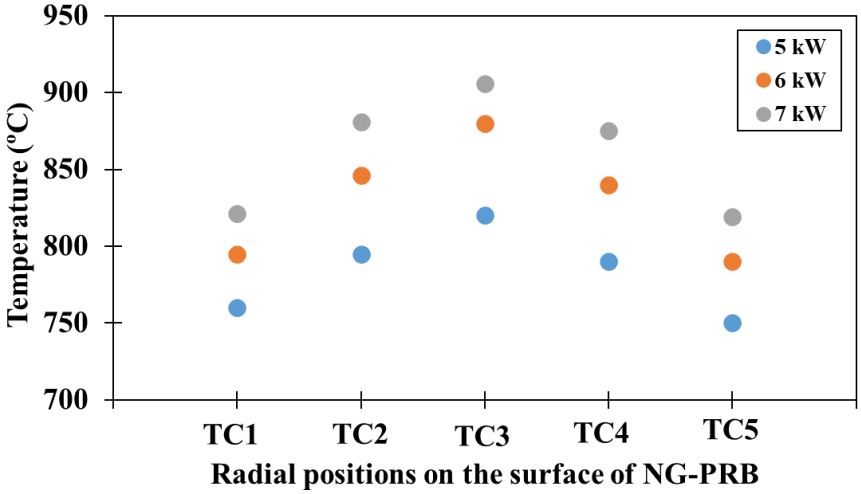

Fig. 4.6: Radial Temperature distribution on the surface of NG-PRB

4.4 Techno-Economic Assessment

Techno-Economic Assessment (TEA) is an important activity to be performed when any product or process is proposed. TEA is a cost analysis that summarizes the economic performance of any product or process. TEA provides insight into aspects of the product/process under study where further research and developments are needed. TEA analyzes the economic impact of the developed product or process when it enters a market, considering the cost of raw materials, operation, construction, etc. Different methods are followed for performing TEA depending on the product or process developed. In the present study, the direct monetary cost associated with the product, which includes purchase cost and operational costs (fuel cost and maintenance cost), is considered. The approach used for direct monetary cost comparison is based on the methods described by Kaushik (2019) and Devi (2020b). In the present study, the developed LPG-PRB (Presented in chapter 3) and NG-PRB are subjected to TEA to assess their economic impacts and compared with Liquefied Petroleum Gas based Conventional Burner (LPG-CB). The TEA method used in this study presents capital cost, life cycle cost, Accounting Rate of Return (ARR) and payback period. The parameters and equations used for TEA are summarized in Table 4.2.

Table 4.2: Formula and Description of Economic metrics considered for present TEA

Economic metrics	Formula	Description
Capital Cost (C)	-	Cost associated with the purchase of the burner
Annual operating cost (C_{OP})	$C_{OP} = C_F + C_M$ $C_F = m_F \times C_f \times N_{op}$	Cost associated with the fuel consumption and maintenance of the burner (m_F - Fuel consumption per hour; C_f - Fuel cost; N_{op} - Total annual operating hours)
Life cycle cost (C_{LC})	$C_{LC} = \frac{C}{L_{LC}} + C_{OP}$	Summation of the actual capital cost ($\frac{C}{L_{LC}}$), and operating cost (C_{OP}) of the burner (L_{LC} - Life of the system)
Annual saving (S)	$S = \left(C_{LC}\right)_{LPG/NG-PRB} - \left(C_{LC}\right)_{LPG-CB}$	Difference between the life cycle cost of LPG-PRB and LPG-CB and NG-PRB and LPG-CB.
Net Present Value (NPV)	$P_a = \frac{F_a}{(1+f)^n} \times \frac{1}{(1+I)^n}$ and $NPV = \sum_{n=0}^{n=L_{LC}} P_a$	It is used for analyzing an investment decision and positive NPV is used as the base to accept a proposed investment. (P_a -Present worth; F_a - future worth; f -inflation rate; I -Interest rate; n - Positive integer)

Payback period ($N_{LPG/NG-PRB}$)	$N_{LPG/NG-PRB} = \frac{(C - RT)}{S}$	The ratio of the amount of initial investment and estimated annual net cash flow. (RT -Running total which is assumed to be zero)
Accounting Rate of Return (ARR)	-	Profitability of the potential investment. ARR is a discount rate that makes the net present value (NPV) of all cash flows from a particular project equal to zero.

4.5 Economic impacts of the developed LPG-PRB and NG-PRB

TEA is performed for the developed LPG-PRB and NG-PRB and the values obtained from the analysis are compared with that of LPG-CB. The capital cost of LPG-CB and NG-PRB is obtained from the market survey and the capital cost of LPG-CB and NG-PRB is assessed by considering the cost of each of its components. The cost of both LPG-PRB and NG-PRB is Rs. 2375 /- which is a little high when compared to that of LPG-CB (Rs. 2100 /-). The burner components in LPG-PRB and NG-PRB namely, casing, SiC foam and Al_2O_3 perforated plate are ceramics. And the remaining components in LPG-PRB and NG-PRB are frame, injector with holder, valve with connector and feeder pipe. The components of LPG-CB are burner head, burner base, valve with injector and frame. The usage of ceramics in LPG-PRB and NG-PRB and their need for replacement periodically is the reason for their high overall cost when compared to LPG-CB. In the present analysis, the life of LPG-PRB, NG-PRB and LPG-CB is considered to be 10 years. The annual maintenance cost of LPG-PRB and NG-PRB is Rs. 725 /-, which includes Rs. 525 /- as replacement cost for ceramic components (SiC foam, Al_2O_3 perforated plate and casing). And the annual maintenance cost of LPG-CB is Rs. 200 /-.

Table 4.3 presents the results obtained from the cost analysis performed in the present TEA. By taking into account the burner's daily operating hours of 8 hours, the annual fuel cost is determined. From the annual appraisal point of view, it was found that the annual fuel cost for operating LPG-PRB at power inputs of 5 kW, 6 kW and 7 kW are Rs. 104088 /-, Rs. 124905.7

/- and Rs. 145723.3 /-, respectively. And the annual fuel cost for operating NG-PRB at power inputs of 5 kW, 6 kW and 7 kW are Rs. 86873.8 /-, Rs. 108266.4 /- and Rs. 130238.3 /-, respectively, which is less when compared to LPG-PRB. But the annual fuel cost for operating LPG-CB at power inputs of 5 kW, 6 kW and 7 kW are Rs. 133446.2 /-, Rs. 160135.5 /- and Rs. 186824.7 /-, which is high compared to LPG-PRB and NG-PRB. Because of the increase in fuel flow rate with an increase in power input, the annual fuel cost of the burners increases with an increase in power input. The annual operating costs for LPG-PRB and NG-PRB (sum of annual fuel cost and maintenance cost) operating at power inputs of 5 kW, 6 kW and 7 kW are Rs. 104813 /-, Rs. 125630.7 /- and Rs. 146448.3 /- and Rs. 87598.8 /-, Rs. 108991.4 /- and Rs. 130963.3 /-, respectively, which is low when compared to LPG-CB (5 kW: Rs. 133646.2 /-, 6 kW: Rs. 160335.5 /- and 7 kW: Rs. 187024.7 /-). Also, the Lifecycle costs of LPG-PRB (5 kW: Rs. 105050.5 /-, 6 kW: Rs. 125868.2 /- and 7 kW: Rs. 146685.8 /-) and NG-PRB (5 kW: Rs. 87836.3 /-, 6 kW: Rs. 109228.9 /- and 7 kW: Rs. 131200.8 /-) are low when compared to LPG-CB (5 kW: Rs. 133856.2 /-, 6 kW: Rs. 160545.5 /- and 7 kW: Rs. 187234.7 /-). The TEA study shows that the overall annual savings that can be obtained by using LPG-PRB when operated at power inputs of 5 kW, 6 kW and 7 kW are Rs. 28805.7 /-, Rs. 34677.3 /- and Rs. 40548.9 /-, respectively. And the overall annual savings by using NG-PRB when operated at power inputs of 5 kW, 6 kW and 7 kW are Rs. 46019.9 /-, Rs. 51316.5 /- and Rs. 56033.9 /-, respectively.

Tables 4.4 and 4.5 present the overall annual savings, present worth of annual savings and cumulative savings that can be obtained by implementation of LPG-PRB and NG-PRB operating at power inputs of 5 kW, 6 kW and 7 kW instead of LPG-CB. With an inflation rate of 6.5% and an interest rate of 8%, the annual savings and present worth of annual savings are calculated. From the cost-benefit analysis, it was observed that investing Rs. 2375 /- in LPG-PRB for commercial cooking can lead to a present cumulative worth of annual savings of Rs. 250651.8 /-, Rs. 301743.7 /- and Rs. 352835.6 /- when operated at power inputs of 5 kW, 6 kW and 7 kW, respectively. And by investing Rs. 2375 /- in NG-PRB for commercial cooking can lead to a present cumulative worth of annual savings of Rs. 400441.4 /-, Rs. 446529.4 /- and Rs. 487577.9 /- when operated at power inputs of 5 kW, 6 kW and 7 kW, respectively.

In the present TEA, ARR is calculated for the developed LPG-PRB and NG-PRB by arriving at the percentage ratio of the net gain over the original investment. The ARR of LPG-PRB was found to be 1121.64%, 1350.55% and 1579.47% when operated at power inputs of 5 kW, 6 kW and 7 kW, respectively. And the corresponding ARR of NG-PRB was found to be

1792.76%, 1999.26% and 2183.17%. With an investment of Rs. 1 /-, LPG-PRB and NG-PRB are anticipated to earn Rs. 11.2 /- and Rs. 17.9 /-, respectively and ARR of 1121.64% and 1792.76%, respectively, at a power input of 5 kW. At a power input of 6 kW, LPG-PRB and NG-PRB with ARRs of 1350.55% and 1999.26% are predicted to earn Rs. 13.5 /- and Rs. 20 /-, respectively, for an investment of Rs. 1/-. Further, at a power input of 7 kW, LPG-PRB and NG-PRB with ARRs of 1579.47% and 2183.17%, are predicted to earn Rs. 15.8 /- and Rs. 21.8 /- for an investment of Rs. 1/-. The payback period that can be achieved using LPG-PRB will be less than 30 days for all power inputs. And the payback period for NG-PRB will be less than 20 days for all power inputs. Because of higher annual savings (5 kW: Rs. 46019.9 /-, 6 kW: Rs. 51316.5 /- and 7 kW: Rs. 56033.9 /-), NG-PRB can achieve a short payback period when compared to LPG-CB. The reason for the increase in the payback period for LPG-PRB is because of the decrease in annual savings (5 kW: Rs. 28805.7 /-, 6 kW: Rs. 34677.3 /- and 7 kW: Rs. 40548.9 /-) in comparison with NG-PRB.

Table 4.3: Results obtained from Cost analysis

Economic metrics		**LPG-PRB**		**NG-PRB**		**LPG-CB**
Capital cost, C		Rs. 2375 /-		Rs. 2375 /-		Rs. 2100 /-
Life of burner, L_{LC}		10 Years		10 Years		10 Years
Annual financial appraisal						
Fuel cost, C_f	5 kW:	Rs. 104088 /-	5 kW:	Rs. 86873.8 /-	5 kW:	Rs. 133446.2 /-
	6 kW:	Rs. 124905.7 /-	6 kW:	Rs. 108266.4 /-	6 kW:	Rs. 160135.5 /-
	7 kW:	Rs. 145723.3 /-	7 kW:	Rs. 130238.3 /-	7 kW:	Rs. 186824.7 /-
Annual operating cost, C_{OP}	5 kW:	Rs. 104813 /-	5 kW:	Rs. 87598.8 /-	5 kW:	Rs. 133646.2 /-
	6 kW:	Rs. 125630.7 /-	6 kW:	Rs. 108991.4 /-	6 kW:	Rs. 160335.5 /-
	7 kW:	Rs. 146448.3 /-	7 kW:	Rs. 130963.3 /-	7 kW:	Rs. 187024.7 /-
Lifecycle cost, C_{LC}	5 kW:	Rs. 105050.5 /-	5 kW:	Rs. 87836.3 /-	5 kW:	Rs. 133856.2 /-
	6 kW:	Rs. 125868.2 /-	6 kW:	Rs. 109228.9 /-	6 kW:	Rs. 160545.5 /-
	7 kW:	Rs. 146685.8 /-	7 kW:	Rs. 131200.8 /-	7 kW:	Rs. 187234.7 /-
Annual saving	5 kW:	Rs. 28805.7 /-	5 kW:	Rs. 46019.9 /-	5 kW:	-
	6 kW:	Rs. 34677.3 /-	6 kW:	Rs. 51316.5 /-	6 kW:	-
	7 kW:	Rs. 40548.9 /-	7 kW:	Rs. 56033.9 /-	7 kW:	-

Table 4.4: Overall savings by LPG-PRB

Year	Annual savings (Rs.)			Present worth of annual savings (Rs.)			Present worth of cumulative savings (Rs.)		
	5 kW	6 kW	7 kW	5 kW	6 kW	7 kW	5 kW	6 kW	7 kW
1	28805.7	34677.3	40548.9	26671.9	32108.6	37545.3	26671.9	32108.6	37545.3
2	30678	36931.3	43184.6	26301.5	31662.7	37023.8	52973.4	63771.3	74569.2
3	32672.1	39331.9	45991.6	25936.2	31222.9	36509.6	78909.6	94994.2	111078.8
4	34795.8	41888.4	48981.1	25575.9	30789.2	36002.5	104485.5	125783.4	147081.3
5	37057.5	44611.2	52164.8	25220.7	30361.6	35502.5	129706.2	156145	182583.8
6	39466.3	47510.9	55555.6	24870.4	29939.9	35009.4	154576.7	186085	217593.3
7	42031.6	50599.1	59166.7	24525	29524.1	34523.2	179101.7	215609.1	252116.4
8	44763.6	53888.1	63012.5	24184.4	29114	34043.7	203286.1	244723.1	286160.1
9	47673.3	57390.8	67108.3	23848.5	28709.7	33570.9	227134.6	273432.8	319731
10	50772	61121.2	71470.4	23517.3	28310.9	33104.6	250651.8	301743.7	352835.6

Table 4.5: Overall savings by NG-PRB

Year	Annual savings (Rs.)			Present worth of annual savings (Rs.)			Present worth of cumulative savings (Rs.)		
	5 kW	6 kW	7 kW	5 kW	6 kW	7 kW	5 kW	6 kW	7 kW
1	46019.9	51316.5	56033.9	42611.1	47515.3	51883.3	42611.1	47515.3	51883.3
2	49011.2	54652.1	59676.1	42019.2	46855.4	51162.7	84630.3	94370.6	103045.9
3	52197	58204.5	63555.1	41435.6	46204.6	50452.1	126065.9	140575.2	153498
4	55589.8	61987.8	67686.2	40860.1	45562.9	49751.4	166926.1	186138.1	203249.4
5	59203.1	66017	72085.8	40292.6	44930	49060.4	207218.7	231068.1	252309.7
6	63051.3	70308.1	76771.3	39733	44306	48379	246951.7	275374.1	300688.7
7	67149.6	74878.1	81761.5	39181.2	43690.6	47707	286132.9	319064.8	348395.7
8	71514.4	79745.2	87076	38637	43083.8	47044.4	324769.9	362148.6	395440.2
9	76162.8	84928.6	92735.9	38100.4	42485.4	46391	362870.2	404634.1	441831.2
10	81113.4	90449	98763.7	37571.2	41895.4	45746.7	400441.4	446529.4	487577.9

4.6 Lifecycle Assessment

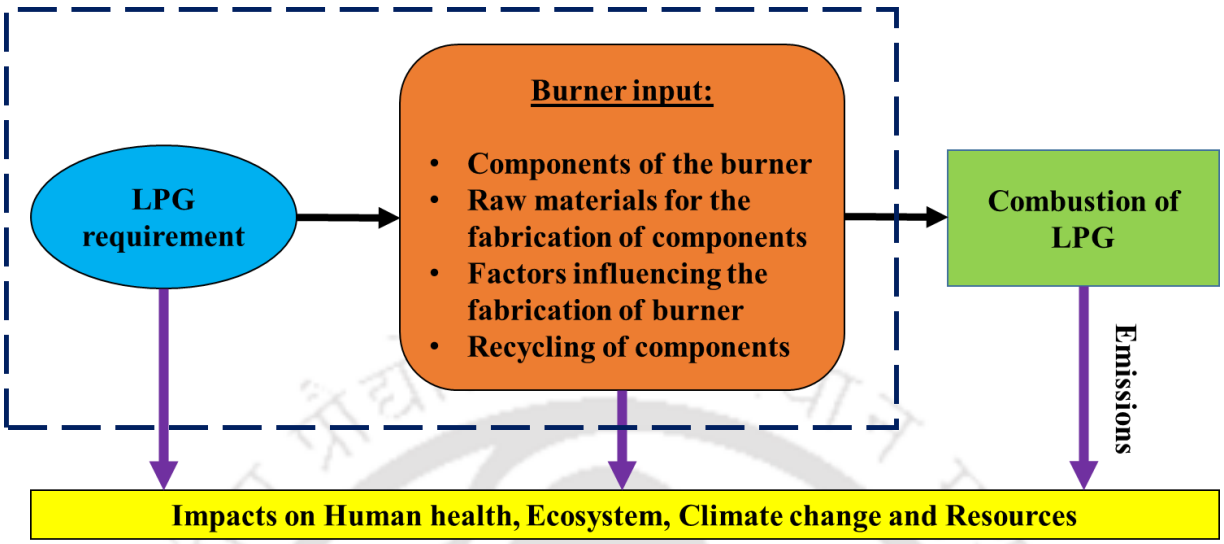

Fig. 4.7: System considered for LCA of LPG-PRB/CB

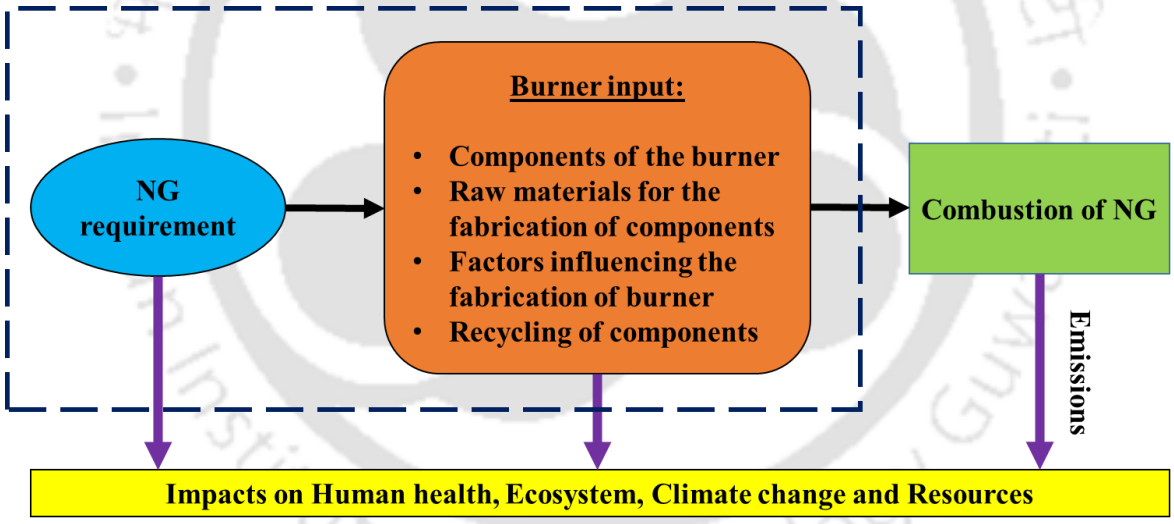

Fig. 4.8: System considered for LCA of NG-PRB

Lifecycle assessment (LCA) is a systematic model performed to determine the environmental impact caused by any product or process. LCA identifies and evaluates the environmental impacts caused by a process or a product. In LCA, material flow (inflow and outflow) and energy utilization are considered to assess the resource depletion, emissions and energy consumption of all processes, starting from transforming raw materials into useful products with by-products to their final disposal. In the present work, the environmental impact caused by LPG-PRB and NG-PRB is analyzed and compared with that of LPG-CB. Figs. 4.7 and 4.8

show the system boundary considered for the present work. For performing LCA, "SimaPro 8.3.0.0" software embedded with the "Ecoinventv3" database is used. The standard LCA method prescribed by the International Organization for Standardization, namely ISO:14040-14044, is adopted in the present work. The IMPACT 2002+ method is adopted to perform LCA for the developed LPG-PRB and NG-PRB suitable for commercial cooking applications.

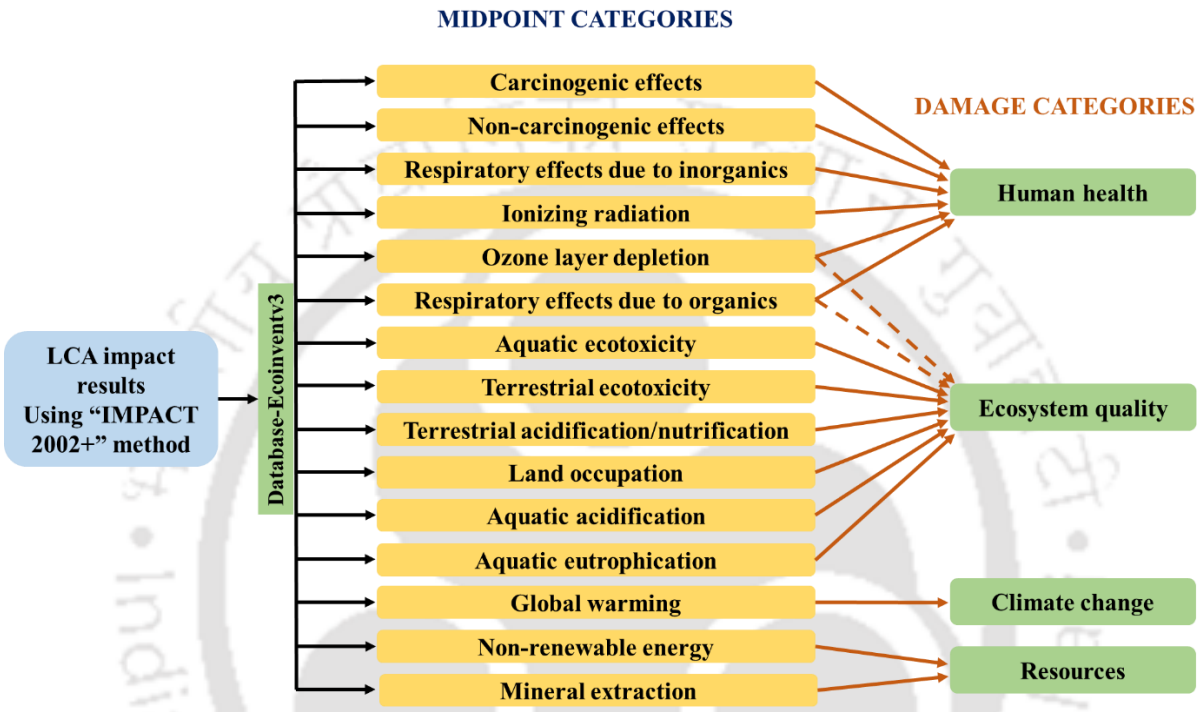

Fig. 4.9: The overall scheme of IMPACT 2002+ LCA method (Jolliet et al., 2003)

Fig. 4.9 represents the scheme of the IMPACT 2002+ method used in the present LCA study, in which the impact results are linked to 4 damage categories (Human health, Ecosystem quality, Climate change, and Resource utilization) via 15 midpoint categories (Human toxicity-carcinogenic effects, Human toxicity-non-carcinogenic effects, Respiratory effects due to inorganics, Ionizing radiation, Ozone layer depletion, Respiratory effects due to organics, Aquatic ecotoxicity, Terrestrial ecotoxicity, Terrestrial acidification/nitrification, Land occupation, Aquatic acidification, Aquatic eutrophication, Global warming, Non-renewable energy consumption and Mineral extraction) (Jolliet et al., 2003). The developed LPG-PRB and NG-PRB operating at power inputs of 5 kW, 6 kW and 7 kW suitable for commercial cooking applications are subjected to LCA study. This study considers the environmental impacts caused by the construction of LPG-PRB and NG-PRB and their operations. This analysis can provide a holistic view of LPG-PRB and NG-PRB's ability to curtail the

environmental impact compared to that of LPG-CB.

4.7 Environmental impacts of the developed LPG-PRB and NG-PRB

In this section, the environmental impacts caused by LPG-PRB, NG-PRB and LPG-CB are presented using the IMPACT 2002+ LCA method. Here, based on the efficiency of LPG-PRB, NG-PRB and LPG-PRB, the fuel needed for 10 years of operation (considering 8 hrs of operation daily) for power inputs of 5 kW, 6 kW and 7 kW is calculated. These data are used for performing the LCA using the IMPACT 2002+ method. Cookstoves with LPG-PRB, NG-PRB and LPG-CB are assessed based on the construction parts (burner, fuel supply line and frame) and input requirement for their impact on 15 midpoint categories (Figs. 4.7 and 4.8). Table 4.6 presents the impacts caused on midpoint categories by LPG-PRB, NG-PRB and LPG-CB when operated at power inputs of 5 kW, 6 kW and 7 kW. The LCA results show that the fuel requirement by LPG-PRB, NG-PRB and LPG-CB contributed more to the total impact. In both cases, the impact from the construction parts is almost equal; only the impact caused by LPG and NG consumption varied. When operated at a power input of 5 kW, the contribution to terrestrial ecotoxicity by LPG-PRB and NG-PRB are 536087.2 kg TEG soil and 10054.4 kg TEG soil, respectively. But LPG-CB operated at 5 kW power input contributed 685164.8 kg TEG soil to the same category, which is higher than LPG-PRB and far more than NG-PRB. The contributions to the terrestrial ecotoxicity category by LPG-PRB, NG-PRB and LPG-CB were found to increase with the increase in power input. When compared to LPG-PRB, NG-PRB contributes more to global warming and non-renewable energy and mineral extraction, categories. This is because of the impacts caused by the process involved in the extraction and purification of NG. Also, compared to LPG-CB, LPG-PRB and NG-PRB contributes more to mineral extraction categories. This is because of the surplus energy spent on the extraction of raw materials. It was observed that the operation of LPG-PRB and NG-PRB irrespective of the power input has less impact on all categories except the mineral extraction category when compared to that of LPG-CB. It was observed that the operation of LPG-PRB leads to a reduction in the range of 19.16%-22.05% compared to LPG-CB in all midpoint categories except the mineral extraction category. And the operation of NG-PRB leads to a reduction in the range of 4.1%-91.1% compared to LPG-CB in all midpoint categories except the mineral extraction category.

Fig. 4.10 represents the comparative assessment of the impact caused by LPG-PRB, NG-PRB and LPG-CB on the damage category in the IMPACT 2002+ LCA method. It was found that the operation of LPG-PRB and NG-PRB irrespective of power input, have a lower environmental impact than LPG-CB in all categories. It must be noted that the impact on the environment is considered from cradle to gate, i.e., from the fuel production stage to the consumption stage via the transportation stage. Another observation from the LCA analysis highlights that the environmental impacts from the construction of cookstoves with LPG-PRB, NG-PRB and LPG-CB are very less compared to the impacts from the energy consumption of the burners, which highlights the importance of employing an efficient burner to curb the overall environmental impact caused by cookstoves. For a considered lifetime of 10 years and 8 hrs of daily cooking, the impact caused by LPG-PRB accounts for the reduction in the range of 21.07%-21.33%, 21.76%-21.82%, 20.79%-21.14% and 21.86%-21.90% in human health, ecosystem quality, climate change and resource utilization damage categories, respectively when operated at power input range of 5-7 kW. And the same for the operation of NG-PRB is 80.27%-79.54%, 97.61%-97.72%, 7.98%-1.89% and 7.6%-1.1% respectively. In the ecosystem quality damage category, the operation of LPG-PRB, NG-PRB and LPG-CB at a power input of 5 kW accounts for about 5040.56 PDF*m^2*yr, 154.25 PDF*m^2*yr and 6442.56 PDF*m^2*yr, respectively. And the impacts on the ecosystem quality damage category increased with an increase in power input because of the increase in fuel consumption. Among the three burners, NG-PRB contributed the least to the ecosystem quality damage category and LPG-PRB contributed less than LPG-CB. Also, in the resources utilization damage category, LPG-PRB, NG-PRB and LPG-CB at a power input of 5 kW accounts for about 473123.34 MJ, 559455.42 MJ and 605457.32 MJ of primary energy utilization, respectively. In this category, the contribution of impact by LPG-PRB is found to be the least and NG-PRB contributed less when compared to LPG-CB. Thus, from the IMPACT 2002+ LCA analysis, it was understood that LPG-PRB and NG-PRB are environmentally superior to LPG-CB, as the overall impact of LPG-PRB and NG-PRB is less compared to LPG-CB.

Table 4.6: Contribution to midpoint categories

Midpoint category	Unit	LPG-PRB			NG-PRB			LPG-CB		
		5 kW	6 kW	7 kW	5 kW	6 kW	7 kW	5 kW	6 kW	7 kW
Carcinogens	kg $C_2H_3Cl_{-eq}$	59.52801	70.74709	81.96611	3.739893	3.815514	3.893183	73.63924	88.02263	102.406
Non-carcinogens	kg $C_2H_3Cl_{-eq}$	172.5605	206.1141	239.6674	7.12484	7.698943	8.288589	218.3007	261.3179	304.3351
Respiratory inorganics	kg $PM2.5_{-eq}$	7.911008	9.451729	10.99244	2.171874	2.65562	3.152462	10.02927	12.00455	13.97983
Ionizing radiation	Bq $C\text{-}14_{-eq}$	193988.8	232833.4	271677.8	18721.14	23388.74	28182.71	248885.2	298685.8	348486.4
Ozone layer depletion	kg $CFC\text{-}11_{-eq}$	0.005755	0.006905	0.008055	6.58E-05	8.02E-05	9.5E-05	0.007371	0.008845	0.010319
Respiratory organics	kg C_2H_{4-eq}	7.574767	9.07905	10.58333	3.5437	4.403194	5.285958	9.659188	11.58775	13.51631
Aquatic ecotoxicity	kg TEG water	1888714	2264131	2639546	89075.44	108145.1	127731	2415324	2896626	3377928
Terrestrial ecotoxicity	kg TEG soil	536087.2	642107.1	748126.4	10054.4	11055.42	12083.54	685164.8	821087.4	957009.9
Terrestrial acid/nutrification	kg SO_{2-eq}	123.9983	148.4675	172.9366	50.81136	62.91672	75.34981	157.4926	188.8633	220.234
Land occupation	m^2org.arable	528.7494	634.0758	739.4016	15.9659	19.37563	22.87767	676.9437	811.9771	947.0105
Aquatic acidification	kg SO_{2-eq}	42.62406	51.06448	59.50485	17.37058	21.54414	25.8307	54.30827	65.12928	75.9503
Aquatic eutrophication	kg PO_4 P-lim	2.741142	3.279013	3.816882	0.066841	0.070546	0.074351	3.500547	4.190123	4.8797
Global warming	kg CO_{2-eq}	3613.262	4319.24	5025.214	4197.636	5210.772	6251.337	4561.813	5466.911	6372.008
Non-renewable energy	MJ primary	473051.1	567435.4	661819.2	559377.4	696845.7	838035.8	605407.9	726413.1	847418.2
Mineral extraction	MJ surplus	72.25009	71.71986	71.18964	78.04263	78.81621	79.61072	49.39882	48.71905	48.03927

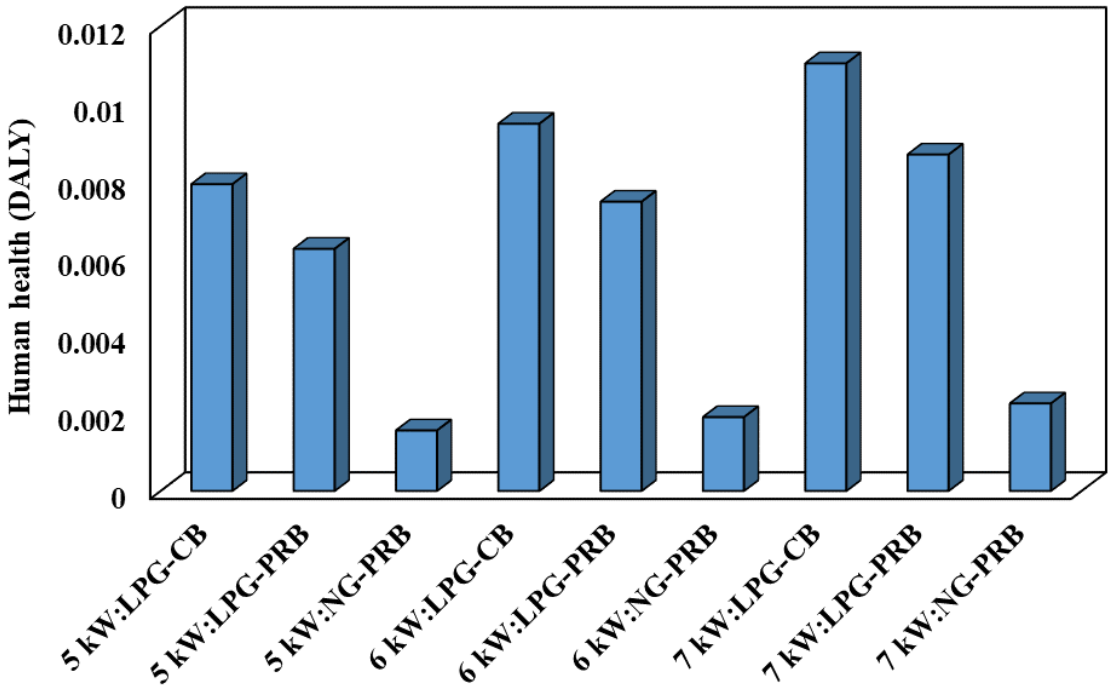

(a) Impact of LPG-CB and NG–PRB on Human health

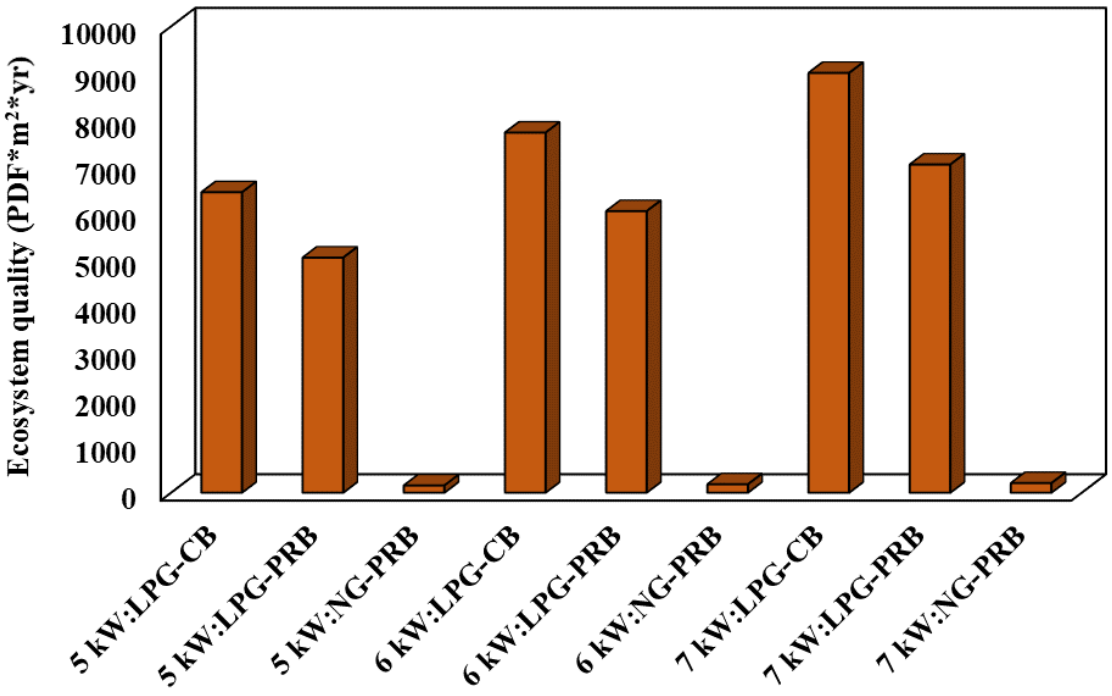

(b) Impact of LPG-CB and NG–PRB on Ecosystem quality

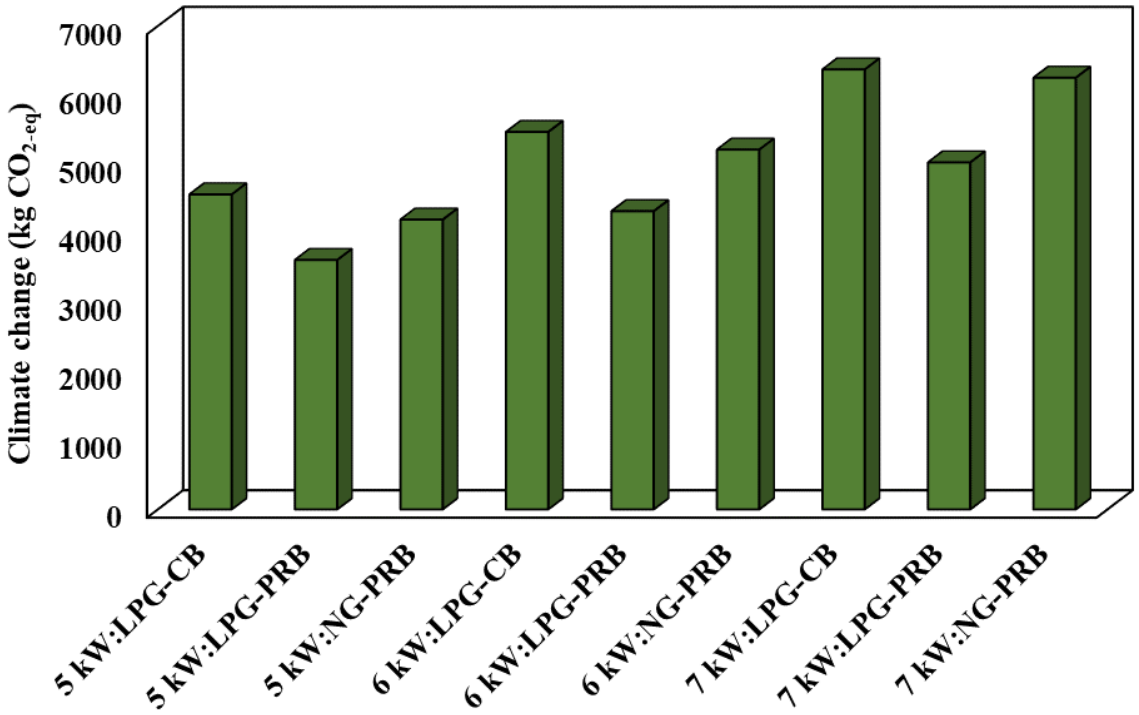

(c) Impact of LPG-CB and NG–PRB on Climate change

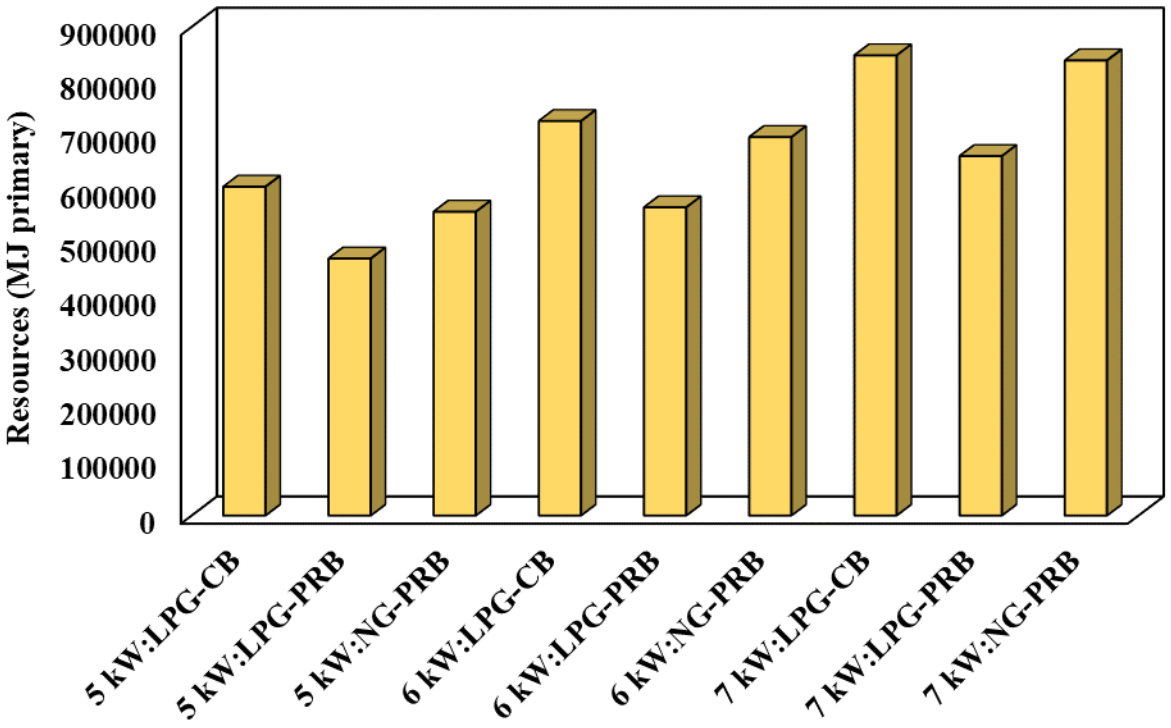

(d) Primary energy requirement by LPG-CB and NG–PRB

Fig. 4.10: The overall impact of LPG-CB and NG–PRB

4.8 Summary

This chapter presents NG-PRB developed by modifying LPG-PRB presented in chapter 3. The developed NG-PRB operates in a partially surface-stabilized mode of operation. Following the procedures prescribed by IS 14612:1999, WBT and emission analysis were performed. From the WBT results, it was observed that NG-PRB has higher thermal efficiency in the range of 61.4%-52.9% and produces lesser emissions (CO: 30-43 ppm and NO_x:3.5-6 ppm) compared to LPG-CB for a power input range of 5-7 kW. Using K-type thermocouples, thermal mapping on the surface of NG-PRB was performed to understand the behavior of NG-PRB. The Surface temperatures in NG-PRB were observed to be less when compared to LPG-PRB because of the less *LCV* of Natural gas compared to LPG. Also, the variation in temperature from the centre to the periphery of NG-PRB surface was less than 100 ºC for all power inputs. In addition to that, TEA and LCA have been performed on the developed LPG-PRB and NG-PRB and the results are compared with that of LPG-CB. The annual maintenance cost of LPG-PRB and NG-PRB is Rs. 725 /-, which includes Rs. 525 /- as replacement cost for ceramic components (SiC foam, Al_2O_3 perforated plate and casing). It was understood that LPG-PRB and NG-PRB are superior to LPG-CB in both economic and environmental aspects. From the TEA results, it was observed that the implementation of developed LPG-PRB instead of LPG-CB can lead to an annual saving of Rs. 28805.7 /-, Rs. 34677.3 /- and Rs. 40548.9 /- when operated at power inputs of 5 kW, 6 kW and 7 kW, respectively. And the implementation of developed NG-PRB instead of LPG-CB can lead to an annual saving of Rs. 46019.9 /-, Rs. 51316.5 /- and Rs. 56033.9 /- when operated at power inputs of 5 kW, 6 kW and 7 kW, respectively. Further from the LCA results, it observed that LPG-PRB accounts for the reduction in the range of 21.07%-21.33%, 21.76%-21.82%, 20.79%-21.14% and 21.86%-21.90% in human health, ecosystem quality, climate change and resource utilization damage categories, respectively when operated at power input range of 5-7 kW. And the same for the operation of NG-PRB is 80.27%-79.54%, 97.61%-97.72%, 7.98%-1.89% and 7.6%-1.1%, respectively.

The developed PRBs have been tested in commercial kitchens in many reputed institutes and restaurants. The PRBs were tested in a real-time scenario in the kitchens by cooking a regular food menu where the caterers used different burners, like T-22, G-35, etc. for cooking applications. The developed PRBs performed better than the existing burners and showed 30-40% fuel savings.

The real-time testing of the developed PRBs has been performed in the following institutes:

- Indian Institute of Technology Tirupati, Andhra Pradesh
- Indian Institute of Information and Technology Kanchipuram, Tamil Nadu
- Anna University-CEG campus, Tamil Nadu
- Anna University-MIT campus, Tamil Nadu
- Pondicherry University, Pondicherry

Indian Institute of Technology Tirupati
Andhra Pradesh

Pondicherry University
Pondicherry

Coimbatore Institute of Technology
Tamil Nadu

Anna University-MIT campus
Tamil Nadu

Indian Institute of Information and
Technology Kanchipuram
Tamil Nadu

Anna University-CEG campus
Tamil Nadu

Fig. 4.11: Real-time testing of the developed PRBs in various institutes

CHAPTER 5

DEVELOPMENT AND PERFORMANCE ASSESSMENT OF BIOGAS BASED POROUS RADIANT BURNER FOR DOMESTIC COOKING

Preface

Chapter 5 presents a Biogas based Porous Radiant Burner (BG-PRB) operating in a partially surface-stabilized mode of operation, i.e., with a secondary blue flame above the red hot surface of BG-PRB for domestic cooking. The specifications of the developed BG-PRB are presented in section 5.1. The developed BG-PRB operates in a self-aspirated mode using the biogas directly supplied from the biogas digester. Sections 5.2 and 5.3 present the experimental and numerical methodology adopted for investigating the performance of the developed BG-PRB. Results obtained from the experimental investigation and numerical simulation are presented in section 5.4. In addition, Techno-economic Assessment (TEA) and Lifecycle Assessment (LCA) were performed for the developed BG-PRB to assess their economic and environmental impact. The methodologies adopted to perform TEA and LCA are presented in sections 5.5 and 5.6, and the results obtained from TEA and LCA are presented in sections 5.7 and 5.8. Finally, the overall conclusion of this specific thesis work is presented in section 5.9.

5.1 Description of construction and working of BG-PRB

The developed BG-PRB consists of SiC foam and Al_2O_3 perforated plate housed inside a high-temperature resistant refractory casing. SiC foam and Al_2O_3 perforated plate act as Combustion Layer (CL) and Preheating Layer (PL), respectively. The high-temperature resistant refractory casing prevents heat loss to the surroundings. Biogas is supplied to the burner through an injector via a mixing pipe without any slots. The mixing pipe has no air slots because less primary air entrainment is needed for the proper combustion of biogas. Biogas enters at high pressure from the injector and enters the mixing pipe. Because of the venturi effect, the high-velocity biogas jet creates a low static pressure near the inlet of the mixing pipe, which in turn causes the suction of primary air through the inlet of the mixing pipe. The fuel-air mixture gets properly mixed in the mixing chamber before reaching PL. The fuel-air mixture enters the Al_2O_3 perforated plate through the holes, where it is preheated and evenly distributed to SiC foam. SiC foam acts as a flame trap, thereby combusting almost most of the combustible fuel-

air mixture percentage and allowing intermediate products like hydrogen and carbon monoxide to combust above the foam. Fig. 5.1 shows the schematic of the developed BG-PRB and Table 5.1 presents its specification.

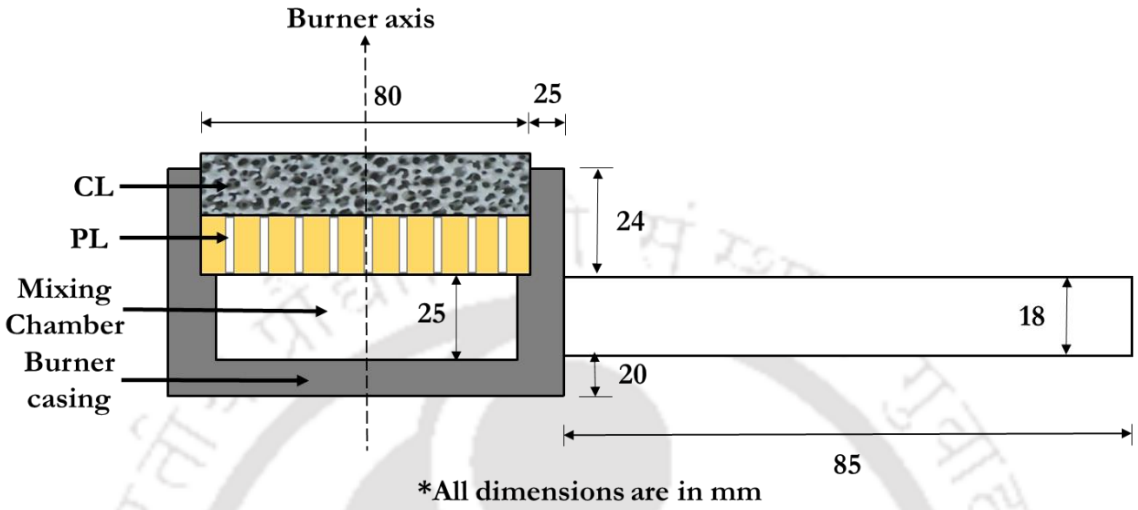

Fig. 5.1: Schematic of the developed BG-PRB

Table 5.1: Specification of the developed BG-PRB

Components	Details	Pictorial view
CL	Material: SiC foam Porosity: 45-55% (10 ppi) Thickness: 15 mm Diameter: 80 mm	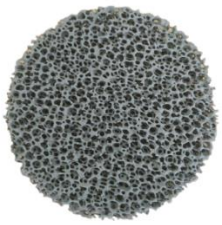
PL	Material: Al_2O_3 perforated plate Porosity: 25% Hole diameter- 2 mm Thickness: 12 mm Diameter: 80 mm	
Casing	Material: Alumina-based high-temperature resistant refractory Thickness: 15 mm	

Mixing pipe	Material: MS pipe Inner diameter: 18 mm Length: 110 mm	
Injector	Diameter: 1.5 mm	
Valve	Type: Needle type	

5.2 Experimental methodology

5.2.1 Experimental setup

The schematic of the experimental setup used for assessing the performance of BG-PRB is shown in Fig. 5.2. The BG-PRB is connected to a fuel supply line comprising of a biogas flow meter, control valve and 3 m^3 biogas digester in series. The biogas is supplied from the biogas digester through a control valve and a biogas flow meter. The control valve is used to control the flow rate of biogas and the biogas flow meter is used to measure the amount of biogas consumed by BG-PRB in operation. Biogas reaches BG-PRB through an orifice fitted in the fuel inlet line of the cookstove. Biogas jet enters the mixing tube of BG-PRB along with primary air. The entrainment of air along with the biogas jet in the mixing tube is mainly due to the venturi effect. Biogas–air mixture gets completely mixed before reaching Al_2O_3 perforated plate. The stable operation of BG-PRB is indicated by the complete red-hot top surface.

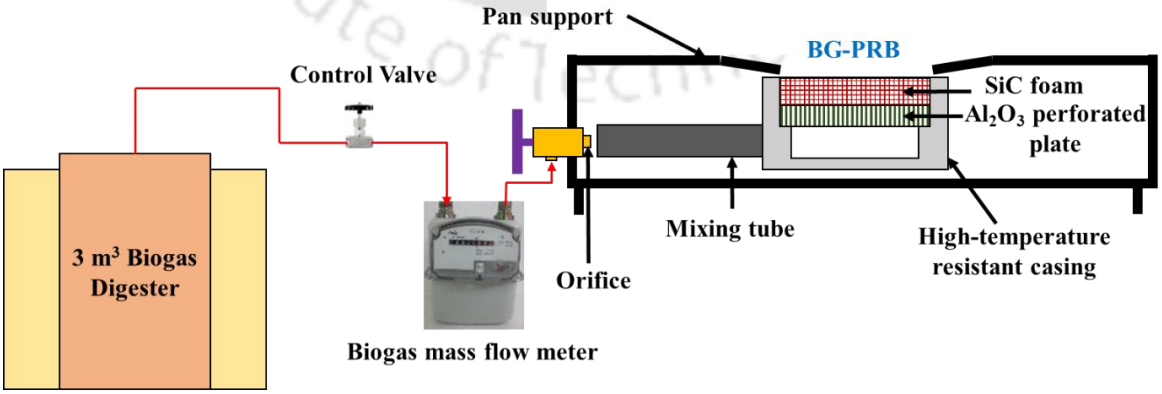

Fig. 5.2: Schematic of the experimental setup

5.2.2 Performance testing

The performance of the BG-PRB is assessed in terms of Thermal efficiency (η_t), CO emission and thermal mapping. The performance of BG-PRB is compared with Biogas based Conventional Burner (BG-CB). The arrangements used for measuring the above-mentioned parameters are discussed in the forthcoming sections.

Thermal efficiency and emission analysis

The thermal efficiency (η_t) of BG-PRB and BG-CB was determined by conducting the Water Boiling Test (WBT) as per IS 8749:2002 (Fig. 5.3) and the details of pan size and mass of water for different biogas flow rates are presented in Appendix–II. The specifications of BG-CB are given in Appendix-III. WBT for BG-PRB and BG-CB was conducted once the burner reached its stable state condition and continued until the temperature of water reached 90 °C. Based on the biogas flow rate, the dimensions of the pan and mass of water were selected to perform WBT (Table 5.2). Mass and temperature measurements were done by weighing balance (accuracy ± 0.001 g) and mercury-in-glass thermometer (accuracy ± 0.5°C), respectively. It was ensured that the flow rate of biogas was kept constant throughout WBT. The amount of biogas consumed during the test was measured using the biogas mass flow meter. WBT was performed thrice, and the average obtained from these three test results was considered for estimating the η_t (Eq. (5.1)).

$$\eta_t = \frac{\left(M \times C_p + m \times C_w\right) \times \left(T_2 - T_1\right)}{m_{BG} \times LCV_{BG}} \tag{5.1}$$

Where M is the total mass of the pan along with the lid (kg), m is the mass of water (kg), C is specific heat (kJ/kg-K, p : pan and w : water), T_2 and T_1 are the temperatures of water (°C) at the end and the start of WBT, m_{BG} is the mass of biogas consumed (kg) to raise water temperature from T_1 to T_2 and LCV_{BG} is the Lower Calorific Value of biogas (kJ/kg). The properties of biogas used for the present study are given in Appendix-I.

Table 5.2: Dimensions of pan and mass of water for performing WBT

Biogas flow rate (l/h)	**Pan diameter (mm)** (± 5 Percent)	**Pan height (mm)** (± 5 Percent)	**Mass of water in Pan (kg)**
0-240	180	100	2
246-300	205	110	2.8

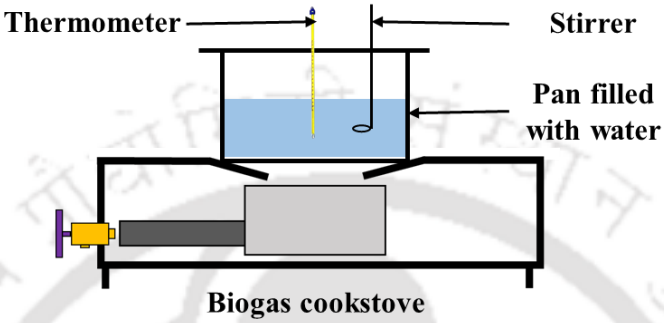

Fig. 5.3: Schematic of the arrangement used for the determination of η_t

In the present study, BG-PRB is explored for domestic cooking applications, for which the measurement of emissions is important, as the user is in direct contact with the burner. In the present case, CO emission from BG-PRB is measured and the values are taken on a dry basis, with a correction to 3% oxygen level. TESTO 350 flue analyzer is used for measuring the CO emissions from both BG-PRB and BG-CB following the protocols specified in IS 8749:2002 (Fig. 5.4). The hood shown in Fig. 3.7 is used in the emission analysis.

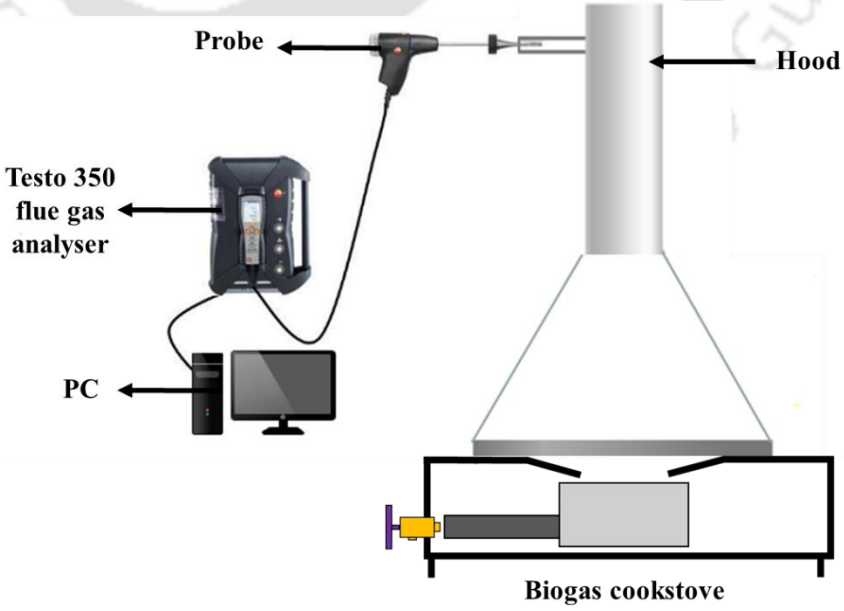

Fig. 5.4: Schematic of the arrangement used for the determination CO emission

Arrangement for thermal mapping

For measuring the temperature distribution in both the axial direction and surface of BG-PRB, calibrated K-type thermocouples having accuracy ± 1°C, the arrangement shown in Fig. 5.5, were used. The outputs of all thermocouples were connected to a data acquisition system (Agilent make) and computer system.

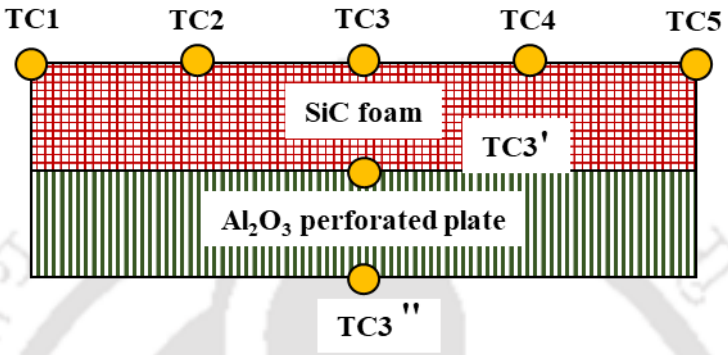

Fig. 5.5: Thermocouple arrangement for surface and axial temperature measurement

Uncertainty analysis

It is important to determine the uncertainty in the calculation of dependent parameters in any experimental investigation. Using the below formula, the error associated with the estimation of η_t is calculated as per the procedure proposed by Moffat, 1988.

$$\delta\eta_t = \sqrt{\left(\frac{\delta\eta_t}{\delta m_{pan}}\Delta m_{pan}\right)^2 + \left(\frac{\delta\eta_t}{\delta m_{water}}\Delta m_{water}\right)^2 + \left(\frac{\delta\eta_t}{\delta(\Delta T)}\Delta(\Delta T)\right)^2 + \left(\frac{\delta\eta_t}{\delta m_{BG}}\Delta m_{BG}\right)^2} \quad (5.2)$$

The uncertainty in the measurement of the mass of water and pan, the mass of biogas consumed and temperature are ±0.1 g, ±0.002 m^3 and ±0.5 °C, respectively.

5.3 Numerical methodology

Fig. 5.6 represents the computational domain considered (BG-PRB) in the present numerical simulation. BG-PRB consists of a mixing chamber, Preheating layer (PL) and Combustion Layer (CL). To simplify the process, the following assumptions are considered.

- Simulations are carried out for a steady flow process, and buoyancy effects and thicknesses of the walls are neglected.
- Solids are considered to be non-catalytic, homogeneous and non-reactive with gas.
- The gases are considered to be incompressible ideal gases.
- Thermo-physical properties of solids, like specific heat capacity, density and thermal conductivity are considered constant.

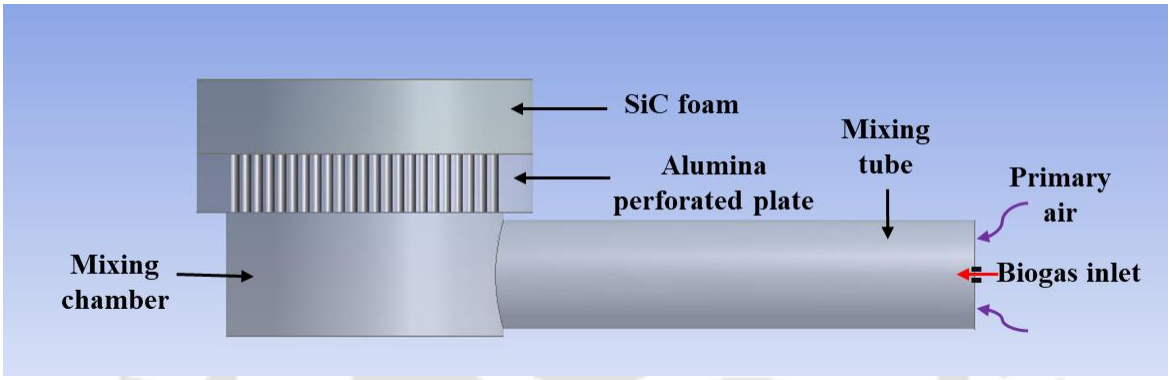

Fig. 5.6: Computation domain considered in the present study

5.3.1 Governing equations

Considering the above-mentioned assumptions, ANSYS 17.2 FLUENT software solves the differential equations listed in Table 3.2 to simulate the combustion.

Table 5.3: Equations solved in the numerical simulation

Equations			Representations
Continuity equation	$\nabla.(\rho_g \vec{u}\varphi) = 0$	(5.3)	**Symbols**
Momentum equation	For MZ and PL $\nabla.(\varphi\rho_g \vec{u}\vec{u}) = -\varphi\nabla P + \nabla.(\varphi\mu\nabla\vec{u})$	(5.4)	ρ Density $\vec{u}$ Velocity vector φ Porosity P Pressure K_1 Permeability of Porous medium C_2 Inertial resistance factor T Temperature k Thermal conductivity
	For CZ $\nabla.(\varphi\rho_g \vec{u}\vec{u}) = -\varphi\nabla P + \nabla.(\varphi\mu\nabla\vec{u})$ $-\left(\frac{\mu}{K_1}\vec{u} + C_2\frac{1}{2}\rho_g\lvert\vec{u}\rvert\vec{u}\right)$	(5.5)	
	Gas-phase		

Energy equation	$\varphi\nabla.(\mathrm{C}_g\ \rho_g T_g \vec{u}) = -\varphi\nabla\left(K_g + \mathrm{C}_g\ \rho_g D_t\right)\nabla T_g - \varphi\sum \dot{w}_i h_i W_i - h_v\left(T_g - T_s\right)$	(5.6)
	Solid-phase	
	$k_s\nabla.(\nabla T_s) - h_v\left(T_s - T_g\right) = 0$	(5.7)
Species conservation equation	$\nabla.(\rho_g\ \vec{u}\, Y_i) = -\nabla.(\rho_g D_m)\nabla Y_i + \dot{w}_i W_i$	(5.8)

C	Specific heat capacity
D_t	Thermal diffusivity
D_m	Mass diffusivity
$\dot{w}$	Molar rate of production
h	Molar enthalpy
W	Molecular mass
h_v	Volumetric heat transfer coefficient
Y	Mass fraction

Subscript

g	Gas
s	Solid
i	Species

5.3.2 Combustion reaction

Eq. (5.9) represents the chemical reaction considered for the numerical simulation. In the present study, Biogas is considered to contain only methane (CH_4) and carbon dioxide (CO_2). Also, a Single-step combustion reaction of methane with CO_2 as diluent is considered. Eddy dissipation model is adopted for calculating the rate of reaction.

$$CH_4 + CO_2 + 2O_2 \rightarrow 2CO_2 + 2H_2O \qquad (5.9)$$

5.3.3 Boundary conditions

The following boundary conditions are considered for the numerical simulation:

I. Fuel inlet (Mass flow inlet)

$\dot{m}_{BG}$ = 0.00006 kg/s (Low power) and 0.0001 kg/s (High power); Y_{CH_4}=0.308; Y_{CO_2}= 0.692

II. Air inlet (Inlet Vent)

Y_{O_2} = 0.233; Y_{N_2} = 0.767

III. Outlet (Pressure outlet)

P_{gauge} (Gauge pressure) = 0; T= 300 K

IV. Walls (SiC Foam)

$$Q_w = -\varepsilon\sigma\left(T_g{}^4 - T_a{}^4\right) - h_c\left(T_g - T_a\right) \tag{5.10}$$

In Eq. (5.10), Q_w, ε, σ, h_c and T_a denote wall heat transfer, emissivity, Stefan-Boltzmann constant, convective heat transfer coefficient and ambient temperature, respectively.

5.3.4 Computation method

In the present study, ANSYS 17.2 FLUENT software is used to solve continuity, momentum, species conservation and energy equations employing the finite volume method. The pressure-velocity coupling is achieved by SIMPLE algorithm and first-order upwind discretization scheme is employed to solve the governing equations.

5.4 Results and discussion

5.4.1 Determination of thermal efficiency and emissions of BG-PRB

η_t and CO emissions from BG-PRB and BG-CB are measured as per IS 8749:2002 protocol. As explained in section 3.4, the developed BG-PRB also operates in a partially surface-stabilized mode of operation, the flame was found to be partially stabilized above CL, resulting in an efficient energy transfer by radiation and convection to the load. From WBT, it was noted that at high power setting (biogas flow rate of 300 L/h), η_t of BG-PRB was found to be 50.5% and the same was 51.1% at low power setting (biogas flow rate of 180 L/h). The decrease in η_t with an increase in power input is due to the increase in heat loss to the surroundings. Whereas η_t of BG-CB at similar power settings were 47.2% and 46.1%, respectively. And it is less when compared to BG-PRB and this variation in the trend is due to flame height. In BG-CB, at low power setting, the flame height is less when compared to the flame height at high power setting, which leads to more convective heat loss to the surroundings. The relative uncertainty in η_t was less than 1 % for all cases. From the emission analysis, It was found that the CO emissions from BG-PRB at low and high power settings were found to be 447 and 513 ppm, respectively, which is less when compared to BG-CB, whose corresponding values were

622 and 816 ppm, respectively. The reason behind the low CO emission in BG-PRB is the higher local temperature and increased residence time of the fuel-air mixture inside SiC foam (CL) which reduces the formation of intermediate CO molecules in the combustion of the fuel-air mixture.

5.4.2 Determination of temperature distribution in BG-PRB

As explained in section 5.3, the temperature distribution in BG-PRB was measured using k-type thermocouples connected to a data logger and a computer in series. Thermal mapping is performed when BG-PRB reaches a stable steady state using the arrangement shown in Fig. 5.5. From the experimental results, it was observed that along the axial direction, higher temperatures were recorded at the interface of SiC foam and Al_2O_3 perforated plates and it gradually decreased towards the top surface of SiC foam (for both high and low power input). This indicates that the combustion of the fuel-air mixture is concentrated more in the region above the interface of the SiC foam and Al_2O_3 perforated plate, which can be clearly understood from Fig. 5.7 ((a) and (b)). The maximum temperature at the interface of BG-PRB was observed to be 1020 ºC at high power setting and the corresponding value at low power setting was 959 ºC. Also, it was observed that along the surface of BG-PRB, the maximum temperature was observed at the centre and decreased towards the periphery (Fig. 5.8). The reason behind such temperature variation across the surface of BG-PRB is the heat loss to the casing by conduction and circular geometry of BG-PRB in which the resistance to the flow of fuel-air mixture is less in the centre when compared to other regions. At low power setting, the maximum surface temperature of 692 ºC was experienced at the centre and high power setting, the same was 752 ºC. Also, the corresponding temperature difference at the surface of BG-PRB from the centre to the periphery was 51 ºC and 39 ºC, respectively. In addition, a blue flame (flame height less than 80 mm) was observed above the top surface of SiC foam, which indicates the combustion of intermediate Carbon monoxide, Hydrogen and other intermediate products formed in the combustion of the fuel-air mixture inside SiC foam. Hence, it can be understood that there is partial combustion happening above the top surface of SiC foam.

In addition to that numerical simulations using ANSYS 17.2 FLUENT were performed and the values were validated with experimental values. Numerical simulation helps in predicting the temperature distribution inside BG-PRB, which in turn helps in confirming the safe operation of BG-PRB. When the local temperature at the entry of the Al_2O_3 perforated plate is less than the auto-ignition temperature of the fuel, it is ensured that there is no possibility of a flashback.

In the present study, both the experimental study and numerical simulation results show that the temperature at the entry of the Al_2O_3 perforated plate is less than the auto-ignition temperature of biogas fuel (650 ºC). Also, the maximum temperature within the SiC foam indicates that the combustion of the biogas-air mixture is taking place inside the voids of the SiC foam indicating the stable operation of BG-PRB. The variations in temperature values are less than 50 ºC for all considered cases. Moreover, the computational domain and the numerical models were simplified based on assumptions, due to which the heat loss from the outlet and the walls was not exactly predicted. To prove the consistency of the model, a grid independence test was performed and the temperature value at the centre of the SiC foam (T3) for low power setting was compared. It was found that in the computational domain containing 799627, 667956 and 596945 elements, the variation in T3 was less than 5 ºC. Hence the numerical simulations were performed for the computational domain having 667956 elements.

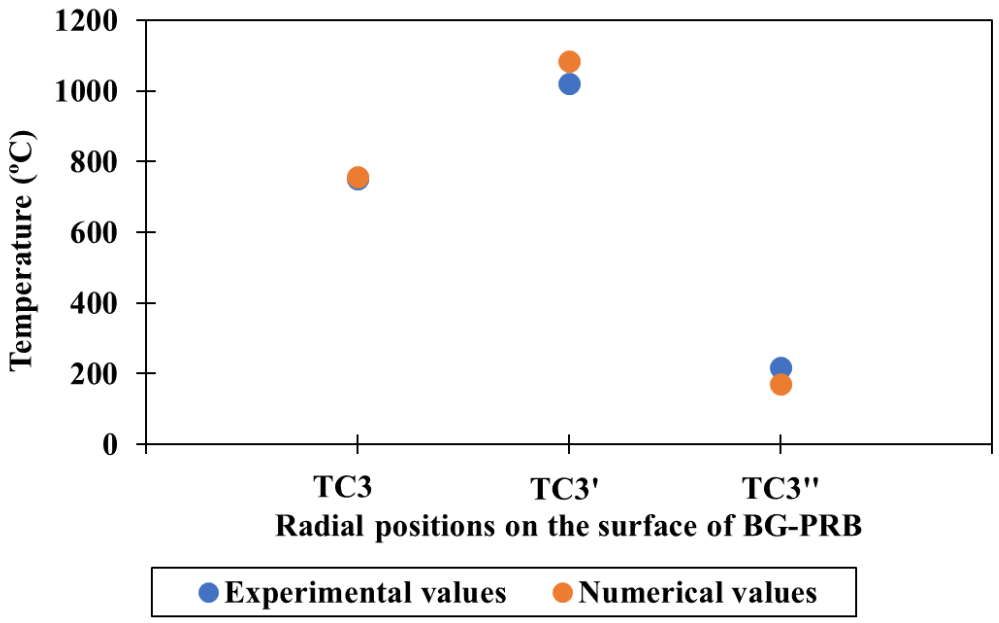

(a) Axial temperature distribution in BG-PRB when operated at high power setting

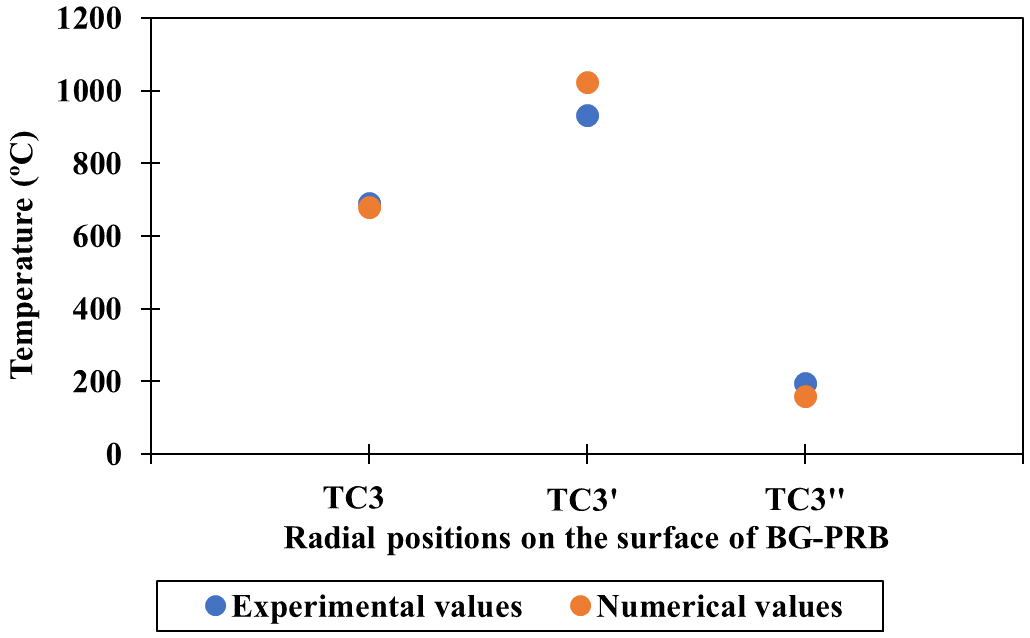

(b) Axial temperature distribution in BG-PRB when operated at low power setting

Fig. 5.7: Axial thermal mapping on BG-PRB operating at different Power settings

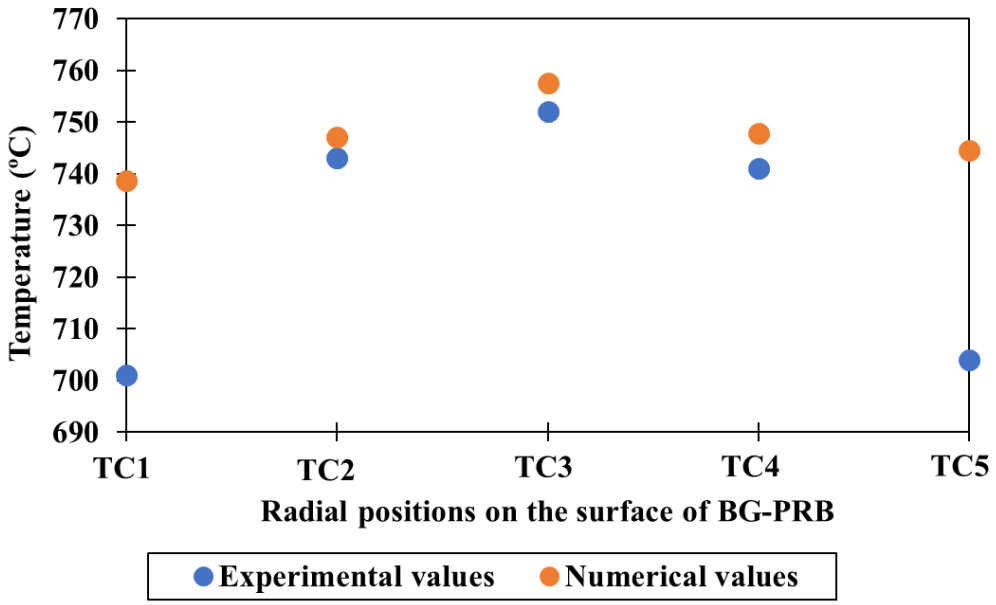

(a) Radial temperature distribution on the surface of BG-PRB when operated at high Power setting

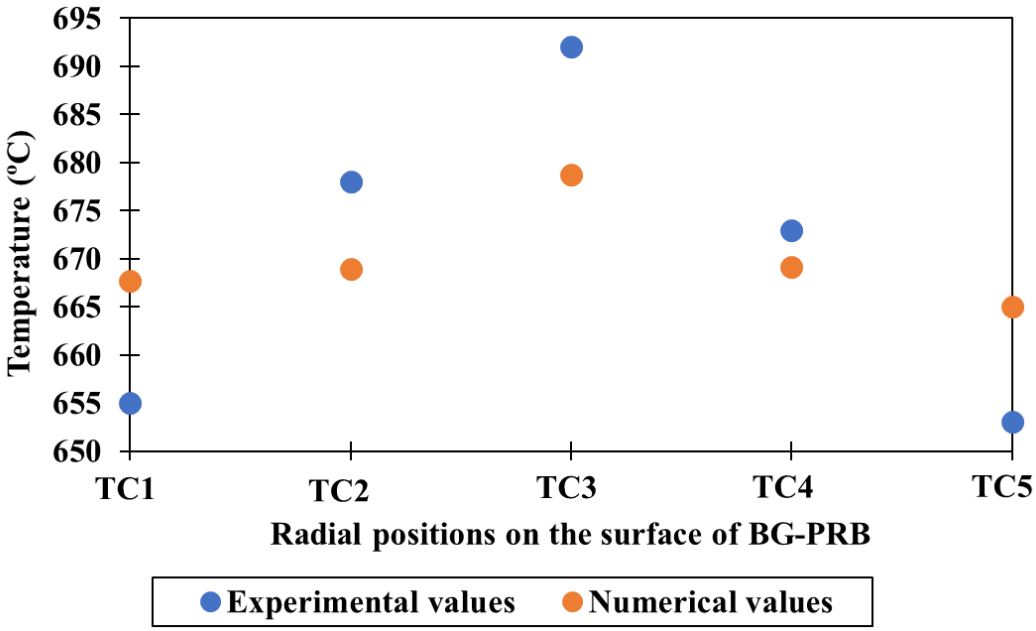

(b) Radial temperature distribution on the surface of BG-PRB when operated at low power setting

Fig. 5.8: Radial Thermal mapping on the surface of BG-PRB operating at different Power settings

Fig. 5.9 shows the temperature contour obtained from the numerical simulation which is plotted on the midplane bisecting BG-PRB in two halves. It can be understood from the contour that the fuel-air mixture gets preheated while entering Al_2O_3 perforated plate and gets combusted on SiC foam. It can also be noted that the flame stabilization zone is enlarged in the high power setting (Fig. 5.9 (b)) when compared to the low power setting (Fig. 5.9 (a)).

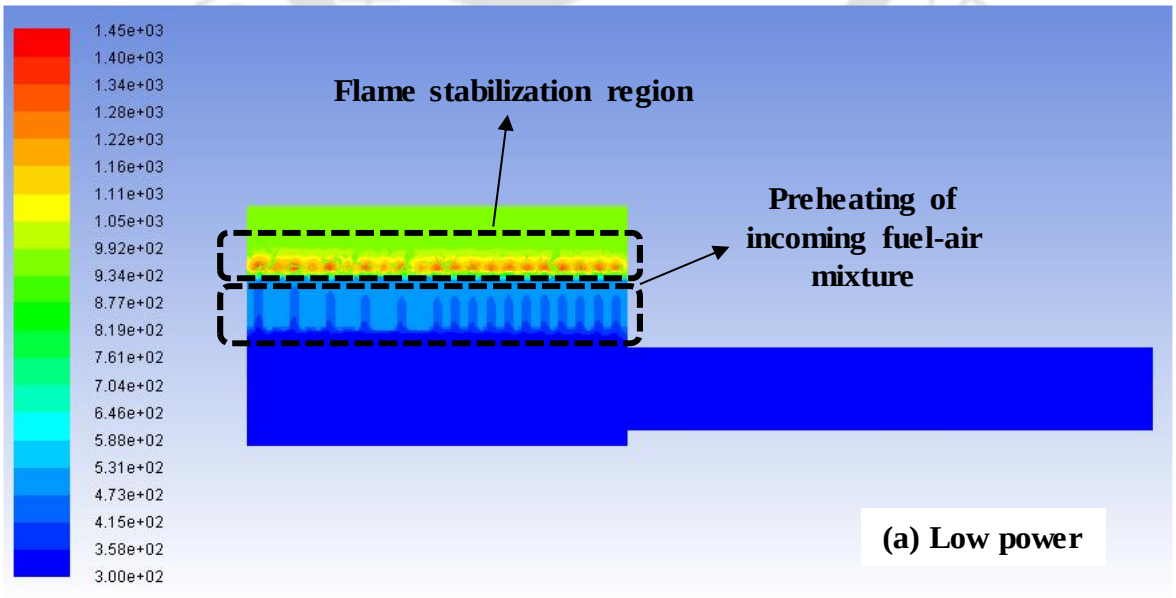

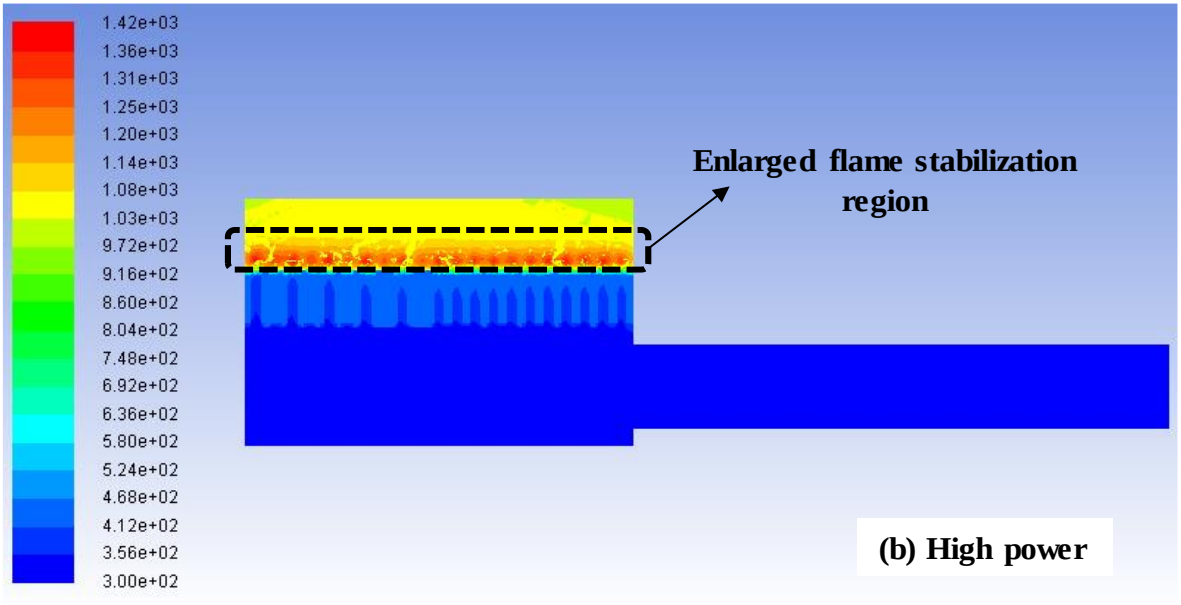

Fig. 5.9. Temperature contour on the midplane of the computational domain at (a) Low power and (b) High power setting

5.5 Techno-Economic Assessment

Techno-Economic Assessment (TEA) is an important activity to be performed when any product or process is proposed. TEA is a cost analysis that summarizes the economic performance of any product or process. TEA provides insight into aspects of the product/process under study where further research and development are needed. TEA analyzes the economic impact of the developed product or process when it enters a market considering the cost of raw materials, operation, construction, etc. Different methods are followed for performing TEA depending on the product or process developed. In the present study, the direct monetary cost associated with the product themselves, which includes purchase cost and operational costs (fuel cost and maintenance cost) is considered. The approach used for direct monetary cost comparison is based on the methods described by Kaushik (2019) and Devi (2020b) is used. In the present study, the developed BG-PRB is subjected to TEA for assessing its economic impacts and it was compared with Liquefied Petroleum Gas based Conventional Burner (LPG-CB). The TEA method used in the study presents capital cost, lifecycle cost, Accounting Rate of Return (ARR) and payback. The methodology adopted in section 4.4 is considered for the present LCA study. And Table 4.2 presents the parameters and equations used for TEA.

5.6 Economic impacts of the developed BG-PRB

TEA is performed for the developed BG-PRB and the values obtained from the analysis are compared with that of LPG-CB. The capital cost of LPG-CB is obtained from the market survey and the capital cost of BG-PRB is assessed by considering the cost of each of its components. The cost of BG-PRB is Rs. 1510 /- which is high when compared to that of LPG-CB (Rs. 1250 /-). The burner components in BG-PRB namely casing, SiC foam and Al_2O_3 perforated plate are ceramics. And the remaining components in BG-PRB namely, frame, valve and supply pipeline are the same as in LPG-CB and their costing will be similar. The usage of ceramics in BG-PRB and their periodical replacement is the reason for its higher overall cost when compared to LPG-CB. In the present analysis, the life of BG-PRB and LPG-CB is considered to be 10 years. The annual maintenance cost of LPG-PRB and NG-PRB is Rs. 610 /-, which includes Rs. 510 /- as replacement cost for ceramic components (SiC foam, Al_2O_3 perforated plate and casing). And the annual maintenance cost of LPG-CB is Rs. 200 /-.

Table 5.4: Results obtained from Cost analysis

Economic metrics	**BG-PRB**		**LPG-CB**	
Capital cost, C	Rs. 1510 /-		Rs. 1250 /-	
Life of burner, L_{LC}	10 Years		10 Years	
Annual financial appraisal				
	Low power	**High power**	**Low power**	**High power**
Fuel cost, C_f	Rs. 2483.5 /-	Rs. 4323.1 /-	Rs. 5294.7 /-	Rs. 8824.4 /-
Annual operating cost, C_{OP}	Rs. 3093.5 /-	Rs. 4933.1 /-	Rs. 5494.7 /-	Rs. 9024.4 /-
Lifecycle cost, C_{LC}	Rs. 3244.5 /-	Rs. 5084.1 /-	Rs. 5619.7 /-	Rs. 9149.4 /-
Annual saving	Rs. 2375.2 /-	Rs. 4065.4 /-	-	-

Table 5.5 presents the results obtained from the cost analysis performed in the present TEA. By taking into account the burner's daily operating hours of 2.5 hr, the annual fuel cost is determined. From the annual appraisal point of view, it was found that the annual fuel cost for operating BG-PRB at low and high power settings is Rs. 2483.5 /- and Rs. 4323.1 /-, respectively. However the annual fuel cost for operating LPG-CB at low and high power settings is Rs. 5294.7 /- and Rs. 8824.4 /-, which is high when compared with results obtained

for BG-PRB. The annual operating cost for BG-PRB (sum of annual fuel cost and maintenance cost) operating at low and high power settings is Rs. 3093.5 /- and Rs. 4933.1 /-, respectively which is low when compared to that of LPG-CB (Low power setting: Rs. 5494.7 /- and High power setting: Rs. 9024.4 /-). Because of the increase in fuel flow rate in BG-PRB at high power setting compared to BG-PRB operating at low power setting, the annual operating cost of BG-PRB operating at high power setting is higher compared to BG-PRB operating at low power setting. The Lifecycle cost of BG-PRB is low (Low power setting: Rs. 3244.5 /- and High power setting: Rs. 5084.1 /-) when compared to LPG-CB (Low power setting: Rs. 5619.7 /- and High power setting: Rs. 9149.4 /-). From the TEA study, it was understood that the overall annual savings that can be obtained by using BG-PRB when operated at low and high power settings are Rs. 2375.2 /- and Rs. 4065.4 /-, respectively.

Table 5.5: Overall savings

Year	Annual savings (Rs.)		Present worth of annual savings (Rs.)		Present worth of cumulative savings (Rs.)	
	Low power	High power	Low power	High power	Low power	High power
1	2375.2	4065.4	2199.3	3764.2	2199.3	3764.2
2	2529.6	4329.6	2168.7	3711.9	4368	7476.2
3	2694	4611	2138.6	3660.4	6506.5	11136.6
4	2869.1	4910.8	2108.9	3609.5	8615.4	14746.1
5	3055.6	5229.9	2079.6	3559.4	10695	18305.5
6	3254.2	5569.9	2050.7	3510	12745.7	21815.5
7	3465.7	5931.9	2022.2	3461.2	14768	25276.7
8	3691	6317.5	1994.1	3413.2	16762.1	28689.9
9	3930.9	6728.2	1966.4	3365.8	18728.5	32055.6
10	4186.4	7165.5	1939.1	3319	20667.7	35374.6

Table 5.6 presents the overall annual savings, present worth of annual savings and present worth of cumulative savings that can be obtained by operating BG-PRB at high power and low power settings instead of LPG-CB. With an inflation rate of 6.5% and an interest rate of 8%, the annual savings and present worth of annual savings are calculated. From the cost-benefit

analysis, it was observed that investing Rs. 1510 /- in BG-PRB for domestic cooking can lead to a cumulative present worth of annual savings of Rs. 20667.7 /- and Rs. 35374.6 /- when operated at low and high power setting, respectively.

The Accounting Rate of Return (ARR) is a financial ratio that is utilized to compute the annual return that can be achieved by investing in the proposed product or process. In the present TEA, ARR is calculated for the proposed BG-PRB by arriving at the percentage ratio of the net gain over the original investment. The ARR of BG-PRB was found to be 144.24% and 247.9% when operated at low power and high power settings, respectively. At a low power setting, with an ARR of 144.24%, BG-PRB is expected to earn Rs. 1.4 /- for the investment of each Rs. 1. Similarly, at a high power setting with an ARR of 247.9%, BG-PRB is expected to earn Rs. 2.5 /- for the investment of each Rs. 1 /-. The payback period that can be achieved by using BG-PRB when operated at low and high power settings is less than 6 months. This short payback period is achievable as BG-PRB resulted in annual savings of Rs. 2375.2 /- and Rs. 4065.4 /- when operated at low and high power settings, respectively.

5.7 Lifecycle Assessment

Lifecycle assessment (LCA) is a systematic model performed to determine the environmental impact caused by BG-PRB. LCA identifies and evaluates the environmental impacts caused by construction and operation of BG-PRB. In LCA, Material flow (both inflow and outflow) for the construction of BG-PRB and its energy utilization are considered to evaluate the resource depletion, emissions and energy consumption of all processes. In the present work, the environmental impact caused by the cookstove with BG-PRB is analyzed and compared with that of the cookstove with LPG-CB. Fig. 5.10 and 5.11 shows the system boundary considered for the present work. For performing LCA, “SimaPro 8.3.0.0” software embedded with the “Ecoinventv3” database is used. In the present work, the standard LCA method as prescribed by the International Organization for Standardization, namely ISO:14040-14044, is adopted. The IMPACT 2002+ method is employed to perform LCA for the proposed cookstove with BG-PRB suitable for domestic cooking applications. The IMPACT 2002+ methodology adopted in section 4.6 is considered for the present LCA study. And Fig. 4.9 shows the schematic of the overall scheme of the IMPACT 2002+ LCA method.

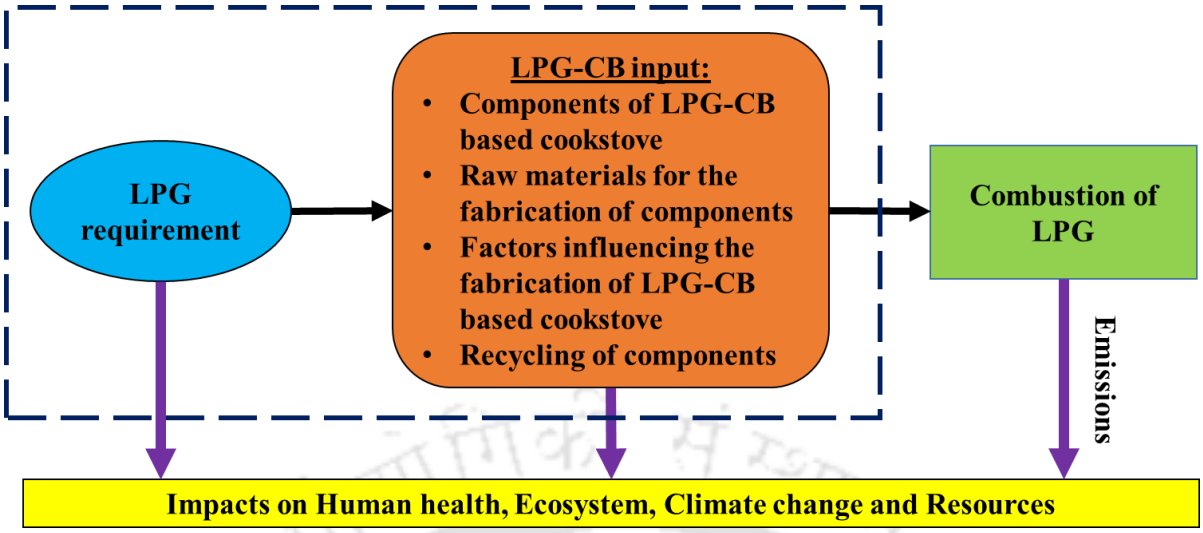

Fig. 5.10: System considered for LCA of LPG-CB

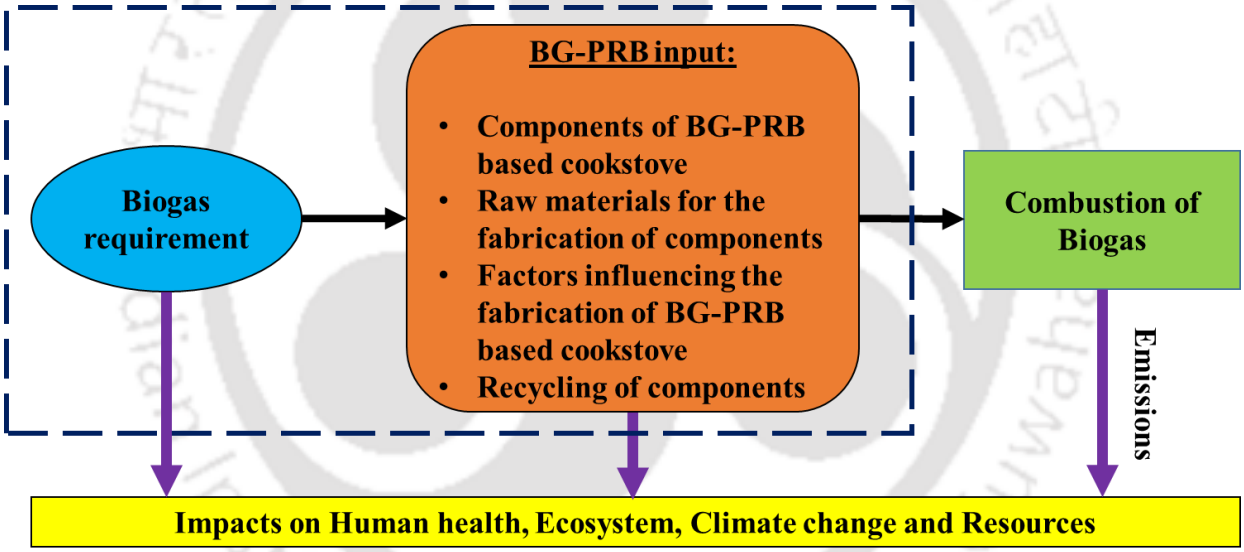

Fig. 5.11: System considered for LCA of BG-PRB

In the present LCA study, the IMPACT 2002+ method links the impact results with damage categories (Human health, Ecosystem quality, Climate change, and Resource utilization) via 15 midpoint categories (Human toxicity-carcinogenic effects, Human toxicity-non-carcinogenic effects, Respiratory effects due to inorganics, Ionizing radiation, Ozone layer depletion, Respiratory effects due to organics, Aquatic ecotoxicity, Terrestrial ecotoxicity, Terrestrial acidification/nitrification, Land occupation, Aquatic acidification, Aquatic eutrophication, Global warming, Non-renewable energy consumption and Mineral extraction) (Jolliet et al., 2003). A Cookstove with BG-PRB operating at a power input of 1.026 kW (low

power setting) and 1.71 kW (high power setting) is considered for the LCA and the results are compared with a cookstove with LPG-CB. In this study, the environmental impacts caused by the construction of cookstoves and the operation of the burners used in the cookstoves are considered. This analysis can provide a holistic view of BG-PRB's ability to curtail the environmental impact compared to that of an LPG-CB.

5.8 Environmental impacts of the developed BG-PRB

In this section, the environmental impacts caused by BG-PRB and LPG-CB are presented using the IMPACT 2002+ LCA method. Here, based on the efficiency of BG-PRB, the amount of biogas needed for 10 years of operation (considering 2.5 hr operation daily) for both high and low power settings was calculated. In this case, the raw materials (Cow dung and water) required for producing biogas required by BG-PRB to operate at high and low power setting is considered. And the corresponding LPG needed for 10 yr of operation of LPG-CB at both high and low power settings was calculated. The above two data were used for performing the LCA using IMPACT 2002+ method. Cookstoves with BG-PRB and LPG-CB were assessed based on the construction parts (burner and frame arrangement) and input requirement for their impact on 15 midpoint categories (Figs. 5.10 and 5.11). Table 5.7 presents the impacts caused on midpoint categories by BG-PRB and LPG-CB when operated at high power and low power settings. From the LCA results, it was understood that fuel requirement by both BG-PRB and LPG-CB contributed more to the total impact. In both cases, the impact from the construction parts is almost equal; only the impact caused by biogas and LPG consumption varied. The contributions to Ozone layer depletion by LPG-CB when operated at high power and low power settings are 0.000794 kg CFC-11$_{-eq}$ and 0.000474 kg CFC-11$_{-eq}$, respectively. However the contribution to the same by BG-PRB when operated at high power and low power settings are 0.00011489 kg CFC-11$_{-eq}$ and 0.0000662 kg CFC-11$_{-eq}$, respectively, which is less when compared to LPG-CB.

When compared to LPG-CB, BG-PRB contributes more to carcinogens, aquatic eutrophication, global warming, and mineral extraction, but this increase is not significant. It was observed that the operation of BG-PRB irrespective of the power settings has less impact on non-carcinogens, Respiratory inorganics, Ozone layer depletion, Respiratory organics, Aquatic ecotoxicity, Terrestrial ecotoxicity, Terrestrial acid/Nutrification, Land occupation, Aquatic acidification, Non-renewable energy when compared to that of LPG-CB. It observed

that the operation of BG-PRB in high power settings leads to a reduction of 85.5%, 82.6, 74.6%, 89.7%, 81.6% and 87% in impacts on the Ozone layer depletion, Respiratory organics, Aquatic ecotoxicity, Terrestrial ecotoxicity, Land occupation, Non-renewable energy categories, respectively in comparison with LPG-CB. And the operation of BG-PRB in low power settings leads to a reduction of 86%, 83%, 75.4%, 89%, 82.1% and 87.3% for the same.

Table 5.7: Contribution to midpoint categories

Midpoint category	Unit	LPG-CB		BG-PRB	
		High power	Low power	High power	Low power
Carcinogens	kg $C_2H_3Cl_{-eq}$	8.085353	4.965285	17.063696	9.930197
Non-carcinogens	kg $C_2H_3Cl_{-eq}$	23.56582	14.23445	19.66325634	11.22534
Respiratory inorganics	kg $PM2.5_{-eq}$	1.094983	0.666502	0.593480112	0.353275
Ionizing radiation	Bq $C\text{-}14_{-eq}$	26818.41	16015.58	-1449.42919	-836.905
Ozone layer depletion	kg $CFC\text{-}11_{-eq}$	0.000794	0.000474	0.00011489	6.62E-05
Respiratory organics	kg $C_2H_{4\text{-}eq}$	1.04205	0.623703	0.181366859	0.106021
Aquatic ecotoxicity	kg TEG water	261981.7	157576.8	66460.32737	38734.44
Terrestrial ecotoxicity	kg TEG soil	74320.79	44836.24	7637.459078	4605.592
Terrestrial acid/nutrification	kg $SO_{2\text{-}eq}$	17.19638	10.3914	16.24882997	9.460921
Land occupation	m^2org.arable	72.87549	43.58383	13.43499243	7.789663
Aquatic acidification	kg $SO_{2\text{-}eq}$	6.03138	3.684068	3.256125702	1.949338
Aquatic eutrophication	kg PO_4 P-lim	0.384601	0.235017	0.501161602	0.287087
Global warming	kg $CO_{2\text{-}eq}$	491.8798	295.5446	678.2244866	392.3546
Non-renewable energy	MJ primary	65199.17	38950.54	8534.07702	4938.009
Mineral extraction	MJ surplus	12.56758	12.71504	72.13726808	44.32464

Figs. 5.13 and 5.14 represent the comparative assessment of the impact caused by BG-PRB and LPG-CB based on the damage category in the IMPACT 2002+ LCA method. It was found

that the operation of BG-PRB in both high and low power settings has a lower environmental impact than LPG-CB in all categories except the climate change category, but this increase is not significant. It should be noted that the impact on the environment is considered from cradle to gate i.e., from the fuel production stage to the consumption stage via the transportation stage. Another observation from the LCA analysis highlights that the environmental impacts from the construction of cookstoves with BG-PRB and LPG-CB are very less compared to the impacts from the energy consumption of the burners, which highlights the importance of employing an efficient burner to curb the overall environmental impact caused by cooking applications. Also, the overall impact of biogas consumption in BG-PRB is found to be less than LPG consumption in LPG-CB. For a considered SMWI life of 10 years and 2.5 hr of daily cooking, the impact from the biogas consumption in BG-PRB accounts for about 41.7%, 86.5% and 87.2% reduction in Human health, Ecosystem quality, and Resource utilization damage categories, respectively when operated at low power setting. And the same for the operation of BG-PRB at high power setting are 40%, 86.4% and 86.8%, respectively. In the Primary energy utilization, the operation of BG-PRB at high and low power settings accounts for about 8606.2 MJ of primary energy utilization and 4982.3 MJ of primary energy utilization, respectively, whereas in the case of LPG-CB, the same is 65211.73 MJ of primary energy utilization and 38963.25 MJ of primary energy utilization, respectively. Thus, from the IMPACT 2002+ LCA analysis, it was understood that BG-PRB is environmentally superior to LPG-CB, as the overall impact of BG-PRB is less compared to LPG-CB.

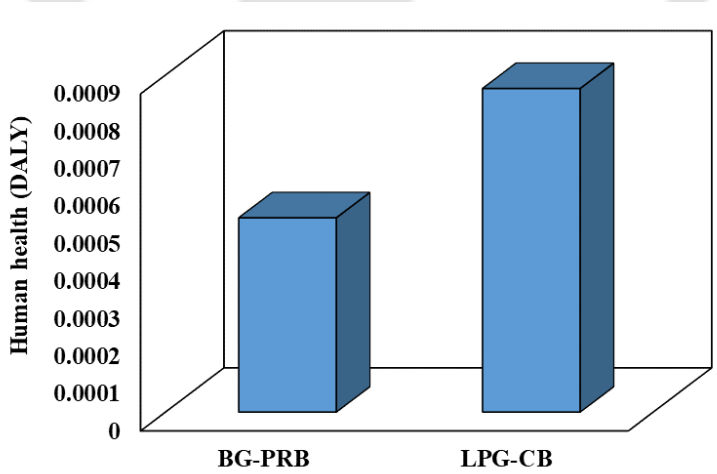

(a) Impact of LPG-CB and BG–PRB on Human health

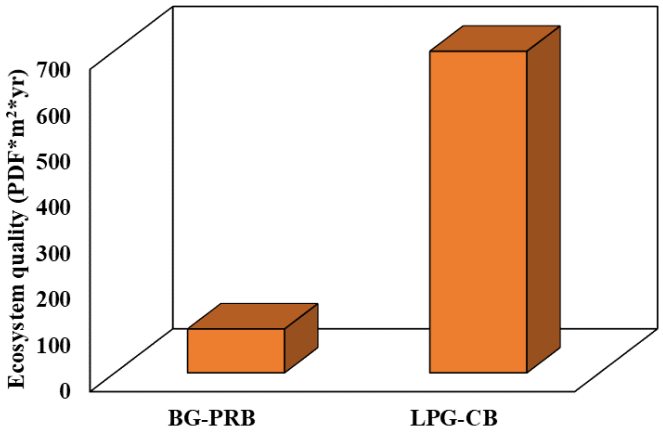

(b) Impact of LPG-CB and BG–PRB on Ecosystem quality

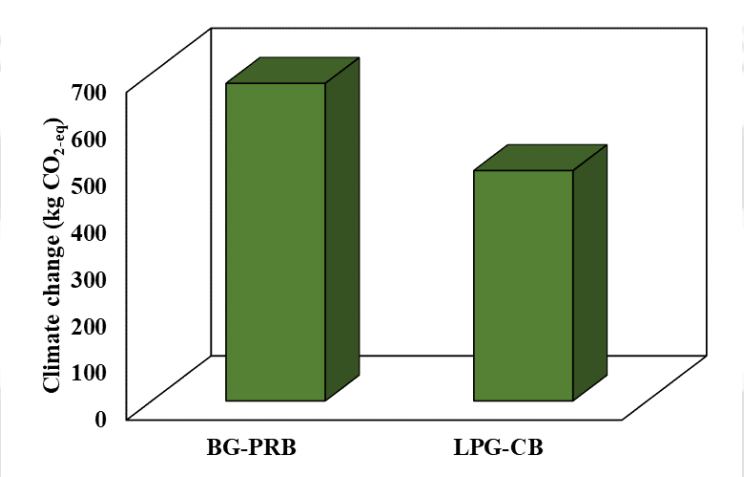

(c) Impact of LPG-CB and BG–PRB on Climate change

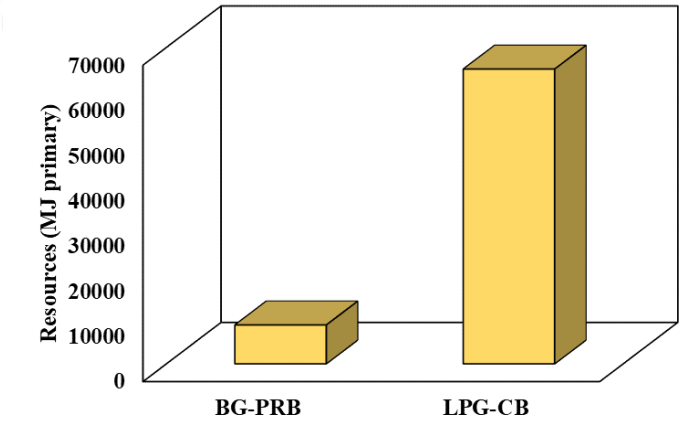

(d) Primary energy requirement by LPG-CB and BG–PRB

Fig. 5.13: The overall impact of LPG-CB and BG–PRB when operated at high power setting

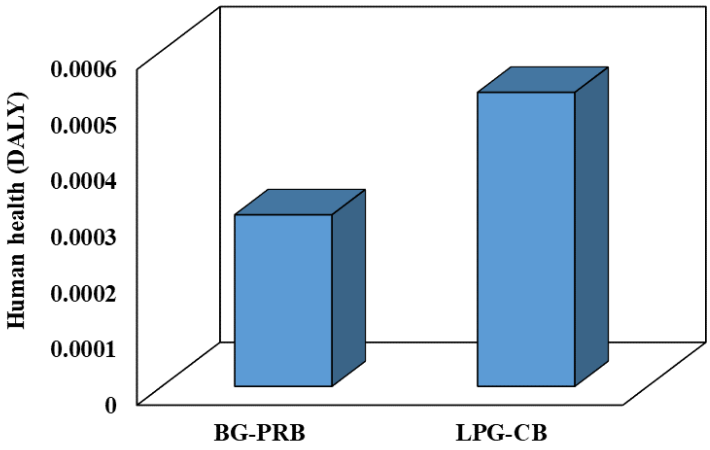

(a) Impact of LPG-CB and BG–PRB on Human health

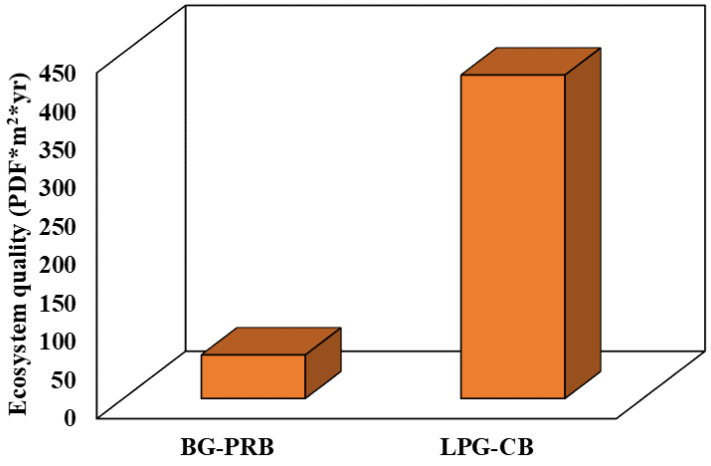

(b) Impact of LPG-CB and BG–PRB on Ecosystem quality

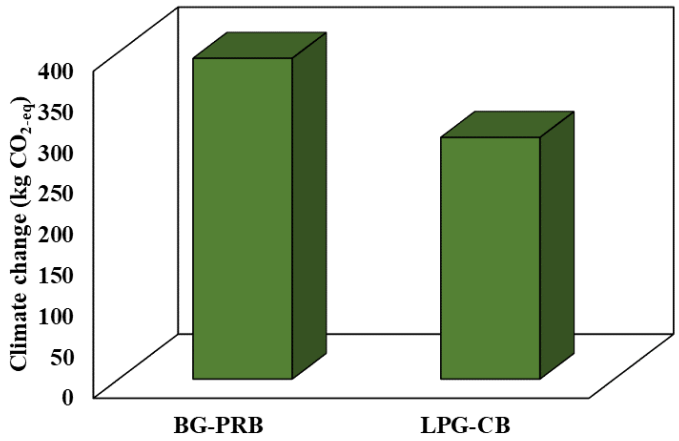

(c) Impact of LPG-CB and BG–PRB on Climate change

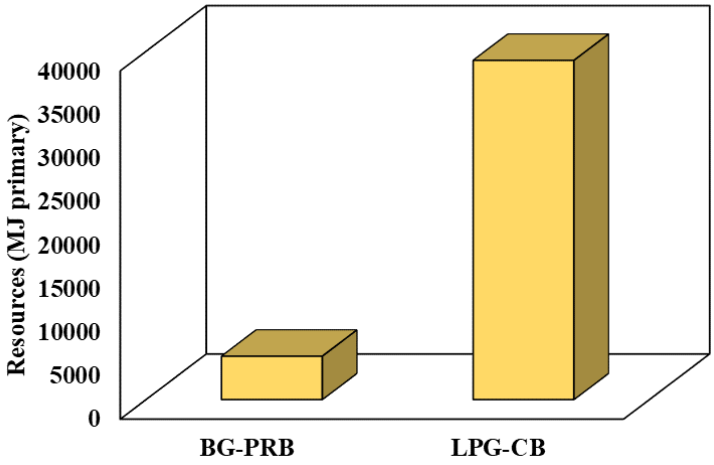

(d) Primary energy requirement by LPG-CB and BG–PRB

Fig. 5.13: The overall impact of LPG-CB and BG–PRB when operated at low power setting

5.9 Summary

This chapter presents BG-PRB as an alternative to BG-CB and its performance is tested under laboratory conditions using IS 8749:2002. It was found that there is an improvement of 7.1% and 10.9% in η_t at high and low power settings, respectively. Also, CO emissions from BG-PRB at low and high power settings were found to be 447 and 513 ppm, respectively, whereas the same for BG-CB, were 622 and 816 ppm, respectively. Using K-type thermocouples, Thermal mapping on the axial direction and surface of BG-PRB was performed to understand the behavior of BG-PRB. In addition, a numerical model was developed and simulations were performed. The results obtained from numerical simulations were compared with the experimental results. It was found that there is less deviation between the results obtained from experiments and numerical simulations. In addition to that, TEA and LCA have been performed on the developed BG-PRB and the results are compared with that of LPG-CB. It was understood that BG-PRB is superior to LPG-CB in both economic and environmental aspects. In the present TEA, the annual maintenance cost of LPG-PRB and NG-PRB is considered to be Rs. 610 /-, which includes Rs. 510 /- as replacement cost for ceramic components (SiC foam, Al_2O_3 perforated plate and casing). And the annual maintenance cost of LPG-CB is Rs. 200 /-. From the TEA results, it was observed that the implementation of developed BG-PRB instead of LPG-CB can lead to an annual saving of Rs. 2375.2 /- and Rs. 4065.4 /- when operated at low and high power settings, respectively. Also, from the LCA results, it was observed that the impact of the biogas consumption in BG-PRB accounts for about 41.7%, 86.5% and 87.2%

reduction in Human health, Ecosystem quality, and Resource utilization damage categories, respectively, when operated at low power setting. And the same for the operation of BG-PRB at high power setting is 40%, 86.4% and 86.8%, respectively.

CHAPTER 6

CONCLUSIONS AND FUTURE SCOPE

Preface

Chapter 6 consolidates the significant observations and conclusions of the research conducted. The primary objective of this thesis is to design energy-efficient and environmentally friendly Porous Radiant Burners (PRBs) that utilize Liquefied Petroleum Gas (LPG), Natural Gas (NG), and Biogas for commercial and domestic cooking applications. Three separate chapters are dedicated to the development of LPG based PRB (LPG-PRB), NG based PRB (NG-PRB) and Biogas based (BG-PRB). The developed PRBs operate in a partially surface-stabilized mode of operation.

Chapter 3 deals with the development of LPG-PRB as an improvement over LPG-PRB developed by Mishra (2015b). LPG-PRB was assessed for its performance in terms of thermal efficiency and emissions. An analytical model for the developed LPG-PRB was developed to determine the primary air entrainment. Further experimental investigations were performed to study the thermal behavior of LPG-PRB with variation in primary air entrainment.

Chapter 4 deals with the development of NG-PRB by modifying the LPG-PRB presented in chapter 3. The developed NG-PRB was assessed for its performance in terms of thermal efficiency and emissions following the methodology adopted for LPG-PRB. In addition, Techno-Economic Assessment (TEA) and Lifecycle Assessment (LCA) were performed for the developed LPG-PRB and NG-PRB to assess their economic and environmental performance.

Further, chapter 5 presents the BG-PRB developed for domestic cooking applications. The developed BG-PRB was assessed for its performance in terms of thermal efficiency and emissions following the protocols prescribed by IS 8749:2002. In addition, Numerical simulations were performed to determine the thermal behaviour of BG-PRB. The results obtained from numerical simulations were compared with that of experimental results. Also, Techno-Economic Assessment (TEA) and Lifecycle Assessment (LCA) were performed for the developed BG-PRB to assess their economic and environmental performance.

6.1 Conclusions on chapter 3 - Development and performance assessment of LPG based Porous Radiant Burner

LPG-PRB operating in a partially surface-stabilized mode of operation is presented as an improvement over LPG-PRB developed by Mishra (2015b). The developed LPG-PRB operates in the power input range of 5-7 kW. Experimental investigations on the performance characteristics of a two-layered self-aspirated LPG-PRB (5–7 kW) have been carried out in terms of thermal efficiency and emissions.

- The developed LPG-PRB showed improved thermal efficiency in the range of 69.7-63.8% for a power input range of 5-7 kW, which is higher compared to LPG-PRB developed by Mishra (2015b) (55-54%) and CB (54.4-49.7%).
- CO and NO_x emissions ranged between 29-34 ppm and 2-5 ppm, respectively.
- An analytical expression has been derived for the air-fuel entrainment ratio in two-layer PRB. From the derived expression, it was understood that the entrainment ratio is a function of the type of fuel used, fuel supply pressure, and geometry of the injector, mixing tube, mixing chamber, Al_2O_3 perforated plate, and SiC foam.
- Investigation of LPG-PRB operating with various injector exit diameters proved that with a decrease in injector exit diameter, there is an increase in primary air entrainment in both hot and cold states.
- LPG-PRB was stable in operation for the studied power input range without flashback.
- The overall performance of LPG-PRB highlights that the newly developed LPG-PRB is a viable alternative to its conventional counterparts.

6.2 Conclusions on chapter 4 - Development and performance assessment of Natural Gas based Porous Radiant Burner

NG-PRB operating in a partially surface-stabilized mode of operation developed by modifying LPG-PRB presented in chapter 3. Techno-Economic Assessment (TEA) and Lifecycle Assessment (LCA) have been performed on the developed LPG-PRB and NG-PRB to assess their economic and environmental impacts and the results obtained from TEA and LCA are compared with that of LPG-CB.

- NG-PRB showed thermal efficiency in the range of 61.4%-52.9% and produced lesser emissions (CO: 30 ppm-43 ppm and NO_x:3.5 ppm-6 ppm) for a power input range of 5-7 kW.
- Maximum surface temperatures of 820 ºC, 880 ºC and 906 ºC for power inputs of 5, 6 and 7 kW, respectively were noted at the centre. Also, the variation in temperature from the centre to the periphery of NG-PRB surface was less than 100 ºC for all power inputs.
- It was understood that LPG-PRB and NG-PRB are superior to LPG-CB in both economic and environmental aspects. From the TEA results, it was observed that LPG-PRB can lead to an annual saving of Rs. 28805.7 /-, Rs. 34677.3 /- and Rs. 40548.9 /- when operated at power inputs of 5 kW, 6 kW and 7 kW, respectively.
- The implementation of developed NG-PRB instead of LPG-CB can lead to an annual saving of Rs. 46019.9 /-, Rs. 51316.5 /- and Rs. 56033.9 /- when operated at power inputs of 5 kW, 6 kW and 7 kW, respectively.
- Further from the LCA results, it observed that LPG-PRB and NG-PRB is superior to LPG-CB in Human health, Ecosystem quality, and Resource utilization damage categories.

6.3 Conclusions on chapter 5 - Development and performance assessment of Biogas based Porous Radiant Burner for domestic cooking

BG-PRB operating in a partially surface-stabilized mode of operation is presented as an alternative to BG-CB. The performance of the developed BG-PRB was tested under laboratory conditions using IS 8749:2002. Numerical investigations have been done to understand the thermal behaviour of BG-PRB. And it provides insight into the reaction zone, which can be used in the future for deciding the optimum design parameters. The results obtained from numerical simulations were similar to that of experimental results.

- BG-PRB showed higher thermal efficiency and produced lesser CO emissions compared to BG-CB. It was found that there is an improvement of 7.1% and 10.9% in η_t at high and low power settings, respectively.
- CO emissions from BG-PRB were found to be 447 and 513 ppm at low and high power settings, respectively, whereas the same for BG-CB, were 622 and 816 ppm, respectively.

- TEA and LCA were performed on the developed BG-PRB and the results were compared with that of LPG-CB. The developed BG-PRB is found superior to LPG-CB in both economic and environmental aspects.
- From the TEA results, it was observed that the implementation of developed BG-PRB instead of LPG-CB can lead to an annual saving of Rs. 2375.2 /- and Rs. 4065.4 /- when operated at low and high power settings, respectively.
- From the LCA results, it observed that the impact of the biogas consumption in BG-PRB accounts for about 41.7%, 86.5% and 87.2% reduction in Human health, Ecosystem quality, and Resource utilization damage categories, respectively, when operated at low power setting. And the same for the operation of BG-PRB at high power setting is 40%, 86.4% and 86.8%, respectively.

From the above conclusions, it can be observed that PRBs, irrespective of the fuel, are energy-efficient and environmentally friendly burners compared to their conventional counterparts. Implementation of PRB can lead to huge economic benefits. Also, the PRBs are safe and suitable for real-time applications.

6.4 Future scope

The following is the scope for future research work:

- Further studies can be focused on the selection of suitable material for the casing.
- Real-time kitchen performance tests can be performed on the developed burners.
- The variation in the performance of the developed PRBs can be studied by varying the parameters mentioned in chapter 3.
- Numerical investigations can be carried out on PRB to find the optimum design.
- Further detailed studies on the performance of PRB can be studied with the change in fuel.
- Apart from cooking applications, the developed PRBs presented in chapters 3 and 4 can be implemented in other industrial applications and can be studied for their performance.

References

Avdic F, Adzic M and Durst F (2010), Small scale porous medium combustion system for heat production in households. Applied Energy, 87: 2148-2155.

Awulu JO, Iyidiobu BN and Ugbede, J (2020), Cooking Performance of a Developed Biogas Burner (Stove). International Journal of Engineering Applied Sciences and Technology, 4(12): 11–16.

Babkin VS., Korzhavin AA., Bunev VA., (1991), Propagation of premixed gaseous explosion flames in porous media. Combustion and Flame, 87: 82-190.

Bangladesh National Biogas Program Monitoring Services. Available online: https://www.upm-cdm.eu/project/bangladesh-national-biogas-program-monitoring-services-12/ (accessed on 28 December 2022).

Bouma PH and De Goey LPH (1999), Premixed combustion on ceramic foam burners, Combustion and Flame, 119 (1-2): 133-143.

BP Statistical Review of World Energy, 71st edition, 2022.

Bureau of Indian standards, Commercial burners using LPG at inlet pressure up to 147.1 kN/m^2 (1500 gf/cm^2)-specification, IS 14612:1999, New Delhi, India.

Bureau of Indian standards, Biogas Stove-Specification (second revision), IS 8749:2002, New Delhi, India.

Bureau of Indian standards, Domestic gas stoves for use with Liquefied Petroleum Gases (fifth revision), IS 4246:2002, New Delhi, India.

Chaelek A, Grare UM and Jugjai S, Self-aspirating/air-preheating porous medium gas burner. Applied Thermal Engineering, 153: 181–189.

Chandra A, Tiwari GN and Yadav YP (1991a), Hydrodynamical Modelling of a Biogas Burner. Energy Conversion and Management, 32(4): 395–401.

Chandra A, Tiwari GN, Srivastava VK and Yadav YP (1991b), Peformance Evaluation of Biogas Burners. Energy Conversion and Management, 32(4): 353–358.

Deb S and Muthukumar P (2021), Development and performance assessment of LPG operated cluster Porous Radiant Burner for commercial cooking and industrial applications. Energy, 219: 119581.

Deb S, Kaushik LK, Kumar MA, Satish SHV and Muthukumar P (2021), Clustered Porous Radiant Burner: A cleaner alternative for cooking systems in small and medium scale applications. Journal of Cleaner Production, 308: 127276.

Decker T, Baumgardner M, Prapas J and Bradley T (2018), A Mixed Computational and Experimental Approach to Improved Bio-gas Burner Flame Port Design. Energy for Sustainable Development, 44: 37–46.

Deshaies B., Joulin G., (1980), Asymptotic study of an excess-enthalpy flame. Combustion Science and Technology, 22: 281-285.

Devi S, Sahoo N and Muthukumar P (2020a), Experimental studies on biogas combustion in a novel double layer inert Porous Radiant Burner. Renewable Energy, 149: 1040-1052.

Devi (2020b), Development and performance analysis of a crude biogas operated sideway faced porous radiant burner, Ph.D. thesis, Department of Mechanical Engineering, IIT, Guwahati.

Dietrich B, Schabel W, Kind M and Martin H (2019), Pressure drop measurements of ceramic sponges-Determining the hydraulic diameter, Chemical Engineering Science, 64(16): 3633-3640.

Dillon J (1999), Combustion in porous media, Los Alamos National Lab, Final report, California Institute of Technology.

Durst F, Trimis D, Dimaczek G (1996), Burners having porous material of varying porosity. Patent Application No.: 392892, United States.

Fulford D (1996), A Short Course on Biogas Stove Design; Kingdom Bioenergy, Ltd.: Wokingham, United Kingdom.

Giwa AS, Ali N, Ahmad I, Asif M, Guo RB, Li FL and Lu M (2020). Prospects of China's Biogas: Fundamentals, Challenges and Considerations. Energy Reports, 6: 2973–2987.

Goeckner BA, Helmich DR, McCarthy TA, Arinez JM, Peard TE, Peters JE, Brewster MQ, Buckius RO (1992), Radiative heat transfer augmentation of natural gas flames in radiant tube burners with porous ceramic inserts, 5(6): 848-860.

Hackert CL, Ellzey JL, Ezekoye OA (1999), Combustion and heat transfer in model two-dimensional porous burners. Combustion and Flame, 116(1-2): 177-191.

Hardesty DR, Weinberg FJ (1973), Burners producing large excess enthalpies. Combustion Science and Technology, 8: 201-214.

Herrera B, Cacua K, Olmos-Villalba L (2015), Combustion stability and thermal efficiency in a porous media burner for LPG cooking in the food industry using Al_2O_3 particles coming from grinding wastes. Applied Thermal Engineering, 91: 1127-1133.

Hoffmann JG, Echigo R, Tada S and Yoshida H (1996), Analytical study on flame stabilization in reciprocating combustion in porous media with high thermal conductivity. Symposium (International) on Combustion, 26(2): 2709-2716.

Hsu PF, Howell JR and Matthews RD (1993), A Numerical Investigation of Premixed Combustion Within Porous Inert Media. ASME Journal of Heat and Mass Transfer, 115(3): 744-750.

Iral L and Amell A (2015), Performance study of an induced air porous radiant burner for household applications at high altitude. Applied Thermal Engineering, 83: 31-39.

Ismail KA, Abdullah MZ, Zubair M, Ahmad ZA, Jamaludin AR, Mustafa KF and Abdullah MN (2013), Application of porous medium burner with micro cogeneration system. Energy, 50: 131-142.

Itodo IN, Agyo GE and Yusuf P (2007), Performance Evaluation of a Biogas Stove for Cooking in Nigeria. Journal of Energy in Southern Africa, 18(4): 14–18.

Jolliet O, Margni M, Charles R, Humbert S, Payet J, Rebitzer G and Rosenbaum R (2003), IMPACT 2002+: A New Life Cycle Impact Assessment Methodology. International Journal of Life Cycle Assessment, 8(6): 324-330.

Jugjai S and Sanitjai S (1996), Parametric studies of thermal efficiency in a proposed porous radiant recirculated burner (PRRB): A design concept for the future burner. RERIC International Energy Journal, 18(2): 97-111.

Jugjai S and Rungsimuntuchart N (2002), High efficiency heat-recirculating domestic gas burners. Experimental Thermal and Fluid Science, 26(5): 581-592.

Kandpal JB, Maheshwari RC and Kandpal TC (1995), Indoor Air Pollution from Combustion of Wood and Dung Cake and Their Processed Fuels in Domestic Cookstoves. Energy Conversion and Management, 36(11): 1073–1079.

Kebede D and Kiflu A (2014), Design of Biogas Stove for Injera Baking Application. International Journal of Novel Research in Engineering and Science, 1(1): 6–21.

Kaushik LK (2019), Performance Study and Feasibility Assessment of Porous Radiant Burner Aided Cook-stoves for LPG, Biogas and Waste Cooking Oil Fuels, Ph.D. thesis, Department of Mechanical Engineering, IIT, Guwahati.

Kaushik LK, Mahalingam AK and Palanisamy M (2021), Performance Analysis of a Biogas Operated Porous Radiant Burner for Domestic Cooking Application. Environmental Science and Pollution Research, 28: 12168–12177.

Khandelwal KC and Gupta VK (2009), Popular Summary of the Test Reports on Biogas Stoves and Lamps Prepared by Testing Institutes in China, India and The Netherlands; SNV Netherlands Development Organization: Hague, The Netherlands.

Kotani Y and Takeno T (1982), An experimental study on stability and combustion characteristics of an excess enthalpy flame. Symposium (International) on Combustion, 19: 1503-1509.

Kurchania AK, Panwar NL and Pagar SD (2010), Design and Performance Evaluation of Biogas Stove for Community Cooking Application. International Journal of Sustainable Energy, 29(2): 116–123.

Kurchania AK, Panwar NL and Pagar SD (2011), Development of Domestic Biogas Stove. Biomass Conversion and Biorefinery, 1: 99–103.

Laphirattanakul P, Laphirattanakul A, and Charoensuk J (2016), Effect of self-entrainment and porous geometry on stability of premixed LPG porous burner. Applied Thermal Engineering, 103: 583–591.

Makmool U, Jugjai S, Tia S, Vallikul P and Fungtammasan B (2007), Performance and analysis by particle image velocimetry (PIV) of cooker-top burners in Thailand. Energy, 32: 1986-1995.

Min DK and Shin HD (1991), Laminar premixed flame stabilized inside a honeycomb ceramic. International Journal of Heat and Mass Transfer, 34(2): 341-356.

Ministry of New & Renewable Energy-Government of India. Available online: https://mnre.gov.in/ (accessed on 28 December 2022).

Ministry of Power, Government of India. Available online: https://powermin.gov.in/en/content/power-sector-glance-all-india (accessed on 20 March 2023)

Mishra NK, Muthukumar P and Mishra SC (2013), Performance Tests on Medium-Scale Porous Radiant Burners for LPG Cooking Applications. International Journal of Emerging Technology and Advanced Engineering, 3(3): 126-130.

Mishra NK, Mishra SC and Muthukumar P (2015a), Performance characterization of a medium-scale liquefied petroleum gas cooking stove with a two-layer porous radiant burner. Applied Thermal Engineering, 89: 44-50.

Mishra NK (2015b), Development of Self-Aspirated Two-Layer Porous Radiant Burners for LPG Cooking Applications, Ph.D. thesis, Department of Mechanical Engineering, IIT, Guwahati.

Mishra NK and Muthukumar P (2018), Development and testing of energy efficient and environment friendly porous radiant burner operating on liquefied petroleum gas. Applied Thermal Engineering, 129: 482-489.

Mital R, Gore JP and Viskanta R (1997), A study of the structure of submerged reaction in porous ceramic radiant burners. Combustion and Flame, 111(3): 175-184.

Moffat RJ (1988), Describing the uncertainties in experimental results. Experimental Thermal and Fluid Science, 1(1): 3–17.

Mujeebu MA, Abdullah MZ, Abu Bakar MZ, Mohamad AA and Abdullah MK (2009), Applications of porous media combustion technology-A review. Applied Energy, 86: 1365-1375.

Mujeebu MA, Abdullah MZ and Mohamad AA (2011), Development of energy efficient porous medium burners on surface and submerged combustion modes. Energy, 36: 5132-5139.

Mulugeta B, Nega DT and Demissie SW (2017), Design, Optimization and CFD Simulation of Improved Biogas Burner for 'Injera' Baking in Ethiopia. International Journal of Engineering Research & Technology (IJERT), 6(1): 58–64.

Muthukumar P, Anand P and Sachdeva P (2011), Performance analysis of porous radiant burners used in LPG cooking stove. International Journal of Energy and Environment, 2(2): 367-374.

Muthukumar P and Shyamkumar PI (2013), Development of novel porous radiant burners for LPG cooking applications. Fuel, 112: 562-566.

Namkhat A and Jugjai S (2010), Primary air entrainment characteristics for a self-aspirating burner: Model and experiments. Energy, 35(4): 1701–1708.

Obada DO, Obi AI, Dauda M and Anafi FO (2014), Design and Construction of a Biogas Burner. Palestine Technical University Research Journal, 2(2): 35–42.

Panigrahy S and Mishra SC (2016a), Analysis of combustion of liquefied petroleum gas in a porous radiant burner. International Journal of Heat and Mass Transfer, 95: 488-498.

Panigrahy S, Mishra NK, Mishra SC and Muthukumar P (2016b), Numerical and experimental analyses of LPG (liquefied petroleum gas) combustion in a domestic cooking stove with a porous radiant burner. Energy, 95: 404-414.

Pantangi VK, Karuna Kumar ASSR, Mishra SC and Sahoo N (2007), Performance analysis of domestic LPG cooking stoves with porous media. International Energy Journal, 8(2): 139-144.

Pantangi VK, Mishra SC, Muthukumar P and Reddy R (2011), Studies on porous radiant burners for LPG (liquefied petroleum gas) cooking applications. Energy, 36(10): 6074-6080.

Petro LM, Machunda R, Tumbo S and Kivevele T (2020), Theoretical and Experimental Performance Analysis of a Novel Domestic Biogas Burner. Journal of Energy, 2020: 8813254.

Pradhan P and Misra PC (2018), Performance evaluation of novel surface flame self-aspirated porous radiant burners for cooking applications. Sadhana, 43: 173.

Pritchard R, Guy JJ and Connor NE (1977), Handbook of industrial gas utilization: Engineering principles and practice.

Sasse L, Kellner C and Kimaro A (1991). Improved Biogas Unit for Developing Countries; Deutsche Gesellschaft für Technische Zusam-menarbeit (GTZ) GmbH: Eschborn, Germany.

Sinha GS, Kaushik LK and Muthukumar P, (2021), A Review on Materials Used for Combustion in Porous Radiant Burners. Proceedings of International Conference on Thermofluids, Lecture Notes in Mechanical Engineering, Springer, Singapore, 633-641.

Smith Jr PL and Winkle MV (1958), Discharge coefficients through perforated plates at reynolds number of 400 to 3000, AIChE Journal, 4: 266–268.

Smith KR, Uma R, Kishore VVN, Lata K, Joshi V, Zhang J, Rasmussen RA and Khalil MAK (2000), Greenhouse Gases from Small-Scale Combustion Devices in Developing Countries Phase IIA, Household Stoves in India; Environmental Protection Agency: Washington, DC, USA.

Suzukawa Y, Sugiyama S, Hino Y, Ishioka M and Mori L (1997), Heat transfer improvement and NO_x reduction by highly preheated air combustion. Energy Conversion and Management, 38(10-13): 1061-1071.

Syamsuri, Suheni and Yustia WM (2015), Performance Analysis of Biogas Stoves with Variations of Flame Burner for the Capacity of Biogas 1 M3/Day. ARPN Journal of Engineering and Applied Sciences, 10(22): 10349–10353.

Takeno T and Sato K (1979), An excess enthalpy flame theory. Combustion Science and Technology, 20: 73-84.

Tong TW, Sathe SB and Peck RE (1990). Improving the performance of porous radiant burners through use of sub-micron size fibers. International Journal of Heat and Mass Transfer, 33(6): 1339-1346.

Trimis D (2000), Stabilized combustion in porous media - Applications of the porous burner technology in energy- and heat-engineering, Fluids 2000 Conference and Exhibit, Denver, Colorado, U.S.A.

Tumwesige V, Fulford D and Davidson GC (2014), Biogas Appliances in Sub-Sahara Africa. Biomass Bioenergy, 70: 40–50.

Weinberg FJ (1971), Combustion temperatures: the future?. Nature, 233: 239-241.

Wu C, Chen K and Yang SY (2014), Experimental study of porous metal burners for domestic stove applications. Energy Conversion and Management, 77: 380–388.

Xiong TY, Khinkis MJ and Fish FF (1995), Experimental study of a high-efficiency, low emission porous matrix combustor-heater. Fuel, 74(11): 1641-1647.

Yasmin N and Grundmann P (2019), Adoption and Diffusion of Renewable Energy—The Case of Biogas as Alternative Fuel for Cooking in Pakistan. Renewable and Sustainable Energy Reviews, 101: 255–264.

Yoksenakul W and Jugjai S (2011), Design and development of a SPMB (self-aspirating, porous medium burner) with a submerged flame. Energy, 36(5): 3092-3100.

Yoshida H, Yun JH, Echigo R and Tomimura T (1990), Transient characteristics of combined conduction, convection and radiation heat transfer in porous media. International Journal of Heat and Mass Transfer, 33(5): 847-857.

APPENDIX – I

Properties of fuel

1. LPG (http://www.gasindia.in)

Particulars	**Value**
Composition	Propane (C_3H_8) - 40% and Butane (C_4H_{10}) - 60%
Ignition temperature (°C)	488-502
Max. flame temperature (°C)	1985
Higher calorific value (kJ/kg)	49540
Lower calorific value (kJ/kg)	45605.6
Density (kg/m^3)	1.9

2. Biogas

Particulars	**Value**
Composition	Methane (CH_4): 52-56% and Carbondioxide (CO_2): 44-48%
Auto Ignition temperature (°C)	650
Lower calorific value (kJ/kg)	17100
Density (kg/m^3)	1.2

3. Natural gas (https://www.unitrove.com/engineering/tools/gas/natural-gas-density)

Particulars	**Value**
Composition	Methane (CH_4) – 90%; Carbondioxide (CO_2) – 6%; Nitrogen (N_2) – 1; Propane (C_3H_8) – 1.2% and Propane (C_4H_{10}) – 1.8%
Ignition temperature (°C)	540
Higher calorific value (kJ/kg)	46520
Lower calorific value (kJ/kg)	41970
Density (kg/m^3)	0.8

APPENDIX – II

Details of pan size and mass of water for Water Boiling Test (WBT)

1. Domestic LPG stoves (IS 4246: 2002)

Gas Rate at STP (l/h)	Pan Diameter (External), mm ±5%	Pan Height (External), mm	Total Pan Mass with lid, g ±10%	Mass of water in pan, kg
Up to 40	180	100	356	2.0
41-50	205	110	451	2.8
51-60	220	120	519	3.7
61-70	245	130	632	4.8
71-80	260	140	750	6.1
81-95	285	155	853	7.7
96-107	295	165	920	9.4

2. Commercial LPG Burner (IS 14612: 1999)

Gas burning rate, kg/h	Pan Diameter (External), mm ±5%	Pan Height (External), mm	Total Pan Mass with lid, g ±10%	Mass of water in pan, kg
1	380	205	2.56	16.5
1.5	420	220	3.07	24.0
2.25	495	265	4.52	37.0
3.5	595	320	8.45	58.0

3. Biogas Stove (IS 8749: 2002)

Gas Rate at STP (l/h)	Pan Diameter (External), mm ±5%	Pan Height (External), mm	Total Pan Mass with lid, g ±10%	Mass of water in pan, kg
Up to 240	180	100	356	2.0
246-300	205	110	451	2.8
306-360	220	120	519	3.7
366-420	245	130	632	4.8
426-480	260	140	750	6.1
486-570	285	155	853	7.7
576-692	295	165	920	-
698-810	320	175	1100	-

APPENDIX – III

Details of burners used for comparison

1. Description of LPG based Conventional Burner used for comparison in chapter-3

LPG-CB chosen is a round-type burner that works on FFC. The burner head is 93 mm in diameter with 170 ports of 2 mm diameter with an injector diameter of 1.1 mm. A photographic image of FFC-CB is shown in Fig. A.

Fig. A. Photographic image of LPG-CB

2. Description of Biogas based Conventional Burner used for comparison in chapter-5

BG-CB chosen is a round-type burner that works on FFC. The burner head is 68 mm in diameter with 23 ports of 5 mm diameter with an injector diameter of 2 mm. A photographic image of BG-CB is shown in Fig. B.

Fig. B. Photographic image of BG-CB

APPENDIX – IV

Technical specifications of the instruments used in the experiments

1. Weighing balance

Make	Sartorius Combics Lite
Model	CLWP1 – 30ED-I
Capacity	30kg
Platform size	400X300mm
Accuracy	± 1g
Power Supply	90 to 260V AC & DC
Indicator	18mm LCD 7 segment backlit

2. Thermocouples

Make	Emerson Process Management Pvt. Ltd.
Type	metal sheathed K-type
Junction	Grounded
Range	20ºC to 1400 ºC
Accuracy	±1 ºC

3. Mass flow meters

Make	Emerson Process Management Pvt. Ltd.
Type	Coriolis mass flow meter
Model	CMF010P323NQB2E222
Flow range	0 to 50 g/min
Flow accuracy	± 0.35% of full scale
Sensitivity	0.001g
Temperature range	-10 to 100 °C
Operating pressure range	0 to 150 bar

4. Portable gas analyzer

Make	Testo
Model	350
O_2	0-25 Vol%
Accuracy	±0.8 Vol.%
Resolution	0.01 Vol%
CO	0-10000ppm
Accuracy	±5ppm (0-199 ppm)
Resolution	1 ppm
NO	0-4000 ppm
Accuracy	±1ppm (0-99 ppm)
Resolution	1 ppm
NO_2	0-500ppm
Accuracy	± 1ppm (0-99.9)
Resolution	0.1 ppm

5. Data Acquisition Unit (DAQ)

Make	Agilent technologies
Model	34970A
Scan rate	60 to 250 channels/second
Scan intervals	0 to 99 hours; 1 ms time step
Accuracy	6 digits of resolution with 0.004%

List of Publications

Patents:

1. Muthukumar P, Kaushik LK, Devi S, **Arun Kumar M**. Biogas Operated Domestic Cook Stove with Naturally Aspirated Porous Radiant Burner. Patent No. 437518 Granted effect from 14/12/2019.
2. Muthukumar P, **Arun Kumar M** and Neela VR, LPG-Operated Fuel-Efficient and Clean Porous Radiant Burner, Patent No. 434432 Granted effect from 14/05/2022.
3. Muthukumar P, Kaushik LK and **Arun Kumar M**. Eco-Friendly and Energy-Efficient LPG Cooking Stove with Naturally-Aspirated Porous Radiant Burner for Commercial Kitchens. *Indian Patent Appl. No.* 202031009304. Dated: 15/5/2020.
4. Muthukumar P, **Arun Kumar M** and Aruna G. Multi-fuel operated Porous Ceramic Burner for catering and industrial applications. (Document under preparation)

Journals/Book chapters:

1. Kaushik LK, **Arun Kumar M**, and Muthukumar P. Performance analysis of a biogas operated porous radiant burner for domestic cooking application, *Environmental Science and Pollution Research*, 2021, 28(10), 12168–12177.
2. Deb S, Kaushik LK, **Arun Kumar M** and Muthukumar P. Performance Characterization of a Cluster Porous Radiant Burner for Clean and Efficient LPG Combustion. *Chemical Engineering Transactions*, 2020, 81, 361-366.
3. Deb S, Kaushik LK, **Arun Kumar M**, Satish SHV and Muthukumar P. Experimental and Numerical Investigation of Cleaner LPG Combustion in a Novel Clustered Porous Radiant Burner. *Journal of cleaner production*, 2020, 308, 127276.
4. **Arun Kumar M**, Kaushik LK and Muthukumar P. Biogas Cook Stove with a Novel Porous Radiant Burner—An Alternate for LPG Cook Stoves in Rural and Semi-urban Indian Households. *In: Muthukumar, P., Sarkar, D.K., De, D., De, C.K. (eds) Innovations in Sustainable Energy and Technology. Advances in Sustainability Science and Technology*, Springer, Singapore, 2021, 121-132.
5. Shaik SR, **Arun Kumar M**, Kalita PC and Muthukumar P. Comprehensive Review on Medical Waste Incineration. *International Journal of Global Warming*, 2021, 27(1), 16-54.

6. **Arun Kumar M**, Shaik SR, Kaushik LK, Kalita PC and Muthukumar P. Design and Lifecycle assessment of small-scale medical waste incinerator. *Indian Chemical Engineer*, 2021, 64(5), 494-507.
7. Muthukumar P, Kaushik LK, **Arun Kumar M**, Deb S, Maurya P, Shaik SR and Mujeebu MA. Evolutions in Gaseous and Liquid Fuel Cook-stove Technologies. *Energies*, 2023, 16(2), 763-800.
8. **Arun Kumar M**, Kaushik LK, Muthukumar P. Experimental investigation on performance characteristics of a naturally-aspirating Porous Radiant Burner. (Submitted to *Sustainable energy technologies and assessment*-Under review)

Conferences:

1. Kaushik LK, **Arun Kumar M** and Muthukumar P. Performance Analysis of a Bio-gas operated Porous Radiant Burner for Domestic Cooking Application. *11th International Exergy, Energy and Environment Symposium (IEEES-11),* SRM university, Chennai, India. 14-18 July 2019.
2. **Arun Kumar M**, Kaushik LK and Muthukumar P. Critical Analysis on Unstable Operation of a Self -aspirated Cook-stove with Porous Radiant Burner. *International Conference on Innovations in Thermo-Fluid Engineering and Sciences (ICITFES – 2020),* Rourkela, India. 10-12 February 2019.
3. **Arun Kumar M**, Shaik SR, Kaushik LK, Muthukumar P and Kalita PC. Life Cycle Assessment of Incinerator equipped with Porous Radiant Burner, Conventional Burner and Electrical Heater- A Comparative Study. *Recent technologies and advanced materials for Green energy and Sustainable Environment (RTAMGESE-2021),* NIT Trichy, India. 12-13 March 2021.
4. **Arun Kumar M** and Muthukumar P. Economic and Environmental performance assessment of Biogas cookstove with Porous Radiant Burner. *International Conference Polygeneration 2023 (ICP-2023),* Bali, Indonesia. 26-28 July 2023.